Oleksandr Dzyapko

# Magnon Kinetics in Quasi-Equilibrium under Parametric Pumping Leading to Bose-Einstein Condensation

2010

## Abstract

The thesis reports on results of experimental investigation of kinetics of magnons in yttrium-iron-garnet (YIG) films under excitation by intense parametric pumping. In particular, processes of magnon-magnon interaction during relaxation of intense wave packet are considered, in order to investigate a possibility and to find appropriate conditions for accumulation of substantial number of non-equilibrium magnons and creation of thermalized quasi-equilibrium magnon gas with non-zero chemical potential. The ultimate goal of this investigation is an observation of quasi-equilibrium Bose-Einstein condensation of magnons.

The studies of kinetic processes in a parametrically excited magnon gas are carried out by means of space- and time- resolved Brillouin light scattering (BLS) technique, which allows direct measurements of magnon spectral distribution function in a wide frequency range.

The choice of YIG as a material for current experimental investigations is caused by the fact that it is characterized by extremely low magnetic losses providing long lifetimes of non-equilibrium magnons ($\tau_{mp}$~0.5 μs at room temperature). The samples were 5.1 μm thick films of YIG grown on optically transparent gallium gadolinium garnet substrates, being therefore a perfect object for BLS measurements.

Time-resolved measurements of the evolution of the spectral distribution of a driven magnon gas allowed detailed investigation of processes of redistribution of parametrically injected magnons over the magnon spectrum (magnon-magnon relaxation processes) before their relaxation into the lattice. The measurements showed an existence of threshold pumping power, above which this redistribution results in a total thermalization of injected magnons and a thermodynamically quasi-equilibrium state, described by Bose-Einstein statistics. The time, the system needs to attain thermalization was found to decrease with the increasing pumping power rapidly reaching down to 50 ns, which is much smaller than the magnon lifetime.

Since the number of magnons in a parametrically driven magnon gas is larger than thermal equilibrium value, the corresponding Bose-Einstein statistic, describing the settled quasi-equilibrium state, is characterized by a nonzero chemical potential. Its value in experiments was directly determined from the measured distributions of magnons. As expected, an increase in the chemical potential of magnon gas with the pumping power was observed. At high enough pumping power the chemical potential

of the magnon gas reaches its maximum value and Bose-Einstein condensation occurs. The effect of condensation is also documented by an observation of accumulation of noticeable part of injected magnons at the bottom of the magnon spectrum, which reveals itself in an emergence of a strong, spectrally narrow magnon population peak at the minimal frequency. The observable width of this peak was found to be determined solely by the frequency resolution of the setup. BLS measurements with the ultimate resolution have shown that the intrinsic width of this peak is less than 50 MHz. It is worthy to emphasize that unlike all other systems observed magnon BEC occurs at room temperature.

As a further proof of Bose-Einstein condensation a radiation of microwave signal by the condensate was observed in experiments with microwave detection of magnons. An existence of such radiation is a clear evidence of the coherent nature of magnon condensate. The frequency of the radiation, as well as its linewidth, was found not to depend on the frequency and the power of the parametric pumping (as long as its value is above the threshold of condensation). At the same time, the frequency of the radiation can be controlled by the applied static magnetic field.

As a next step in investigation of magnon Bose-Einstein condensation the spatial properties and the dynamics of the condensate were studied experimentally. In accordance with the fact that the condensate arises as a result of action of parametric pumping a direct correspondence between the spatial profile of the condensate cloud and the configuration of the pumping field was observed. In particular, using a specific character of dynamic fields produced by a pumping resonator, simultaneous excitation of two spatially separated condensate clouds was realized. Moreover, it follows from the measurements that the separation between the condensates excited in this experiment, as well as their spatial width, can be varied in a controllable way.

## Contents

# Chapter 1

# Introduction

The concept of spin waves was introduced in physic by Bloch [1], who first suggested dynamic excitations of spin system of magnetic crystal to have a character of collective precession of individual spins which can be represented as a propagating wave. Corresponding quasiparticles, which come out as a result of quantization of spin waves were called magnons. Magnons are very similar to phonons. Like phonons they are bosons and can be described by Bose-Einstein distribution function; however a spin of a magnon, as a magnetic quasiparticle, is equal to 1. For temperatures far below Curie temperature magnetic system of magnetically ordered crystal can be well represented as a gas of magnons on the top of the ground state. Such representation has appeared to be successful and allowed to determined thermodynamic characteristics of ferromagnets such as temperature dependence of the magnetization and contribution to heat capacity and thermal conductivity.

Discovered later by Griffith effect of ferromagnetic resonance [2] started continuous experimental study of dynamic properties of magnons in microwave experiments. Shortly after that a nonlinear behavior in a system of excited spin waves was experimentally discovered [3, 4] which was then explained by Suhl [5] in terms of spin-wave parametric excitation. Possibility of parametric excitation of spin waves by microwave pumping provided powerful method for experimental investigation of different nonlinear processes [6, 7] and relaxation of magnetic excitations in magnetically ordered solids [8].

All nonlinear processes as well as the relaxation processes are caused by the non-ideality of magnon gas, i.e. by the presence of interaction between magnons. There are different types of such interaction processes (two-, three-, four-magnon interaction processes, processes involving phonons) and their effectiveness depends on the frequency and wave vector of the participating magnons. At the same time, most experiments are devoted to the processes with the participation of magnons directly excited by pumping (so-called primary magnons), whereas the magnons which

appears as a results of the relaxation of primary magnons are neglected. Such approach, of course, cannot give total information about the kinetics and thermodynamics of the magnon system driven by microwaves. Moreover, standard microwave technique, which is mainly used for pumping experiments, is sensitive only for magnons with small values of wave vector, which also limits range of magnons that could be investigated.

In the last few decades Brillouin light scattering technique [9, 10] has successively became a leading technique for experimental investigation of linear and nonlinear spin waves. First of all, this technique is very sensitive allowing for detection of thermal magnons [9]. Second, it provides possibility of direct measurements of frequency and wave vector of magnons, being therefore very informative (it was successfully used for determination of wave vectors of parametrically excited magnons in [11]). Developed in [10] time and space resolved BLS technique allows to go further and to investigate non-stationary processes of magnon interaction. The current work represents the results of such experimental investigation of kinetic processes in magnon system, strongly excited by parametric pumping.

An interest to the investigation of kinetics of magnon gas is mainly connected with the rapidly rising interest of scientists to the quantum effect of Bose-Einstein condensation. This field has been explosively growing since the first experimental observation of the effect in a vapor of sodium atoms in 1995 [12-14]. To date BEC has been observed for gases of 9 different elements [12-21] and such quasiparticles as excitons [22, 23] and polaritons [24], representing systems with both repulsive and attractive interaction, long-range anisotropic interaction and gases of metastable atoms. Recently observed BEC of magnons in YIG [25], which is the scientific basis for this thesis, has enriched this list, proving a universal nature of this effect. Moreover, magnon BEC has shown the possibility of room temperature condensation, which distinguish it from other systems.

Besides results on kinetics of magnon gas leading to the quasi-equilibrium condensation, which are important for understanding of the nature of this effect, the properties of the condensate are studied as well in this work. In particular spatiotemporal dynamics of the condensate for different spatial configurations of pumping and a radiation of microwaves by the condensate are investigated.

The structure of the thesis is following:

In Chapter 2 general concepts of magnetic ordering, magnons in ferromagnets, their properties and interaction with each other and with phonons as long as brief introduction into general properties of bosons and effect of Bose-Einstein condensation, necessary for understanding of the described experiments are given.

Chapter 3 contains information about experimental techniques used for current investigation along with the description of experimental setup.

Finally, experimental results on thermalization and condensation of magnon gas and investigation of properties of magnon Bose-Einstein condensate are represented in Chapter 4. Chapter 5 concludes this thesis.

# Chapter 2

# Fundamental Concepts

## 2.1 Magnetic ordering

Depending on their reaction on applied magnetic field at high temperatures all materials are divided into diamagnetic and paramagnetic. Elementary magnetic moments of atoms of paramagnets are nonzero even without applied magnetic field. Being subjected into the external magnetic field these moments are oriented by it, and, as a consequence, magnetic ordering arises. However, if one decreases the temperature of a paramagnet below a critical value, it becomes magnetically ordered: a spontaneous magnetization due to interaction between the atoms is built even in the absence of the applied magnetic field. Depending on the character of this interaction one arrives at ordered states with different arrangement of magnetic moments of individual atoms. Main types of the magnetically ordered materials are:

1. Ferromagnets.

Elementary magnetic moments of atoms in ferromagnets are oriented parallel to each other in one direction forming a lattice of magnetic moments. As a result a large macroscopic magnetization arises. Metals like Fe, Ni, Co, Dy and insulators like EuO and EuS are classical examples of ferromagnets.

2. Antiferromagnets.

Elementary moments in antiferromagnets are ordered in such a way, that a resultant magnetization of the unit cell is equal to zero. In the simplest case antiferromagnet consists of two equivalent sublattices with oppositely directed magnetizations which compensate each other. However, materials with more than two magnetic sublattices also exist. Antiferromagnetic ordering is typical for oxides MnO, Feo, CoO and fluorides $MnF_2$, $CoF_2$, $FeF_2$.

3. Ferrimagnets.

Similarly to antiferromagnets ferrimagnets also have several magnetic sublattices, which however do not compensate each other completely. Thus, ferrimagnets, similarly to ferromagnets, have nonzero spontaneous macroscopic magnetization. Classical example of ferrimagnets is Yttrium Iron Garnet (YIG) $Y_3Fe_5O_{12}$ which has 20 magnetic sublattices.

Beside these three types of magnetically ordered materials such groups as helicomagnets, canted antiferromagnets and magnetic glasses also exist. Despite of such variety of the materials, the nature of the magnetic ordering and the most of dynamic effects can be understood on the example of ferromagnets. For instance, in YIG at reasonable low frequencies (<100 GHz) and temperatures far below the critical temperature all sublattices are oscillating in-phase due to the strong interaction between them. Therefore, the material can be described by one vector of the total magnetization, similar to ferromagnets. Below in this work we will mainly address ferromagnets.

It is worth noting that the fully ordered ground state exists only at the zero temperature. From the thermodynamical point of view state with all magnetic moments aligned has minimal entropy therefore the thermal motion attempt to destroy it. Due to thermal excitation the order parameter (the magnetization for ferromagnets) decreases with increasing temperature. At the critical temperature (Curie temperature $T_C$ for ferromagnets, Néel temperature $T_N$ for antiferromagnets) when the thermal energy is high enough the correlation between directions of single moments vanishes and the order parameter becomes equal to zero.

### 2.2 Elementary magnetic moments; Magnetic interaction

The elementary moments, mentioned above are in most cases intrinsic (spin) moments of electrons of outer unfilled shells of the atoms. In insulators, which are often used in experiments, these electrons are localized on crystal lattice sites. This

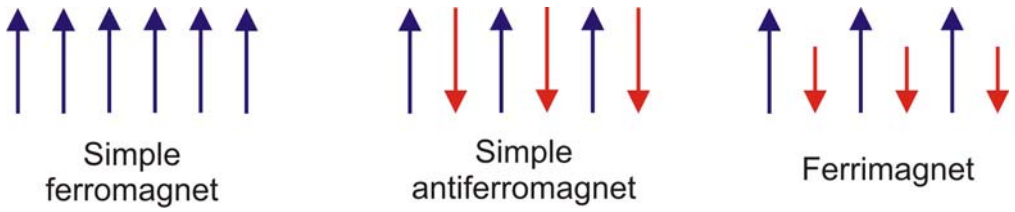


**Figure 1.** Arrangement of electron spins in magnetically ordered crystals

fact allows one to consider a ferromagnetic media as a lattice of localized magnetic moments. The alignment of the elementary magnetic moments is caused by the interaction between them. Consider now two magnetic dipoles $\vec{\mu}_1$ and $\vec{\mu}_2$ from classical point of view. Each of them is found in magnetic field created by other. The energy of such dipole-dipole interaction is [26]

$$\varepsilon_{dd} = -\frac{3(\vec{\mu}_1\vec{r}_{1,2})(\vec{\mu}_2\vec{r}_{1,2})}{r_{1,2}^5} + \frac{(\vec{\mu}_1\vec{\mu}_2)}{r_{1,2}^3} \qquad (1)$$

This interaction possibly could cause an alignment of magnetic moments. However, as measurements of the Curie temperature $T_C$ for different ferromagnets have shown, this energy is far too small to provide magnetic ordering in observable temperature range. As mentioned above, at Curie point magnetic ordering is destroyed by the thermal motion, which means that at this temperature thermal energy $\varepsilon_T \sim \kappa T_C$ ($\kappa$ is the Boltzmann constant) must be equal to the energy of dipole-dipole interaction referred to one atom $\varepsilon_{dd} \sim \mu_B^2 / a^3$ (from (1)), where $\mu_B$ - intrinsic magnetic moment of the electron (Bohr magneton) and $a$ – is the mean distance between magnetic moments. For typical values of $a \sim 3 \cdot 10^{-8}$ cm one obtains $\varepsilon_{dd} \sim 3 \cdot 10^{-18}$ erg, whereas for the most ferromagnets $\varepsilon_T \sim k$(10-1000 K)~($10^{-15}$-$10^{-13}$ erg). This shows that the origin of ferromagnetism cannot be explained by classical physics. The nature of magnetic ordering was explained by Heisenberg in terms of quantum mechanics. Considering as previously two atoms at neighboring crystal lattice sites one should also take into account electrostatic interaction between them. The energy of this interaction $\varepsilon_e \sim e_0^2 / a \sim 10^{-11}$ erg is high enough to provide the alignment of the spins. It turns out, that this energy $\varepsilon_e$ depends on the mutual direction of spins of electrons of both atoms. According to the Pauli exclusion principle total wave-function of two electrons $\psi(r_1, s_1, r_2, s_2) = \varphi(r_1, r_2)\sigma(s_1, s_2)$ should be antisymmetric under their exchange (here $r_i$, $s_i$ – position and spin of the $i$-th electron, $\varphi$ and $\sigma$ – coordinate and spin parts of total wave-function). Thus, when spins of the electrons are parallel ($s_1 = s_2$) spin part of the wave-function $\sigma$ is symmetric and $\varphi$ – antisymmetric. Correspondingly, in antiparallel spin configuration ($s_1 = -s_2$) $\varphi$ is symmetric. Thus, the energy of Coulomb interaction, which depends on the spatial configuration of wave-function, will be

different in these two cases. This difference is called exchange energy. According to Dirac [27], the Hamiltonian of the exchange energy can be written in the following form:

$$\hat{H}_{ex} = -2J(r_{1,2})\hat{s}_1\hat{s}_2 \ , \qquad (2)$$

where $J$ is the exchange integral. When positive it favors spins to be parallel causing ferromagnetic ordering. Effective interaction, reflecting a tendency of magnetic moments to be in a state with minimal exchange energy, is called exchange interaction. Exchange integral $J$ decreases quickly with increasing distance between the particles, so the exchange interaction is a short-range interaction.

Described here model of a ferromagnet as a system of localized spin magnetic moments coupled through the exchange interaction defined by Hamiltonian (2) is called Heisenbeg-Dirac-Van Vleck model (briefly - Heisenberg model). For correct description of processes in real substances one should generalize this model by taking into account other magnetic interactions, present in the system. These are: dipole-dipole interaction of the moments between each other (1); their interaction with external magnetic field, the so-called Zeeman interaction (energy of a moment $\vec{\mu}$ in a magnetic field $\vec{H}$ $\varepsilon_Z = -\vec{\mu}\vec{H}$) and the energy of magnetic anisotropy (dependence of the energy of a ferromagnet on the direction of elementary moments with respect to the crystal lattice axes). The latter, however, is often very small and should be taken into account only in specific cases.

It is worth noting that although the dipole-dipole interaction is much weaker then the exchange one it also decreases weaker with distance i.e. it is a long-range interaction. Therefore it plays important role in processes with characteristic scales much larger than interatomic distance $a$, when exchange is already weak.

### 2.3 Macroscopic theory of spin waves; Landau-Lifshitz equation

As discussed above, all magnetic moments in ferromagnets are coupled to each other through the exchange interaction. This strong correlation between moment's directions leads to the existence of specific excitations in these materials. If, for some reason, the direction of one moment is changed, the neighboring moments will

immediately be affected due to the exchange interaction. Thus, any small deviation will not stay localized but will propagate in a wave-form over the whole sample. Since the moments involved are spins, these propagating wave-like excitations were called spin waves. Although the exchange interaction, which is determinant, has quantum nature, a classical approach can be used to describe spin waves. Historically classical approach was developed after the quantum theory, but for some applications (for instance for consideration of long wavelength excitations of samples of different geometries) it appears more convenient to use the classical theory. In this approach the continuum model of ferromagnet is used. Instead of system of localized moments it is characterized by the magnetization vector $\vec{M}$ (density of the magnetic moment)

$$\vec{M} = \frac{\sum_{\Delta V} \vec{\mu}_i}{\Delta V}, \qquad (3)$$

where $\Delta V$ is small, but macroscopic volume. At that, the deviation of spins mentioned above, are now represented as an oscillations of magnetization $\vec{M}$. It is obvious, that this approach is valid, when the characteristic scale of the processes $l >> a$ ($a$ – distance between neighboring spins).

From classical physics it is known, that motion of the single moment $\vec{m}$ in magnetic field $\vec{H}$ is described by

$$\frac{\partial \vec{m}}{\partial t} = -\gamma \vec{m} \times \vec{H} \qquad (4)$$

Here $\gamma$ is the so-called gyromagnetic ratio. For electron spin $\gamma = 2\mu_B/\hbar$ with $\hbar$ being the Plank constant. The main assumption of the classical theory is that because of the strong exchange interaction, which tries to align all spins, the sample could be treated as the set of small macroscopic volumes $\Delta V$ with "rigid" magnetic moment $\vec{m} = \vec{M}\,\Delta V$. In other words, the dynamic of the magnetization $\vec{M}$ is also described by (4). $\vec{H}$ in this case is considered to be an effective field representing all interactions in the system. Thus, the equation of motion of the magnetization $\vec{M}$ of a ferromagnetic sample is

$$\frac{\partial \vec{M}}{\partial t} = -\gamma \vec{M} \times \vec{H}_{eff} \qquad (5)$$

This equation was first written by Landau and Lifshitz in 1935 [28]. The effective field $\vec{H}_{eff}$ contains in general case following terms:

- external magnetic field $\vec{H}_{e0}$ (corresponds to the Zeeman energy);
- effective field of the exchange interaction $\vec{H}_{ex}$;
- effective field of dipole-dipole interaction $\vec{H}_{dd}$;
- effective field of magnetic anisotropy (will be omitted in this consideration).

Effective field of exchange interaction takes into account an increase of the exchange energy when the neighboring magnetic moments are not exactly parallel, i.e. when $\vec{M}$ depends on spatial coordinates. It can be written as [29]

$$\vec{H}_{ex} = q\nabla^2 \vec{M}, \qquad (6)$$

where $q$ is the exchange constant, which is proportional to the exchange integral $J$ (see Section 2.6).

The dipole-dipole field $\vec{H}_{dd}$ accounts for the fact that the magnetic moment of a given small volume of the sample is found in the magnetic field created by the magnetization of the rest of the sample. In other words, it depends on $\vec{M}$. For the case of homogeneous magnetization it is simply found from the equations of magnetostatics $\nabla \cdot (\vec{H}_{dd} + 4\pi \vec{M}) = 0,\ \nabla \times \vec{H}_{dd} = 0$ along with the boundary conditions. In the theory of magnetostatics this field is called demagnetizing field and it can be written in the form [29]

$$\vec{H}_{dd} = -\hat{\vec{N}}\vec{M}, \qquad (7)$$

where $\vec{N}$ is a tensor of the demagnetization factors, which components are determined by the shape of the sample. When the sample is an ellipsoid (sphere, disc/slab, rod – limiting cases of the ellipsoid) and its axes coincide with the coordinate axes $\vec{N}$ becomes diagonal, i.e. $N_{i,j} = \delta_{i,j} N_i$ (here $\delta_{i,j}$- Kronecker's delta and $i, j = x, y, z$). If the external magnetic field $\vec{H}_{e0}$ is also parallel to one of the axes, both the demagnetizing field $\vec{H}_{dd}$ and the magnetization vector $\vec{M}$, are parallel to $\vec{H}_{e0}$.

An important feature of the equation of motion (5) is that it ensures the conservation of the length of the magnetization vector $\vec{M}$. Multiplying (5) scalarly with $\vec{M}$ one gets

$$\vec{M}\frac{\partial \vec{M}}{\partial t} = \frac{1}{2}\frac{\partial}{\partial t}\vec{M}^2 = -\gamma \vec{M}(\vec{M} \times \vec{H}_{eff}) = 0 \Rightarrow$$
$$\Rightarrow \vec{M}^2 = const \qquad (8)$$

For consideration of non-uniform wave excitation one needs to extend the above approach and to take into account spatio-temporal variations of the magnetization. A spectrum of the spin waves in macroscopic approximation was first obtained by Herring and Kittel [30]. In this approach the magnetization of the sample is considered as a sum of a large static $\vec{M}_0$ and a small dynamic $\vec{m}_{\sim}$ components

$$\vec{M} = \vec{M}_0 + \vec{m}_{\sim} \qquad (9)$$

It is assumed, that the dynamic component $m_{\sim} << M_0$ and can be presented as a set of plane waves $\vec{m}_{\sim}(r,t) = \sum_k \vec{m}_k = \sum_k \vec{m}_{0k} e^{i(\omega t - kr)}$. In this case the exchange field becomes

$$\vec{H}_{ex} = q\nabla^2 \vec{m}_{\sim} = -q\sum_k k^2 \vec{m}_k \qquad (10)$$

For the unbounded sample the static component of the dipole-dipole field $\vec{H}_{dd}$ (demagnetizing field) is parallel to the magnetization just because of the symmetry

reasons. Therefore, its contribution to the torque (5) $\vec{M} \times \vec{H}_{dd}$ equals to zero and $\vec{H}_{dd}$ can be neglected in this analysis. For determination of the dynamic component $\vec{h}_{dd}$, strictly speaking, the Maxwell's equations should be used (in the case of magnetic insulator we can set $j = 0$ )

$$\nabla \cdot (\vec{h}_{dd} + 4\pi \vec{m}_{\sim}) = 0$$
$$\nabla \times \vec{h}_{dd} = \frac{\varepsilon}{c} \frac{\partial \vec{e}}{\partial t} \qquad (11)$$

However, as soon as the wavelength of a spin wave is much smaller than that of the electromagnetic wave of the same frequency the right hand part of the second equation accounting for the retardation effects can be omitted. This approximation is called magnetostatic, since the obtained equations for $\vec{h}_{dd}$ and $\vec{m}_{\sim}$ resembles equations for static magnetic field. In the framework of this approximation for the plain waves $\tilde{m}_k$ one obtains

$$\vec{h}_{dd} = -4\pi \vec{k} (\vec{m}_k \vec{k}) / k^2 \qquad (12)$$

Thus, the effective field $\vec{H}_{eff}$ which enters the equation (5) is

$$\vec{H}_{eff} = \vec{H}_{eff\,0} + \vec{h}_{eff} = \vec{H}_{e0} - q \sum_k k^2 \vec{m}_k - 4\pi \sum_k \vec{k} (\vec{m}_k \vec{k}) / k^2 \qquad (13)$$

In similar way as for the magnetization, one gets $h_{eff} \ll H_{eff\,0}$, which allows one to use the method of successive approximations. In zero approximation one obtains

$$\vec{H}_{e0} \times \vec{M}_0 = 0, \qquad (14)$$

which means, that for an isotropic ferromagnet the direction of the static magnetization coincides with the direction of the external magnetic field. It is

convenient to direct *z* axis along this direction i.e. $\vec{H}_{e0} = \vec{z}_0 H_{e0}, \vec{M}_0 = \vec{z}_0 M_0$. Then, in the first approximation on $\vec{m}$ one gets for each individual wave $\vec{m}_k$

$$i\omega_k \vec{m}_{0k} + \omega_H \vec{m}_{0k} \times \vec{z}_0 - \frac{q\omega_M k^2}{4\pi} \vec{z}_0 \times \vec{m}_{0k} - \frac{\omega_M}{k^2} (\vec{m}_{0k} \vec{k}) \vec{k} \times \vec{z}_0 = 0, \quad (15)$$

where $\omega_H = \gamma H_{e0}, \omega_M = 4\pi\gamma M_0$.

Projecting (15) onto the coordinate axes one directly obtains $m_{0kz} = 0$, and a system of equations for other two components. Equating the determinant of the obtained system to zero, one gets a dispersion relation for spin waves

$$\omega_k^2 = (\omega_H + \gamma q M_0 k^2)(\omega_H + \gamma q M_0 k^2 + \omega_M \sin^2 \theta_k), \quad (16)$$

where $\sin^2 \theta_k = \frac{k_x^2 + k_y^2}{k^2}$, i.e. $\theta_k$ is the angel between $\vec{k}$ and the *z*-axis.

A typical spectrum of spin waves in a ferromagnet is shown in Fig.2. As seen from (16) the spectrum of the spin waves has several peculiarities. First of all, it has a gap. The minimal frequency of the spin waves $\omega_H = 2\pi f_H = \gamma H_{e0}$ is determined by the external magnetic field. The contribution of dipole-dipole interaction (term $\omega_M \sin^2 \theta_k$) leads to the anisotropy of the dispersion relation, i.e. the frequency of a spin wave depends on the direction of its wave vector. At a given $|\vec{k}|$ minimal frequency corresponds to the waves propagating along the direction of the static magnetization ($\theta_k = 0$) and maximum – to those, perpendicular to $\vec{M}_0$ ($\theta_k = \frac{\pi}{2}$). In the long wavelength limit ($k \to 0$): $\omega_{\min} = \omega_H, \omega_{\max} \equiv \omega_\perp = 2\pi f_\perp = \sqrt{\omega_H(\omega_H + \omega_M)}$ (see Fig. 2). If the external magnetic field $H_{e0}$ is changed, the whole spectrum slides along the frequency axis. Higher frequencies correspond to higher field values.

As expected, short-range exchange interaction does not play significant role at small *k*-values (when the wave length $\lambda = 2\pi / k$ is much larger than the interatomic

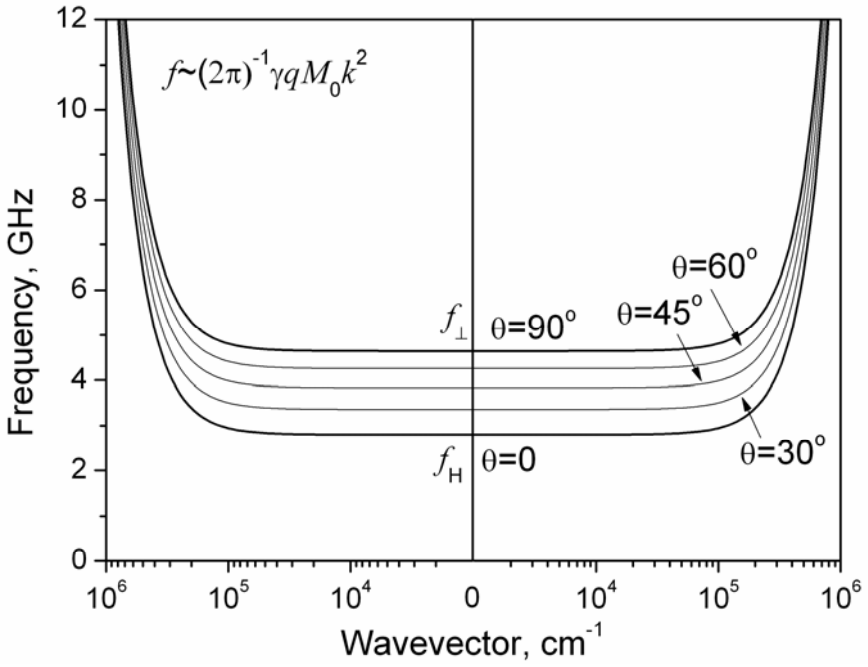


**Figure 2.** Spectrum of spin waves in an unbounded ferromagnet with $4\pi M_0$=1750 G and $q$=3×10$^{-12}$ cm$^2$ (YIG at room temperature) for $H_0$=1 kOe.

distance $a$) but its contribution quickly increases with increasing wave vector $\sim k^2$. At $\gamma q M_0 k^2 >> \omega_H, \omega_M$ the dispersion of spin waves has simple quadratic form

$$\omega_k \approx \gamma q M_0 k^2 \qquad (17)$$

Finally, using equation (15) one can derive for the ratio of the magnetization components

$$\frac{m_{0ky}}{m_{0kx}} = -i\left(1 + \frac{\omega_M \sin^2\theta_k}{\omega_H + \gamma q M_0 k^2}\right)^{-\frac{1}{2}} \qquad (18)$$

From (18) follows, that spin waves have right-hand circularly polarization. This polarization is, for a general orientation of the wave vector, elliptical, but it approaches to the circular one with increasing *k*. The oscillations are exactly circular for $\vec{k} \| \vec{z}_0$. Thus, if one goes back to the representation of the ferromagnet as a set of the magnetic moments, a spin wave can be imagined as a precession of the individual moments with the phase of the precession changing along $\vec{k}$ direction (see Fig. 3)

For the excitation of certain spin wave $\vec{m}_k$ one, obviously, needs to apply dynamic field $\vec{h}_k$ with the corresponding frequency and wave vector ($\omega_k, \vec{k}$). Then, in equation (15) one obtains additional term $\frac{\omega_M}{4\pi}\vec{h}_k$, which describes the excitation of the corresponding spin wave.

The most simple, from the point of view of experimental realization, is the excitation of uniform mode ($k = 0$). The first investigations of the dynamical properties of the ferromagnets, subjected both to the static and dynamic microwave magnetic fields, were carried out by Griffiths [2]. The effect of the resonant excitation of the uniform oscillations in ferromagnetic sample by dynamic microwave field of certain frequency $\omega = \omega_{k=0}(\vec{H})$ is called ferromagnetic resonance [31].

In the case of unbounded ferromagnet, the frequency of the uniform mode $\omega_0$ (at $k \to 0$) is not determined, since spectra corresponding to different $\theta$ do not approach to the same limit as $k \to 0$. However, in real samples this problem is removed by taking into account of the boundary conditions which are crucial for the uniform mode. For the case of an ellipsoidal sample in the magnetostatic approximation using

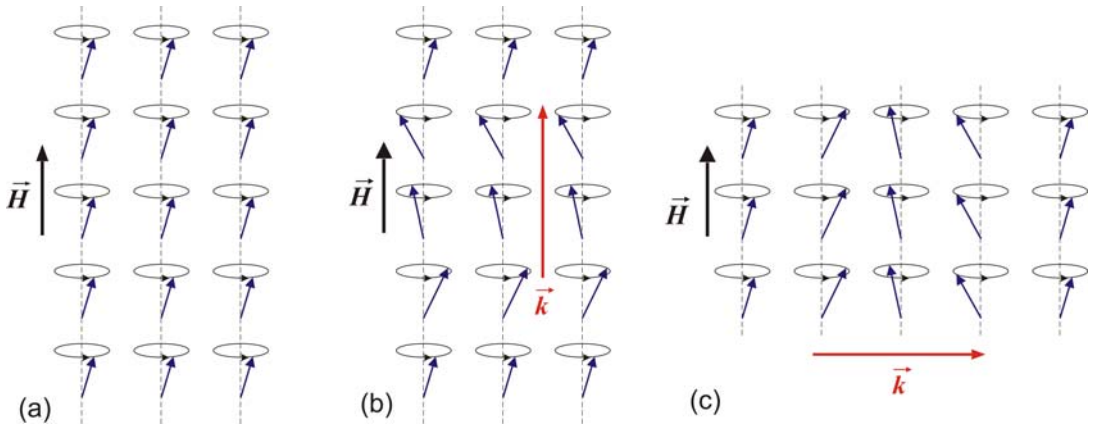


**Figure 3.** Schematic illustration of (a) the uniform mode and spin waves propagating along the direction of the static magnetic field (b) and perpendicularly to it (c).

(7) one gets for the uniform mode $\vec{H}_{dd} = -\vec{\vec{N}}\vec{M} = -\vec{\vec{N}}\vec{M}_0 - \vec{N}\vec{m}_0$. Substituting this into (15) and equating $k = 0$ one obtains for the frequency of the uniform mode

$$\omega_0^2 = \left( \omega_H + \frac{N_x - N_z}{4\pi} \omega_M \right) \left( \omega_H + \frac{N_y - N_z}{4\pi} \omega_M \right) \qquad (19)$$

Equation (19) was obtained by Kittel [31]. From the classical point of view uniform mode is a precession of the total magnetic moment of the sample $\vec{\mathcal{M}} = \vec{M}V$ with the right-hand polarization and the frequency given by (19).

It is worth noting, that the Landau-Lifshitz equation (5) does not describe damping of the spin waves, which is always present in real systems. One approach to take the relaxation into account is to introduce phenomenologically an additional dissipative term $\vec{R}$ into the right hand part of the equation (5). The term proposed by Landau and Lifshitz [28] can be written as follows: $\vec{R} = -\frac{\alpha}{M^2} \vec{M} \times (\vec{M} \times \vec{H})$ with $\alpha$ - damping parameter having the dimensions of frequency. Sometimes another dissipative terms in form proposed by Gilbert [32] or Bloch and Bloembergen [33] are used. The real processes of dissipation in ferromagnets are numerous and complicated, therefore, the choice of the dissipative term depend on the particular experimental situation. However for the most relevant cases relaxation parameter of the spin waves $\eta_k$ is small compared to their frequency $\eta_k / \omega_k \ll 1$ which allow for accounting of the damping at the very end of the consideration by simple substitution of the frequency of the certain spin wave $\omega_k \to \omega_k + i\eta_k$. For the calculation of $\eta_k$ detailed theory of the processes responsible for the relaxation should be used. Along with the relaxation frequency $\eta_k$ the life time of the spin wave $\tau_k = 1/(2\eta_k)$, which characterize the damping of the energy of the spin wave, is often used.

### 2.4 Spin waves in ferromagnetic films

In real experiments on spin waves samples of finite size are always used. Therefore, the size and the shape of the sample mainly determine the long-range dipole-dipole interaction, leading to the substantial modification of the spin wave spectrum at $k \le 2\pi / l$, where $l$ is the characteristic dimension of the sample.

Mathematically this is represented by the fact that the magnetostatic equations for the dipole-dipole field should be provided with the boundary conditions on the samples surfaces (which results in static and dynamic demagnetizing fields).

One of the most frequently used sample geometry is that of films (slabs). In addition, film geometry, as geometry with a confinement in one direction, is the simplest one for the consideration of the effects in bounded ferromagnets. Since these effects are caused by dipole-dipole interaction and affect only long wavelength excitation, first theoretical studies of the problem of the spin waves in ferromagnetic films did not take into account the exchange interaction [34-37]. The first work in this direction was made by Damon and Eschbach [34], who considered a ferromagnetic slab, magnetized in its plane. They showed that the normal modes for this geometry are waves propagating in the plane of the slab, but standing in the direction along its normal. The wave vector of these modes can be presented as $k^2 = k_{\|}^2 + (k_{\perp}^n)^2$, where the continuously changing in-plane component $k_{\|}$ describes the propagation of the spin wave mode, whereas the quantized $k_{\perp}^n$ characterize the mode pattern across the thickness. The value of the latter differs for two neighboring modes for $\Delta k_{\perp} = k_{\perp}^{n+1} - k_{\perp}^n = \frac{\pi}{d}$ with *d* being the thickness of the slab. Furthermore, beside these modes (which can be imagined as a superposition of two plain waves) a new, surface, mode, propagating along one of the interfaces, arises in the spectrum, which does not have analogue in the spectrum of spin waves of unbounded sample. This mode has imaginary transverse wave vector $k_{\perp} = iq$, so the distribution of the dynamic magnetization of this wave over the slabs thickness is hyperbolic. It exists only at $\theta = \angle(\vec{k}_{\|}, \vec{M}_0) > \theta_c = \tan^{-1}\left(\frac{\omega_H}{\omega_M}\right)$ [37]. Fig. 4 shows typical dispersion of the volume modes of the slab propagating along the magnetization direction ($\vec{k}_{\|} \| \vec{M}_0$, $\theta$=0) and of the surface mode with $k_{\|} \perp \vec{M}_0$ ($\theta$=90º), along with the distribution of dynamic magnetization $m_{\sim\perp}$ over the slabs thickness.

Since Damon and Eshbach used the magnetostatic approximation for the derivation of $h_{dd}$ they called the modes, obtained in such a way, magnetostatic waves.

The Damon-Eshbach theory is only applicable for small values of $k$, when exchange interaction still can be neglected. However, for thin films the separation between neighboring modes in $k$-space $\Delta k_{\perp} = \frac{\pi}{d}$ can be already high enough to require accounting of the exchange interaction. The theory of spin waves in ferromagnetic films including both dipole-dipole and exchange interaction was developed in [38-40]. Introduction of exchange requires additional boundary conditions for the dynamic magnetization $\vec{m}$, accounting for the fact that the precession of the surface spins can differ from that in the bulk [41-43]. In general case, introduction of the exchange complicates the problem noticeable, but for some applications approximate expression can be useful. From [39] in diagonal approximation for "unpinned" surface spins (surface spins are considered not to differ from bulk) the approximate dispersion relation in explicit form can be obtained

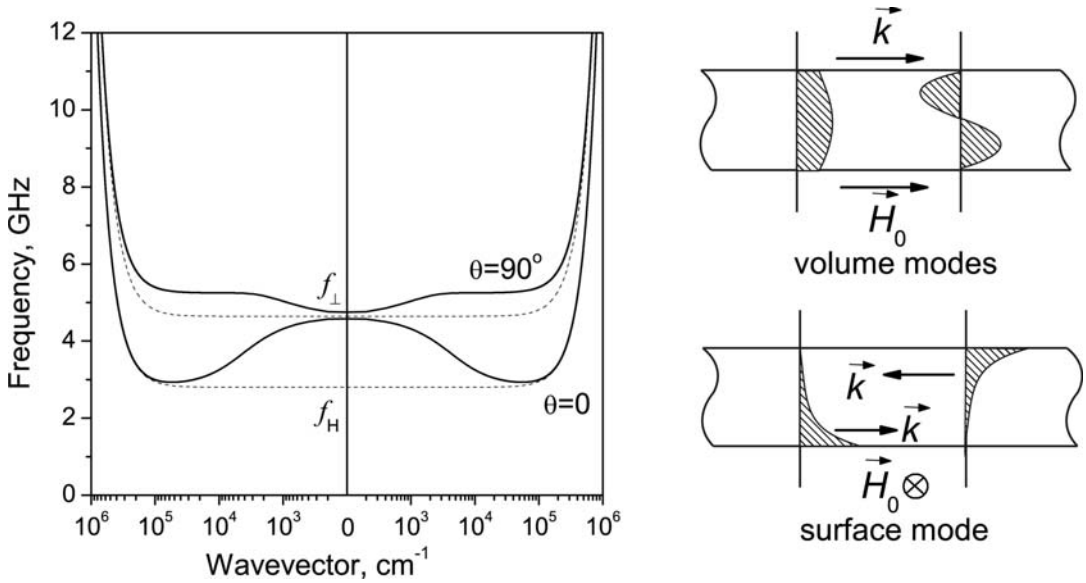


**Figure 4.** Spectrum of the spin waves in 5 μm thick in-plane magnetized YIG film at $H_0$=1 kOe (solid lines) along with the spectrum of the bulk ferromagnet (dotted lines) (a); (b) – schematics of the profiles of the volume and surface magnetostatic modes.

$$\omega_k^2 = (\omega_H + \gamma q M_0 k^2 + \omega_M (1 - P_n))(\omega_H + \gamma q M_0 k^2 + \omega_M P_n \sin^2 \theta_k) \qquad (20)$$

$$P_n = \frac{k_\parallel^2}{k_\parallel^2 + \kappa_n^2} - \left( \frac{k_\parallel^2}{k_\parallel^2 + \kappa_n^2} \right)^2 \frac{F_n}{\sqrt{2(1+\delta_{0n})}}$$

$$F_n = 2 \frac{1 - (-1)^n \exp(-k_\parallel d)}{k_\parallel d}$$

$$k^2 = k_\parallel^2 + \kappa_n^2, \kappa_n = \frac{n\pi}{d}$$

where $k_\parallel$ is in-plane wave vector, *n* denotes the number of the mode and $\theta_k = \angle(\vec{k}_\parallel, \vec{M}_0)$. In diagonal approximation used in (20) it is assumed that the normal modes are either uniform across the thickness of the film (*n*=0) or harmonic ($n \neq 0$), therefore this equation badly describes the dispersion of the surface mode (with hyperbolic dependence of $\vec{m}$ over the thickness), i.e. (20) should be carefully applied at large $\theta_k$. However, for thin films the distribution of the magnetization for surface mode can be considered as uniform in a wide range of wave vector values ($k_\parallel d << 1$) and dispersion relation (20) can be used.

### 2.5 Parametric excitation of spin waves

The system of the spin waves in a ferromagnet is intrinsically nonlinear. In particular, the condition of the conservation of total length of the magnetization vector $\left|\vec{M}\right| = \left|\vec{M}_0 + \vec{m}\right| = const$ results in the dependence of the static magnetization vector on the dynamic one. Assuming that $\vec{M}_0 \parallel \vec{z}_0$ and $\vec{m}$ lying in the *x0y* plane one can write

$$M_0 = \sqrt{M^2 - m^2} \approx \left| m << M_0 \right| \approx M(1 - \frac{m^2}{2M^2}) \qquad (21)$$

This value of $M_0$ should be used in equations for dynamic magnetization $\vec{m}$, which cause an interaction between different spin waves. The interaction enables an energy transfer from one spin wave modes to another. In particular, the excitation of non-

uniform spin wave modes (waves with $\vec{k} \neq 0$) by the uniform field becomes possible. It was found [5, 44] that this excitation has a character of parametric resonance – applied dynamic field (which is in this case called pumping) changes alternatively one of the parameters of the media (local magnetic field or magnetization) and when the amplitude of this changes exceeds a threshold value, an effective growth (instability) of certain modes starts and almost entire pumped energy is transferred into them. From the theory of oscillation and waves [45] it is known that for the effective energy transfer in the parametric process the following condition between the frequency and the wave vector of the pumping and those of the pumped modes should hold:

$$\begin{aligned} n\omega_p &= \omega_1 + \omega_2 \\ n\vec{k}_p &= \vec{k}_1 + \vec{k}_2 \end{aligned}, \qquad (22)$$

where $n$=1, 2, 3… is the order of the parametric process. These conditions ensure the stable phase difference between the pumping and the pumped modes in time and space correspondingly. The most effective and commonly observed is the process of the 1st order.

In the theory of parametric instability of spin waves two types of parametric processes depending on the orientation of the microwave pumping field $\vec{h}_{\sim}$ are distinguished.

Instability of the first type arises when the pumping field $\vec{h}_{\sim} = \vec{h}_{\perp} e^{i\omega_p t}$ is perpendicular to the direction of the static magnetic field and static magnetization, i.e. $\vec{H}_{e0} \| \vec{M}_0 \| \vec{z}_0, \vec{h}_{\sim} \perp \vec{z}_0$. In the linear case (introducing $\vec{h}_{\sim}$ into the effective field (13)) one can see, that this uniform magnetic field would excite only the uniform precession at the frequency $\omega_p$ (the closer this frequency to the ferromagnetic resonance frequency $\omega_0$ the more effective is the excitation). However, due to the nonlinearity of the spin system excited uniform mode is coupled to the other (non-uniform) modes and can pass energy into them. Generally speaking, these could be any two spin waves, which fulfill (22). However, in almost all cases spin waves with $\omega_1 \approx \omega_2 \approx \omega_p / 2,\ \vec{k}_1 = -\vec{k}_2$ are excited. The instability of spin waves under the action of transverse pumping is also called subsidiary absorption or Suhl's first order instability.

In the second case dynamic instability is caused by the magnetic field $\vec{h}_{\sim} = \vec{z}_0 h_{\parallel} e^{i\omega_p t}$, which is parallel to the static one. In the linear approximation on small values $h_{\sim}, m_{\sim} \ll H_{e0}, M$ of equation (5) magnetic field $\vec{h}_{\sim} \parallel \vec{z}_0$ cannot excite any separate spin wave. However, in the second approximation, when the coupling between different modes is taken into account, the simultaneous transfer of the energy from the field to two spin waves becomes possible. In the same way as for the subsidiary absorption the most effective is the excitation of spin waves with $\omega_1 \approx \omega_2 \approx \omega_p / 2,\ \vec{k}_1 = -\vec{k}_2$.

It can be shown (see e.g. [29, 46, 47]) that the account of the dynamic field $\vec{h}_{\sim}$ in the equation of motion (5) leads to the following equations for the amplitudes of the spin waves:

$$\begin{aligned} \frac{dc_k}{dt} &= i\tilde{\omega}_k c_k + \rho_{\perp,\parallel}(k, h_{\sim}) c^*_{-k} \\ \frac{dc^*_{-k}}{dt} &= -i\tilde{\omega}^*_k c^*_{-k} + \rho^*_{\perp,\parallel}(k, h_{\sim}) c_k \end{aligned}, \qquad (23)$$

where $c_k = c^0_k(t) e^{i\tilde{\omega}_k t} \sim \frac{m_k}{M_0}$ - reduced amplitude of the spin wave with wave vector $\vec{k}$, $\tilde{\omega}_k = \tilde{\omega}_{-k} = \omega_k + i\eta_k$ ($\eta_k \ll \omega_k$ accounts for the dissipation) and $\rho_{\perp,\parallel}(k, h_{\sim})$ - coupling coefficient between spin waves $c_k$ and $c_{-k}$, which depends on the magnetic parameters of the media. For the case of transverse parametric pumping this parameter is the magnetization $\vec{M}$, which precesses due to the excitation of uniform mode $c_0$ by the transverse field $\vec{h}_{\sim}$:

$$\begin{aligned} \rho_{\perp}(k, h_{\sim}) &= -ic_0 \frac{\omega_M}{4\omega_k} (\omega_k + \omega_H + \gamma q M_0 k^2) \sin 2\theta_k e^{i\varphi_k} = \\ &= -i \frac{\gamma h_{\perp} e^{i\omega_p t}}{\omega_0 - \omega_p + i\eta_0} \frac{\omega_M}{4\omega_k} (\omega_k + \omega_H + \gamma q M_0 k^2) \sin 2\theta_k e^{i\varphi_k} = i V^{\perp}_k h_{\perp} e^{i\omega_p t} \end{aligned}, \qquad (24)$$

where it is assumed that dynamic field $h_{\sim}$ has right-hand circular polarization.

For the parallel pumping, coupling coefficient depends on the value of the magnetic field inside the sample, which is modulated by $\vec{h}_{\sim}$:

$$\rho_{\parallel}(k, h_{\sim}) = i\gamma h_{\parallel} e^{i\omega_p t} \frac{\omega_M}{4\omega_k} \sin^2\theta_k e^{2i\varphi_k} = iV_k^{\parallel} h_{\parallel} e^{i\omega_p t} \qquad (25)$$

In (24), (25) $\theta_k$ and $\varphi_k$ are azimuth and polar angles of wave vector $\vec{k}$ ($\theta_k = 0$ corresponds to the direction of the static magnetization). Since $c_k \sim e^{i\omega_k t}$, $c_{-k}^* \sim e^{-i\omega_k t}$, $\rho_{\perp,\parallel} \sim e^{i\omega_p t}$, it is obvious from (23) that the most efficient energy transfer from the pumping field into the spin waves is realized when $\omega_k \approx \omega_p / 2$. When this energy transfer becomes enough to overcome the relaxation of the spin waves, an exponential grows of the amplitudes of the latter starts. From (23) it can be shown, that the threshold value of the dynamic field $h_{\perp,\parallel}$, above which the instability occurs is

$$h_{thr\,\perp,\parallel} = \frac{\sqrt{\eta_k^2 + (\omega_p / 2 - \omega_k)^2}}{\left|V_k^{\perp,\parallel}\right|} \qquad (26)$$

Since the spectrum of spin waves is degenerated (see for example Fig. 3), i.e., for a certain value of frequency $\omega_k$ there are many possible values of wave vector $\vec{k}$, to find the actual threshold field one needs to minimize (26) over the all existing spin waves with $\omega_k = \omega_p / 2$. When assumed that $\eta_k$ does not depend on $\vec{k}$ the minimal threshold corresponds to the waves with maximum coupling coefficient $V_k^{\perp,\parallel}$. For the case of transverse pumping these are waves with $\theta_k \approx 45°$ and for parallel - $\theta_k = 90°$. Corresponding waves are indicated in the Fig. 5 by circles and stars respectively. The necessary condition for the observation of the parametric instability of the first order is $\omega_p \geq 2\omega_{\min} = 2\omega_H$.

Parametric instability of spin waves in bounded samples, in particular in thin films, has its peculiarities if the frequency of the pumped modes $\omega_p / 2$ lies in the

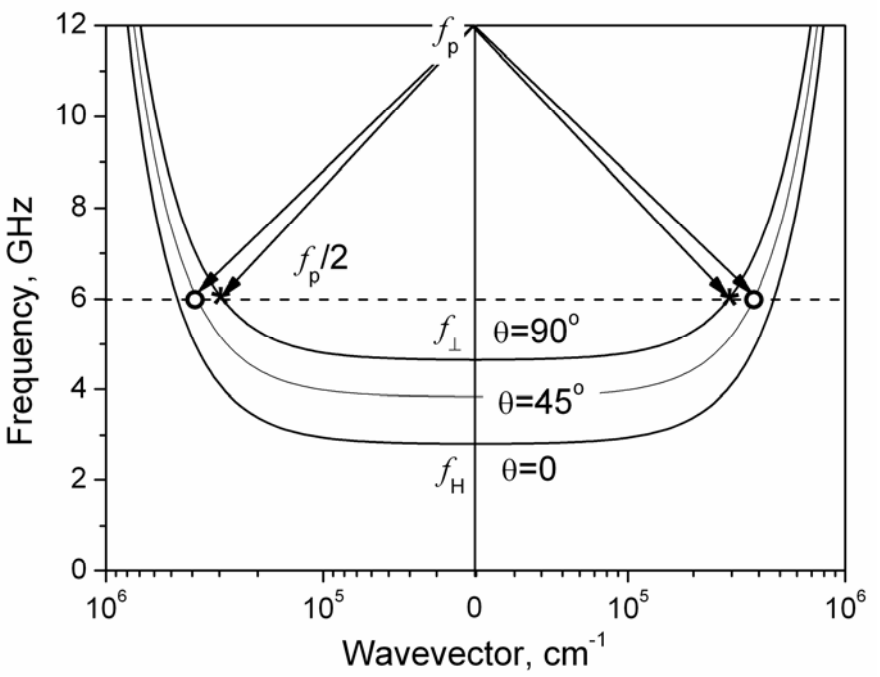


**Figure 5.** Illustration of the parametric pumping instability process. Circles and stars indicate the waves, which first become unstable under the influence of the perpendicular and parallel pumping respectively.

dipole part of the spectrum [48-51]. However, the approach for the analysis of the problem remains the same. Equations (23) are still valid, only the expressions for the coupling coefficients $V_k^{\perp,\parallel}$ are modified.

### 2.6 Quantum theory of spin waves; Magnons

Macroscopic description of the dynamical properties of a ferromagnetic media by means of oscillations and waves of the magnetization has advantages in the sense of demonstrativeness and use of conventional methods of the wave physics. However, classical approach remains phenomenological and cannot be rigorous, since the exchange interaction, which is the prime cause of the ferromagnetism, has quantum nature. For quantum description the Heisenberg model of a ferromagnet as a system of localized spins coupled to each other through the exchange interaction is used. For the first time this approach was used by Bloch [1], who introduced the concept of spin waves. Later Holstein and Primakoff [52] generalized this model by taking into

account weaker dipole-dipole interaction between spins and their interaction with external magnetic field (Zeeman interaction). To analyze the excitations, which can exist in the system, they used the method of second quantization (see e.g. [53, 54]). This method involves a series of transformations of initial Hamiltonian (written in the "natural" variables of the system) with the purpose to cast it into the harmonic oscillator-form $\hat{H} = \sum_k \hbar\omega_k c_k^+ c_k + \hat{H}_{\text{int}}$. In this representation $c_k^+, c_k$ are the operators of creation and annihilation of the quasiparticles corresponding to the elementary excitations of the system and their product $c_k^+ c_k \equiv \hat{n}_k$ is the operator of the number of these quasiparticles; $\hbar\omega_k$ - their energy. $\hat{H}_{\text{int}}$ contains terms of third and higher orders in $c_k$ and describes transitions between states with different excitations (represents energy of interaction of quasiparticles between each other).

The "natural" variables of the Heisenberg ferromagnet are, obviously, the operators of spin projections at the lattice site *i*: $\hat{s}_i^{x,y,z}$. To obtain the initial microscopic Hamiltonian one should take expressions for the exchange and dipole-dipole interaction of two magnetic moments (Eqs. (2) and (1) respectively) and for the Zeeman energy of a single moment in a magnetic field and perform a summation over the all lattice sites (classical dipole moments $\mu$ should be replaced by $2\mu_B\hat{s}$).

$$\hat{H} = -2\sum_i \mu_B H\hat{s}_i - \sum_i \sum_{j\neq i} J(r_{i,j})\hat{s}_i\hat{s}_j - \frac{1}{2}\sum_i \sum_{j\neq i} \frac{4\mu_B^2}{r_{i,j}^5}\left[3(\vec{r}_{i,j}\hat{s}_i)(\vec{r}_{i,j}\hat{s}_j) - r_{i,j}^2(\hat{s}_i\hat{s}_j)\right] \quad (27)$$

Since the projections of each individual spin satisfy commutation rules $[\hat{s}_i^x, \hat{s}_i^y] = i\Delta_{i,j}\hat{s}_i^z$, the total number of independent variables in (27) is 2*N*, where *N* is the number of lattice sites in the sample. The approach used in [52] involves three transformations of initial Hamiltonian (27). In the first one spin operators should be first replaced by operators $\hat{a}_i^+$ and $\hat{a}_i$, which satisfy commutation relations for Bose operators $\left[\hat{a}_i, \hat{a}_j^+\right] = \Delta_{i,j}, \left[\hat{a}_i, \hat{a}_j\right] = 0, \left[\hat{a}_i^+, \hat{a}_j^+\right] = 0$. The connection between spin operators and new ones is:

$$\hat{s}_i^+ = \sqrt{2s}\left(1-\frac{1}{2s}\hat{a}_i^+\hat{a}_i\right)^{\frac{1}{2}}\hat{a}_i$$
$$\hat{s}_i^- = \sqrt{2s}\hat{a}_i^+\left(1-\frac{1}{2s}\hat{a}_i^+\hat{a}_i\right)^{\frac{1}{2}}, \qquad (28)$$
$$\hat{s}_i^z = s-\hat{a}_i^+\hat{a}_i$$

where $\hat{s}_i^\pm = \hat{s}_i^x \pm i\hat{s}_i^y$ are cyclic spin operators. New operators $\hat{a}_i^+, \hat{a}_i$ are the operators of the creation and annihilation of spin deviation at *i*-th lattice site.

One can expand the operator expressions (28) in Taylor series

$$\hat{s}_i^+ = \sqrt{2s}\left(\hat{a}_i - \frac{\hat{a}_i^+\hat{a}_i\hat{a}_i}{4s}+...\right) \qquad (29)$$

and similar one for $\hat{s}_i^-$. The main assumption of the Holstein-Primakov theory is that the expansion (29) converges very rapidly and we can restrict ourselves with the first term only. Substituting now this expansion into (27) one gets for the Hamiltonian of the ferromagnet

$$\hat{H} = W_0 + \hat{H}^{(2)} + \hat{H}^{(3)} + \hat{H}^{(4)} + ... , \qquad (30)$$

where $W_0$ does not contain $\hat{a}_i^+, \hat{a}_i$ and $\hat{H}^{(2)}, \hat{H}^{(3)}, \hat{H}^{(4)}$ are forms of second, third and forth order in $\hat{a}_i^+, \hat{a}_i$. As the initial Hamiltonian (27) describes interaction between moments at different lattice sites, quadratic form $\hat{H}^{(2)}$ is not diagonal (contain terms $\sim \hat{a}_i^+\hat{a}_j$). A standard method to diagonalize such forms is the Fourier transformation, which allows one to pass from the operators $\hat{a}_i$ related to a single site *i* to new "collective" operators which belong to all sites simultaneously. Thus, the second transformation is

$$\hat{a}_i^+ = \frac{1}{\sqrt{N}}\sum_k \exp(-i\vec{k}\vec{r}_i)\hat{b}_k^+ \qquad \hat{a}_i = \frac{1}{\sqrt{N}}\sum_k \exp(i\vec{k}\vec{r}_i)\hat{b}_k \qquad (31)$$

Here $N$ is the number of lattice sites in the sample and $\vec{k}$ is the wave vector of the reciprocal lattice $\vec{k} = \frac{1}{\sqrt[3]{N}}\left(l\vec{e}_1 + m\vec{e}_2 + n\vec{e}_3\right)$ ($\vec{e}_i$ are vectors defining unit cell of the reciprocal lattice and $l, m, n = 0, \pm 1, .. \pm \frac{\sqrt[3]{N}}{2}$).

In new variables $\hat{b}_k$ quadratic term of the Hamiltonian has a form:

$$\begin{aligned}
&\hat{H}^{(2)} = \sum_k A_k \hat{b}_k^+ \hat{b}_k + \frac{1}{2}\sum_k \left(B_k \hat{b}_k \hat{b}_{-k} + B_k^* b_{-k}^+ b_k^+\right) \\
&A_k = \sum_l 2sJ(\vec{r}_l)\left[1 - \exp\left(-i\vec{k}\vec{r}_l\right)\right] + 2\mu_B H + 4\pi\mu_B M \sin^2\theta_k \\
&B_k = 4\pi\mu_B M \sin^2\theta_k \exp\left(-i2\varphi_k\right)
\end{aligned} \qquad (32)$$

with $M = 2\mu_B sN$ - saturation magnetization (magnetic moment of the unit volume).

Obtained Hamiltonian $\hat{H}^{(2)}$ is much simpler as that in (30), since each term in the sums contains only the operators corresponding to the same value of $|\vec{k}|$. However, for its diagonalization one should apply linear transformation, popularly known as Bogolubov *u-v* transformation $b_k = u_k c_k + v_k^* c_{-k}^+$, $b_k^+ = u_k^* c_k^+ + v_k c_{-k}$.
This will give $\hat{H}^{(2)} = \sum_k \varepsilon_k c_k^+ c_k$ with

$$\varepsilon_k = \sqrt{A_k^2 - |B_k|^2} \qquad (33)$$

representing the energy of the excitation. Detailed derivation of (33) can be found in [8] (Chp3), [29] (Chp5).

Thus, summarizing all above mentioned in terms of second quantization, one obtains, that the eigen-excitations of a ferromagnet are quasiparticles with energies $\varepsilon_k$ given by (33). These quasiparticles are called magnons.

From the point of view of the principle of wave-particle duality (e.g., [53]) there should be straight correspondence between magnons and spin waves. In fact, using $\varepsilon_k = \hbar\omega_k$ one obtains, that the spectrum of magnons (33) almost coincides with the dispersion of the spin waves (16). The only difference is in the form of the exchange

term $\varepsilon_{ex} = \sum_l 2sJ(r_l)\left[1 - \exp(-i\vec{k}\vec{r}_l)\right]$, which now contains microscopic parameters *s* and *J*. Since the exchange integral *J(r)* decreases quickly with the distance, it is reasonable for the calculation of $\varepsilon_{ex}$to take into account only nearest spins. For instance, in a simple cubic lattice each spin has 6 neighbors at distance *a* (size of the unit cell) and

$$\varepsilon_{ex} = \sum_l 2sJ(r_l)\left[1 - \exp(-i\vec{k}\vec{r}_l)\right] = 4sJ(a)(3 - \cos k_x a - \cos k_y a - \cos k_z a) \qquad (34)$$

In the long-wave-length limit ($ka << 1$) (34) reduces to $\varepsilon_{ex} = 4sJ(a)a^2k^2$, which coincides with the microscopic term if $q = \dfrac{4sJ(a)a^2}{\gamma M_0}$.

Thus, for $ka << 1$ the results of the microscopic and the continuum theory coincide. Detailed microscopic treatment results in the strong dependence of the energy of magnons on the direction of their wave vector $\vec{k}$ with respect to the axes of spin lattice (34) at large values. It is worth noting, whereas in the macroscopic approach values of wave vector are unlimited, in the microscopic theory they are defined only in the first Brillouin zone ($|k| \le \dfrac{\pi}{a}$).

### 2.7 Properties of magnons

As shown in the previous section, magnons are elementary excitations of the spin system of the ferromagnet. Consequently, any processes of the excitation, damping or propagation of the magnetization waves in ferromagnetic media can be regarded as a creation or annihilations of magnons or their flows. The energy and quasimomentum of a magnon is given by

$$\begin{aligned} \varepsilon &= \hbar\omega \\ p &= \hbar k \end{aligned} \qquad (35)$$

All "linear" properties of magnon are defined by the dispersion law $\varepsilon(p)$ or $\omega(k)$. For most relevant cases the classical expression for the spectrum can be used. By analogy with quasiparticles in semiconductor an effective mass $m_{eff} = \hbar^2 \left(\frac{d^2\varepsilon}{dk^2}\right)^{-1}$ can be attributed to magnons.

Other important properties of magnons can be obtained directly from the properties of the Holstein-Primakov transformations. Thus, for example, since the operators $\hat{a}_i$ introduced in the first transformation obey commutation relations for Bose operators, obtained by their means quasiparticles (magnons) are bosons. Besides, it can be shown (Chapter 4 in [8]) that for low excitation levels (or temperatures far below $T_c$) when $n_k = c_k^+ c_k \ll N$ and neglecting the dipole-dipole interaction it is valid

$$\mathcal{M}_z = MV - 2\mu_B \sum_k n_k , \quad (36)$$

where $MV = \mathcal{M} = 2\mu_B sN$ is the total magnetic moment of the sample. From (36) it follows that every magnon reduces the value of the $z$ projection of the magnetic moment by quantity $2\mu_B = \gamma\hbar$, in other words, each magnon carries the angular momentum $-\hbar$, i.e. the spin of the magnon is equal to 1.

Equating the energy of the certain spin wave in the macroscopic approximation with $n_k\varepsilon_k$ one can find the connection between the numbers of magnons and the dynamic magnetization amplitudes. For the case of circularly polarized spin waves $(\theta_k = 0)$ one gets:

$$\frac{n_k}{V} = \frac{m_{0k}^2}{2M_0\gamma\hbar}, \quad (37)$$

where $m_{0k} = \sqrt{m_{0kx}^2 + m_{0ky}^2}$. For waves with arbitrary value of $\theta_k$ (37) can be used for estimations.

### 2.8 Interaction of magnons

Beside the quadratic part $\hat{H}^{(2)}$, which determines the spectrum of magnons, the total Hamiltonian of the system includes terms of higher orders, which describe an interaction of magnons with each other [29]:

$$\begin{aligned}\hat{H}^{(3)} &= \sum_{k_1,k_2,k_3} \left(V_{12,3} c_{k_1} c_{k_2} c_{k_3}^{+} + H.c.\right)\delta(k_1 + k_2 - k_3), \\ \hat{H}^{(4)} &= \sum_{k_1,k_2,k_3,k_4} \left(T_{12,34} c_{k_1} c_{k_2} c_{k_3}^{+} c_{k_4}^{+} + H.c.\right)\delta(k_1 + k_2 - k_3 - k_4) + \\ &+ \sum_{k_1,k_2,k_3,k_4} \left(W_{123,4} c_{k_1} c_{k_2} c_{k_3} c_{k_4}^{+} + H.c.\right)\delta(k_1 - k_2 - k_3 - k_4)\end{aligned} \qquad (38)$$

Terms $\hat{H}^{(3)}$ and $\hat{H}^{(4)}$ in the microscopic magnetic Hamiltonian corresponds to the nonlinear terms of the second and third order in dynamic magnetization $\underset{\sim}{m}$ in the classical equation of motion of the magnetization (5), which arise when the condition of the conservation of the magnetic moment (21) is taken into account. However, the approach of the second quantization allows for the simple interpretation of these terms. The first term in $\hat{H}^{(3)}$ corresponds, obviously, to the annihilation of the magnons $c_{k_1}$ and $c_{k_2}$ with the simultaneous creation of the magnon $c_{k_3}^{+}$, i.e. describes a process of a confluence of two magnons into one. Correspondingly, the Hermitian conjugate term, designated as *H.c.*, depicts a splitting of a magnon into two quasiparticles. By analogy, Hamiltonian $\hat{H}^{(4)}$ describes processes of scattering of two magnons into other two magnons (first sum) and a confluence of three magnons into one along with the inverse splitting process (second sum). The presence of the $\delta$-function in (38) ensures the momentum (impulse) conservation law to be fulfilled in these processes.

Generally speaking, the probability of the many particle processes decreases when the number of interacting particles increases and one might restricts the consideration of the magnon interaction by $\hat{H}^{(3)}$ only. However, it appears that three-magnon processes are caused solely by the dipole-dipole interaction, the total spin of the magnetic system is not conserved by this process. The stronger exchange interaction preserves the total spin of the system and, therefore, can result only in four-magnon

interaction, in which two magnons are annihilated and two are created. Hence, the efficiency of the four-magnon processes can be comparable with that of the three-magnon ones and even dominate over them.

Similarly, parametric instability process can be represented as an interaction of quasiparticles. From this point of view the perpendicular pumping instability is a three magnon splitting process, in which a magnon of the uniform precession splits into two magnons with the half frequency. The corresponding Hamiltonian term is $\Delta\hat{H}^{(3)} = \sum_k V_{0,k,-k} c_0 c_k^+ c_{-k}^+$ . In the case of parallel pumping, additional term for Zeeman energy in the dynamic magnetic field of the pumping should be introduced into the total Hamiltonian $\hat{H}_Z = \sum_k \left( h_z e^{i\omega_p t} V_k c_k^+ c_{-k}^+ + H.c. \right)$, which describes the annihilation of the photon of the electromagnetic pumping with the simultaneous creation of two magnons.

### 2.9 Thermodynamics of magnons

The minimum of the magnetic energy of the Heisenberg ferromagnet corresponds to the ground state with all spins being parallel to each other and aligned along the direction of the external magnetic field. However, at any temperature $T > 0$ there are deviations from the ground state due to the thermal fluctuations. From the point of view of the second quantization method, described above, this deviations can be represented as a gas of magnons, which are in thermal equilibrium with the other (non magnetic) systems of the crystal, first of all with the lattice (phonons). They are often called thermal magnons. The properties of the magnon gas are determined by the dispersion law of magnons and their statistics and influence the thermodynamic properties of ferromagnets. In particular, thermal magnons determine the character of the temperature dependence of magnetization $M\ (T)$ .

Since magnons are bosons, the average number of magnons in the quantum state $k$ in thermal equilibrium at temperature $T$ is given by the Bose-Einstein distribution

$$n_k = \frac{1}{\exp(\frac{\varepsilon_k - \mu}{\kappa T}) - 1}, \qquad (39)$$

where $\varepsilon_k$ is the energy in the *k* state, given by the dispersion law, $\kappa$ is the Boltzmann constant and $\mu$ is the chemical potential. If the total number of particles in the system is not fixed, the chemical potential $\mu$ is to be set to zero. This is the case of magnons at the thermal equilibrium with the lattice since their number can change due to their interaction with phonons. Hence, for magnons the distribution function with $\mu = 0$ should be used (it is also called Plank's distribution, since it was first derived by Plank for other quasiparticles – photons at thermal equilibrium with the black body).

Since every particular magnons carries spin $-\hbar$ the magnetic moment of the ferromagnet at a finite temperature *T* can be written as

$$M(T)V = M(0)V - \gamma\hbar\sum_k n_k = M(0)V - \gamma\hbar\sum_k \frac{1}{\exp(\frac{\varepsilon_k}{\kappa T}) - 1}, \qquad (40)$$

where the first term (*M(0)*) is the magnetization at *T*=0 and the second one represents the contribution of the thermal magnons (summation is carried out over the all *N* sites of the reciprocal lattice). Replacing the sum with the integral over the *k*-space ( $\sum_k = \frac{1}{\Delta k}\int_k d^3k = \frac{V}{(2\pi)^3}\int_k d^3k$ ) one gets [47]:

$$\begin{aligned}
M(0) - M(T) &= \frac{\gamma\hbar}{(2\pi)^3}\int_k \frac{d^3k}{\exp(\frac{\hbar\omega(k)}{\kappa T}) - 1} = \left|\omega \approx \omega_H + \gamma q M_0 k^2\right| = \\
&= \int_{\omega_H}^{\infty} d\omega \frac{1}{4\pi^2}\sqrt{\frac{\omega - \omega_H}{\gamma q M_0}}\frac{1}{\exp\left(\frac{\hbar\omega}{\kappa T}\right) - 1} = \left|\begin{matrix} z = \frac{\hbar(\omega - \omega_H)}{\kappa T} \\ \omega = \omega_H + z\frac{\kappa T}{\hbar} \end{matrix}\right| = \\
&= \frac{\kappa T}{4\pi^2\hbar}\sqrt{\frac{\kappa T}{\hbar\gamma q M_0}}\int_0^{\infty} \frac{dz\sqrt{z}}{\exp(\frac{\hbar\omega_H}{\kappa T})\exp(z) - 1} = \\
&= \frac{\gamma\hbar}{\sqrt{2}}\left(\frac{\kappa T}{2\pi\hbar\gamma q M_0}\right)^{3/2} \mathrm{Li}_{3/2}\left(e^{-\frac{\hbar\omega_{\min}}{\kappa T}}\right) \approx \alpha T^{3/2}
\end{aligned}, \qquad (41)$$

which is the well-known $T^{3/2}$ law first obtained by Bloch [1].

In a similar manner the contribution of the thermal magnons into the heat capacity of the ferromagnet can be calculated

$$(c_V)_{mag} = \frac{\partial U_{mag}}{\partial T} = \frac{\partial}{\partial T}\left(\sum_k \varepsilon_k n_k\right) = \beta T^{3/2} \qquad (42)$$

In temperature range $T < T_D^2 / T_C$ ($T_D$ – Debye temperature) magnon heat capacity appears to be higher than that of the phonons and determines the properties of the ferromagnet.

### 2.10 Ferromagnetic relaxation processes

For the detailed theoretical investigation of the ferromagnetic relaxation processes microscopic approach using concept of magnons appears to be very convenient. In this approach a magnetic excitations of a ferromagnetic insulator (free electrons are neglected) is represented as a gas of weekly interacting quasiparticles. Beside the interaction of magnons with each other (described by Hamiltonian terms of order higher then two), they are also coupled to the lattice, which is often treated as a phonon bath. In a thermal equilibrium state both, magnon and phonon gases are described by Bose-Einstein distribution $n_k^0 = \left(\exp\left(\frac{\varepsilon_k - \mu}{\kappa T}\right) - 1\right)^{-1}$ with $\mu_m = \mu_p = 0$ and $T_m = T_p$. An excitation of a certain spin wave with the wave vector $\vec{k}$ means that the corresponding occupation number $n_k$ exceeds the equilibrium value $n_k^0$. Accordingly, the relaxation reflects the tendency of the system to reduce the occupation number $n_k$ to the equilibrium level $n_k^0$, resulting in transfer of the energy brought into the system by the excitation of mode $\vec{k}$ finally to the bath (lattice). For the correct description of the relaxation all processes which can change the occupation numbers of excited magnons should be taken into account. Generally, these are divided into two parts: inherent or magnon-magnon processes and spin-lattice (magnon-phonon) processes.

Magnon-magnon processes describe energy redistribution within the magnetic system of the crystal. Beside three- and four-magnon scattering processes (which are described by the magnetic Hamiltonian terms $H^{(3)}$ and $H^{(4)}$) two-magnon process is also considered in the theory of ferromagnetic relaxation. They stand for the scattering of magnons on the nonuniformities of the sample, which is accompanied by the change of a wave vector of magnons. As a result of this process a magnon with a frequency $\omega_1$ and a wave vector $\vec{k}_1$ is annihilated and another magnon with the

frequency $\omega_2 = \omega_1$ and the wave vector $\vec{k}_2 \neq \vec{k}_1$ is created. However, these processes plays important role only for the relaxation of the long-wavelength excitation with $k \approx 0$.

Spin-lattice relaxation describes the energy transfer from the magnetic system into the lattice through the elementary scattering processes involving both magnons and phonons. These are the processes of the radiation or absorption of a phonon by magnon and a confluence of two magnons into a phonon.

Each of the above mentioned scattering process can be characterized by the magnon life time $\tau_i$ with respect to this process. At that the total magnon life time τ is determined as $1/\tau = \sum_i 1/\tau_i$. For the calculation of the individual characteristic lifetimes $\tau_i$ a technique of transition probabilities is often used. Any scattering process means annihilation and creation of quasiparticles in certain states, which in the second quantization representation corresponds to the transition of the system from one quantum state to another. Treating the interaction of magnons, which cause the scattering, as a perturbation of the main quadratic Hamiltonian $H^{(2)} = \sum_k \hbar\omega_k c_k^+ c_k$ one can use the quantum mechanics perturbation theory [53] for the calculation of the probability of the elementary scattering process:

$$w_{lm} = \frac{2\pi}{\hbar} \left| \left\langle m \left| H_p \right| l \right\rangle \right|^2 \delta(\varepsilon_l - \varepsilon_m) \qquad (43)$$

Here $\left\langle m \left| H_p \right| l \right\rangle$ is the matrix element of the Hamiltonian term responsible for the transition between quantum states $l$ and $m$ with corresponding energies $\varepsilon_l$ and $\varepsilon_m$. Performing a summation over all possible scattering processes of a certain type, in which the number of magnons $n_k$ in the state $\vec{k}$ can be changed, one obtained total probability

$$w_\Sigma = \frac{dn_k}{dt} = L\left\{n_{k_i}\right\}, \qquad (44)$$

$L\left\{n_{k_i}\right\}$ is the collision integral, which depends on the occupation numbers $n_{k_i}$ of all quasiparticles (magnons or phonons) involved in the scattering process. For the equilibrium case, when $n_{k_i} = n_{k_i}^0$ (given by Bose Einstein distribution), $L\left\{n_{k_i}^0\right\} = 0$.

When, however, magnon mode $\vec{k}$ is excited $n_k = n_k^0 + \delta n_k$, and in the linear approximation on $\delta n_k$ ($|\delta n_k| << n_k$) collision integral can be represented in the following form:

$$\frac{dn_k}{dt} = \frac{d(\delta n_k)}{dt} = L\left\{n_{k_i}\right\} = \frac{\delta n_k}{\tau_k}, \quad (45)$$

where $\tau_k$ is a life time of magnons $\vec{k}$ with respect to the processes included in the collision integral (the so-called $\tau$-approximation). The occupation numbers of all other quasiparticles, involved in these processes are assumed to be equal to its equilibrium value.

The relaxation times of magnon-magnon processes is always smaller than of magnon-phonon ones, since the former is usually determined by the exchange interaction, whereas the latter is mainly due to the relativistic spin-orbit coupling. Thus, the relaxation of magnetic excitations occurs in a following way: on the first stage the excited magnons is redistributed over the magnetic system of the crystal by means of relatively fast three- and four-magnon scattering on thermal magnons in a way that a Bose-Einstein distribution is settled. However this distribution appears to be not equilibrium but quasi-equilibrium, since after this step of the relaxation the temperature and the chemical potential of the magnon gas, in general case, differs from that of the phonons. The true equilibrium state is achieved by means of slower magnon-phonon relaxation, which provides the energy and magnetic moment transfer from the spin system into the lattice, resulting in $T_m = T_p$ and $\mu_m = \mu_p = 0$.

A contribution of three- and four-magnon processes to the relaxation of a certain magnons with wave vector $\vec{k}$ appears also to be of different magnitude. First of all, three-magnon processes are caused by the weaker dipole-dipole interaction. Second, the simultaneous fulfillment of the energy and momentum conservation laws ($\vec{k} \pm \vec{k}_1 - \vec{k}_2 = 0, \omega_k \pm \omega_1 - \omega_2 = 0$ with $\pm$ standing for confluence and splitting correspondingly) is required for the scattering process. The peculiarities of the magnon spectrum (presence of a gap and quadratic anisotropic dependence on wave vector) make three-magnon processes to be often forbidden or allowed only in a narrow region of values of wave vectors $\vec{k}_2, \vec{k}_3$, resulting in small probabilities of this

processes. On the contrary, the conservation laws for the four-magnon processes are easier to fulfill and they allow for the participation of magnons from different spectral regions. Therefore, in a wide spectral and temperature range, four-magnon processes are dominant and determines the relaxation of magnetic excitations.

### 2.11 Interaction of magnons with light

When passing through a solid, light can interact with it and gain energy from or pass it to the system. These processes are regarded as inelastic scattering. In a quantum mechanical treatment inelastic light scattering is a process when the medium absorbs a photon and radiates a photon of a different energy, thereby passing into a new quantum state. As a result, a quasiparticle, which characterizes the energy of the medium in the second quantization approach, is annihilated or created. For the case of interaction of the light with the magnetic system this quasiparticles are magnons. Historically the scattering from high-frequency (>300 GHz) optical phonons is called Raman scattering, whereas the scattering from low-frequency acoustic phonons and magnons is called Brillouin scattering.

The energy and the wave vector of the absorbed and the radiated photon are uniquely connected with those of the magnon by the laws of the energy and momentum conservation:

$$\begin{aligned} \hbar\omega_S &= \hbar\omega_I \pm \hbar\omega_m \\ \vec{k}_S &= \vec{k}_I \pm \vec{k}_m \end{aligned} \qquad (46)$$

Indices $S$ and $I$ correspond to the scattered and incident photon and $m$ – to the magnon. The upper sign means that the magnon is annihilated (anti-Stokes frequency shift) in the scattering process and the lower one corresponds to the creation of the magnon (Stokes frequency shift). Both processes are further illustrated in Fig. 6.

The microscopic origin of the inelastic light scattering on magnons is the spin-orbit and exchange interaction. First detailed microscopic description of the above mechanism was given in [55, 56].

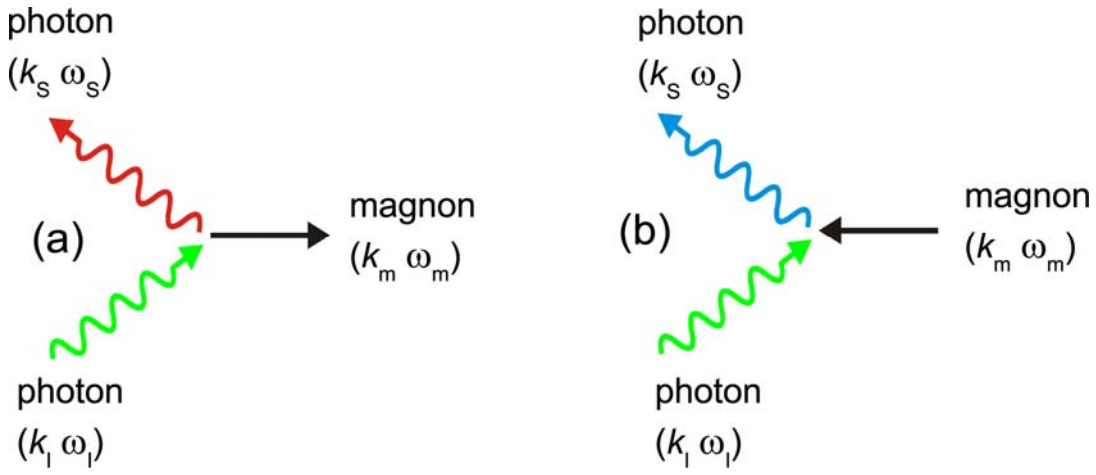


**Figure 6.** Illustration of Brillouin scattering process; panels (a), (b) corresponds to the Stokes $((k_S,\omega_S)=(k_I-k_m,\omega_I-\omega_m))$ and anti-Stokes $((k_S,\omega_S)=(k_I+k_m,\omega_I+\omega_m))$ frequency shift respectively.

From the classical point of view magnetic system of a magnetically ordered crystal can affect the light, propagating in it, which is regarded as a magneto-optic effect (e.g. [57]). It is usually described by the introduction of the additional term $\vec{\vec{\varepsilon}}^{(m)}=\Delta\varepsilon_{\alpha\beta}$ into the permittivity tensor $\vec{\vec{\varepsilon}}$ of the crystal. This magnetic contribution to the total permittivity can be represented as a series in the powers of the magnetization vector $\vec{M}$

$$\Delta\varepsilon_{ik}=\sum_{\gamma}f_{\alpha\beta\gamma}M_{\gamma}+\sum_{\gamma\delta}g_{\alpha\beta\gamma\delta}M_{\gamma}M_{\delta}+\ldots \qquad (47)$$

($i,k,l,m=x,z,y$). The tensors $\vec{\vec{f}}$ and $\vec{\vec{g}}$ are, in general case, complex and represent magneto-optic effects ($\vec{\vec{f}}$ describes circular birefringence (Faraday effect) and linear dichroism, $\vec{\vec{g}}$ - linear birefringence and circular dichroism). The presence of a spin wave with dynamic magnetization $\vec{m}\sim e^{j(\omega_m t-\vec{k}_m\vec{r})}$ results in the modulation of the permittivity tensor components $\Delta\varepsilon_{\alpha\beta}$. Physically this means the creation of the phase grating, which has spatial period determined by $\vec{k}_m$ and propagates with the phase velocity of the spin wave ($\omega_m/k_m$). The propagating light is then scattered by the grating and changes its direction (wave vector) due to the Bragg diffraction and the frequency due to the Doppler effect in accordance with (46).

For the quantitative characterization of the scattering process the differential light scattering cross section is used. It is the ratio of the intensity of the light, scattered into an elementary solid angle $d\Omega$ with the scattered frequency between $\omega_s$ and $\omega_s + d\omega_s$ per unit time and volume to the intensity density of the incident light [58]

$$\frac{d^2h}{d\Omega d\omega_s} = \frac{\omega_I \omega_S^3 \tilde{n}_2}{c^4 \tilde{n}_1} \sum_{\alpha\beta\alpha'\beta'} e_I^{\alpha} e_I^{\beta} \left\langle (\delta\varepsilon_{\alpha\beta})^* \delta\varepsilon_{\alpha'\beta'} \right\rangle_{k_I - k_S, \omega_I - \omega_S} e_S^{\alpha'} e_S^{\beta'} \tag{48}$$

Here $\tilde{n}_{1,2}$ - refractive index at frequencies $\omega_{I,S}$ respectively, $c$ is the velocity of light in vacuo and $e_{I,S}^{\alpha}$ - components of unit vector of polarization of the incident and scattered light. $\delta\varepsilon_{\alpha\beta}$ is dynamic (fluctuating) component of $\Delta\varepsilon_{\alpha\beta}$ caused by the dynamic magnetization of spin waves and $\left\langle (\delta\varepsilon_{\alpha\beta})^* \delta\varepsilon_{\alpha'\beta'} \right\rangle_{k,\omega}$ is Fourier component of the correlation function of this dynamic component of dielectric permittivity

$$\left\langle \delta\varepsilon^* \delta\varepsilon \right\rangle_{k,\omega} = \iint d(t_2 - t_1) d^3(\vec{r}_2 - \vec{r}_1) \exp\left[ i\omega(t_2 - t_1) - i\vec{k}(\vec{r}_2 - \vec{r}_1) \right] \times \\ \times \left\langle \left[ \delta\varepsilon(\vec{r}_1, t_1) \right]^* \delta\varepsilon(\vec{r}_2, t_2) \right\rangle, \tag{49}$$

where $\langle ... \rangle$ denotes statistical averaging. From (47) it follows that $\left\langle \delta\varepsilon^*(\vec{r}_1, t_1) \delta\varepsilon(\vec{r}_2, t_2) \right\rangle \propto \left\langle m^*(\vec{r}_1, t_1) m(\vec{r}_2, t_2) \right\rangle$ and, therefore, the problem of the calculation of the differential scattering cross section is reduced to the calculation of the correlation functions of the magnetization components. For the scattering on thermal magnons, one obtains [59]:

$$\left( \frac{d^2h}{d\Omega d\omega_s} \right)_{Stokes} = \frac{\hbar\gamma M_0 \omega_I \omega_S^3 \tilde{n}_2}{2\pi c^4 \tilde{n}_1} \left| A^- \right|^2 (n_m + 1) \delta(\omega_I - \omega_S - \omega_m) \\ \left( \frac{d^2h}{d\Omega d\omega_s} \right)_{anti-Stokes} = \frac{\hbar\gamma M_0 \omega_I \omega_S^3 \tilde{n}_2}{2\pi c^4 \tilde{n}_1} \left| A^+ \right|^2 n_m \delta(\omega_I - \omega_S + \omega_m) \tag{50}$$

where $n_m$ is the thermal magnon population factor, given by Bose-Einstein distribution and $A^{\pm}$ are functions accounting for the peculiarities of the magneto-optic effects

containing the coefficients $f_{\alpha\beta\gamma}$ and $g_{\alpha\beta\gamma\delta}$ of the expansion (47) and depending on the polarization of the incident and scattered light.

An important feature of the light scattering on magnons is that in most practical experimental situations the process of scattering is accompanied by the rotation of the polarization of the scattered light by 90° since the non-diagonal terms of the tensors $f_{\alpha\beta\gamma}$ and $g_{\alpha\beta\gamma\delta}$ dominate over the diagonal terms.

Finally, it is worth noting, that the momentum conservation law (46) $\vec{k}_S = \vec{k}_I \pm \vec{k}_m$ for the wave vectors of the incident and scattered light is a consequence of the translational invariance of the scattering media. If the scattering volume has finite thickness (sample of a slab shape, or a flat surface of the absorptive media resulting in the finite penetration depth of the light) the conservation condition (46) is fulfilled only for the in-plane component of the wave vector $\vec{k}_{\|}$ parallel to the surface $\vec{k}_{S\|} = \vec{k}_{I\|} \pm \vec{k}_{m\|}$. The value of the wave vector component perpendicular to the surface $\vec{k}_{\perp}$ appears to be not well defined (the uncertainty $\Delta k_{\perp} \sim \frac{2\pi}{\xi}$ with $\xi$ being the size of the confinement region). The specifics of the light scattering in ferromagnetic films have been addressed in [9, 10, 60-63].

### 2.12 Bose-Einstein condensation

From the quantum statistical point of view all particles are divided into bosons and fermions. The latter obey the Pauli exclusion principle: only one fermion can be found in any quantum state. On the contrary, the number of bosons in single quantum state is unlimited. Moreover, due to the indistinguishability of the elementary particles, statistical probability of the processes involving boson transition between different quantum states appear to be proportional to the number of bosons in the final state. In other words, the more bosons are in the certain quantum state the higher is the probability for other boson to be scattered into this state, i.e. bosons trend to gather themselves.

The characteristic properties of bosons and fermions are reflected in their statistics. For bosons it is the already mentioned Bose-Einstein distribution function

$$n_k = \frac{1}{\exp(\frac{\varepsilon_k - \mu}{\kappa T}) - 1} \qquad (51)$$

Here $n_k$ is an average number of bosons in the state $k$ with energy $\varepsilon_k$, $T$ is the temperature, $\kappa$ - Boltzmann constant and $\mu$ - chemical potential. For the systems with fixed number of bosons the chemical potential $\mu$ arises from the additional condition

$$\sum_k n_k = N = const \qquad (52)$$

and, in a certain sense, it is a parameter, which characterizes the number of the particles in a system. From the thermodynamic point of view, the chemical potential represents the change of the energy of the system (strictly speaking, one of the thermodynamical energy potentials, which is minimized in equilibrium state at a given conditions) when the number of particles is changed.

$$\mu = \left(\frac{\partial U}{\partial N}\right)_{S,V} = \left(\frac{\partial F}{\partial N}\right)_{T,V} = \left(\frac{\partial H}{\partial N}\right)_{S,p} = \left(\frac{\partial G}{\partial N}\right)_{T,p} \qquad (53)$$

Thus, if the number of bosons is not fixed (which applies to qasiparticles), the corresponding thermodynamical potential can be minimized by varying *N*. As a result, at the true thermodynamic equilibrium the chemical potential $\mu = 0$.

From (51) it is obvious, that for bosons $\mu$ cannot be larger than the minimum energy in the system $\mu < \varepsilon_{\min}$, otherwise one would obtain negative population for the state with $\varepsilon_k < \mu$.

When considering physically relevant problem of a gas of elementary particles, the continuous distribution over the energies (spectral distribution) instead of discrete (51) is often used. For that, the transition to the distribution in *k*-space is first made:

$$dn_k = n_k d\tau = \frac{V}{(2\pi)^3} \frac{d^3k}{\exp(\frac{\varepsilon_k - \mu}{\kappa T}) - 1}, \qquad (54)$$

where $d\tau = \frac{V}{(2\pi)^3} d^3k$ is a number of states in the element of the phase volume $d^3k$.

The energy of an elementary particle in general case can be represented as a sum of the potential and the kinetic energies:

$$\varepsilon = \varepsilon_0 + \frac{p^2}{2m} = \varepsilon_0 + \frac{\hbar^2 k^2}{2m} \qquad (55)$$

Since for an isotropic system $\varepsilon$ depends only on $k = |\vec{k}|$, one can pass to the distribution over the absolute value of the wave vector in spherical coordinate system for $\vec{k}$ ($d^3k \to \iint\limits_{\theta,\varphi} k^2 \sin\theta dk d\theta d\varphi = 4\pi k^2 dk$) and further, using (55) to the energy distribution

$$dN_\varepsilon = \frac{Vm^{3/2}}{\sqrt{2}\pi^2\hbar^3} \frac{\sqrt{\varepsilon - \varepsilon_0}\, d\varepsilon}{\exp(\frac{\varepsilon - \mu}{\kappa T}) - 1} \qquad (56)$$

Here $dN_\varepsilon$ is the number of particles having energy within the interval $\varepsilon \div \varepsilon + d\varepsilon$. The equation (56) is often written in the form $dN_\varepsilon = D(\varepsilon) n_\varepsilon d\varepsilon$, where $D(\varepsilon) = \frac{Vm^{3/2}\sqrt{\varepsilon - \varepsilon_0}}{\sqrt{2}\pi^2\hbar^3}$ is the density of the states (number of states within the energy interval $d\varepsilon$) and $n_\varepsilon$ is the Bose-Einstein occupation function (51). The normalization condition (52) now can be rewritten as

$$N = \int\limits_{\varepsilon_{\min}}^{\infty} dN_\varepsilon = \frac{Vm^{3/2}}{\sqrt{2}\pi^2\hbar^3} \int\limits_{\varepsilon_0}^{\infty} \frac{\sqrt{\varepsilon - \varepsilon_0}\, d\varepsilon}{\exp(\frac{\varepsilon - \mu}{\kappa T}) - 1} = N(\mu, T) \qquad (57)$$

From (54) it follows that the chemical potential $\mu$ grows with increasing number of particles *N*. At the same time, $\mu$ cannot be larger than the minimal energy $\varepsilon_{\min} = \varepsilon_0$.

In other words, at a given temperature $T$, there is a critical number of particles (concentration), which can be in the system, given by (54) with $\mu = \varepsilon_0$

$$\frac{N_c(T)}{V} = \frac{m^{3/2}}{\sqrt{2}\pi^2\hbar^3}\int_{\varepsilon_0}^{\infty}\frac{\sqrt{\varepsilon-\varepsilon_0}\,d\varepsilon}{\exp(\frac{\varepsilon-\varepsilon_0}{\kappa T})-1} = \frac{(m\kappa T)^{3/2}}{\sqrt{2}\pi^2\hbar^3}\int_0^{\infty}\frac{\sqrt{x}dx}{e^x-1} = \frac{1}{\sqrt{2}}\left(\frac{m\kappa T}{2\pi\hbar^2}\right)^{3/2}\varsigma\left(\frac{3}{2}\right) \quad (58)$$

At $N > N_c$ there is no physically relevant solution ( $\mu < \varepsilon_0$ ) of (57) although there are also no apparent physical restrictions on the existence of a system with $N > N_c$. The solution of this problem is based on the fact that the normalization condition in integral form (57) turns out not to represent the original summation over the discrete states (51) correctly. In fact, the particles, which are in the state with minimal energy $\varepsilon = \varepsilon_{\min}$, are not taken into account in the integral (57) since the density of the states $D(\varepsilon = \varepsilon_{\min}) = 0$ and, hence, the occupation function $n_{\varepsilon_{\min}}$ is multiplied by zero. At the same time, the number of particles in this lowest state can be arbitrary large at $\mu \to \varepsilon_{\min}$ . Thus, the following picture is actually observed: $N_c$ particles are distributed over the states with $\varepsilon > \varepsilon_{\min}$ according to integral distribution (56) with $\mu = \varepsilon_{\min}$ and other $N_0 = N - N_c$ particles occupy the lowest energy state.

Similar argumentation can be used for the system with the fixed number of particles *N=const* but with its temperature being changed. As $T$ is decreased, the chemical potential $\mu$ increases. It approaches its maximum value $\mu = \varepsilon_{\min}$ at non-zero critical temperature $T_c$. Equating (58) with respect to the temperature one gets

$$T_c = 3.31\frac{\hbar^2}{m\kappa}\left(\frac{N}{V}\right)^{2/3} \quad (59)$$

As $T$ is further decreased ( $T < T_c$ ) the integral (57) decreases ( $\int_{\varepsilon_{\min}}^{\infty} dN_\varepsilon(T) < N$ ) i.e. the states with $\varepsilon > \varepsilon_{\min}$ are no more able to accommodate all the particles. Only $N(T/T_c)^{3/2}$ of them occupy these states, whereas the rest $N_0 = N\left[1-(T/T_c)^{3/2}\right]$ are found in the state with the minimal energy.

The effect of accumulation of the macroscopic part of the particles in the lowest energy state is called Bose-Einstein condensation (BEC). It was theoretically predicted by Einstein in 1925 [64]. Actually, BEC implies something more than simple build-up of the population of the lowest state. In fact, according to the statistical distribution (51), the number of particles in this state is always higher than in any of the other. But at $N > N_c$ or, what is equivalent, $T < T_c$ the population is so high, that these particles start to "feel" each other, namely the correlation between the wave functions of the individual particles arises and they become coherent. The collective state of the particles described by the single wave functions (Bose-Einstein condensate) is formed.

For a long time, superfluids and superconductors (see e.g. [65]) were considered the only physical systems were effect of BEC had been observed. However, due to large density of the particles in these systems the condensation process is strongly affected by the interaction of the particles. Recently BEC was experimentally observed for the dilute gases of various atoms [66] and for different quasiparticles [22-25, 67-69]. In both cases some specific aspects can be pointed out.

The density of the atomic gases is limited by the condensation in real space (at small interparticle distances atoms are attracted to each other, they can build a liquid phase). Therefore, the following scenario of Bose-Einstein transition is realized in the experiments with atomic gases: the gas with a given number of particles is cooled until its temperature goes down below the critical value $T_c$ (determined by its concentration). For the dilute atomic gases characteristic densities achieved in the experiments are in the range $10^{13}$-$10^{15}$ cm$^{-3}$, which corresponds to the temperatures from 100 nK to a few μK. Such temperatures require complicated cooling procedure along with the extreme thermal isolation involving implementation of different experimental techniques: laser and evaporative cooling and magnetic and optical trapping [66].

On the contrary, quasiparticles can be easily excited in solids by external pumping and restrictions on their density are not as tight as for atoms. Therefore, to observe BEC in such systems, an external source is applied to the sample at a given temperature and the concentration of the particles is increased until $N > N_c(T)$ is fulfilled. Moreover, effective masses of electronic excitations are comparable with the mass of an electron (i.e. is much smaller than mass of the atoms), which also favours

the observations of BEC in these systems at reasonable temperatures. However, quasiparticles in solids have finite lifetime due to their interaction with the lattice, i.e. their numbers are conserved only at a certain time scale. Therefore the necessary condition for the observation of BEC of quasiparticles is that their lifetime is much longer than the time they need to scatter with each other [70, 71]. The latter determines how fast the quasi-equilibrium in the system will be achieved when the number of particles is increased, i.e. the time needed for BEC to occur. In fact, cold trapped atoms in atomic BEC experiments also have effective lifetime (due to heating effects and three-body interactions) but in the recent experiments it is up to two orders of magnitude larger than their scattering time and, therefore, does not prevent condensation.

# Chapter 3

# Experimental methods

## 3.1 Epitaxial yttrium iron garnet films

The main objective of the given work is to investigate experimentally kinetic processes in excited magnon gas, in particular from the point of view of possible observation of quasi-equilibrium Bose-Einstein condensation under conditions of quasi-equilibrium in the magnetic subsystem. This implies certain natural requirements to the material of the samples, which can be used in the experiments. First, the material should possess as low as possible spin lattice relaxation rates, determining how long the excited magnons remains within the magnetic system before decaying. In other words one needs a magnetic material with long lifetimes of magnons. Second, as mentioned in the theoretical part, the important parameter for a possibility of quasi-equilibrium in the subsystem of quasiparticles is not the lifetime of the quasiparticles itself, but rather the ratio between the latter and the time quasiparticles need for the thermalization [70, 71]. Thus, the desired material should be also characterized by high magnon-magnon interaction rates, i.e. high nonlinearity at reasonable pumping powers. The material, which fits the above requirements most, is the yttrium iron garnet $Y_3Fe_5O_{12}$ (YIG). It has the narrowest known line of ferromagnetic resonance ($\Delta H_0$=0.5 Oe) (corresponding to a long lifetime of magnons). Due to these unique properties of YIG it is widely used in such applications as high $Q$ microwave oscillators, generators and other [72]. Besides, a long lifetime of magnons results in a low thresholds of different nonlinear processes, including parametric pumping and four-magnon scattering [6, 7].

YIG is 20 sublattices cubic ferrimagnet with rather large unit cell of a size $a_{YIG}$=12.376 Å and magnetic moment 10$\mu_B$. Its Curie temperature $T_C$=560 K enables applications at room temperature. Detailed description of magnetic properties of YIG can be found in [72, 73]. Main of them, relevant for the current investigation are, obviously, the magnon-phonon relaxation time $\tau_{mp}$, which is of order of 0.5 $\mu$s for room temperature and magnon-magnon interaction time $\tau_{mm}$ which is at usual conditions one order of the magnitude smaller. Strictly speaking, in addition to quasi-

ferromagnetic modes (all sublattices precess in-phase) YIG possess many modes, where different sublattices precess out-of-phase). However, due to the strong exchange interaction between the sublattices the latter modes have their frequencies at much higher frequencies than 2-10 GHz used in these experiments. Therefore, one can consider YIG as a simple ferromagnet in this frequency interval.

The wide use of YIG for industrial applications and experimental physics became possible after the process of almost perfect growth of single crystals was developed [74, 75]. However, for some applications (delay lines, memory applications) thin film samples are preferable. These are produced by the liquid phase epitaxy (LPE) technique [76-78], involving high temperature solution growth of the films on gallium gadolinium garnet (GGG) substrates with a mixture of PbO and $B_2O_3$ as a solvent. The LPE technique provides supreme control over the film composition allowing for growth of the samples with extremely low concentration of impurities. At the same time lattice constant of GGG crystals ($a_{GGG}$=12.383 Å) is very close to those of YIG (the misfit is about $6\times10^{-4}$), allowing, therefore, for the production of high quality defect free films without elastic stress [79].

Early optical measurements on YIG [59, 80] has shown, that besides outstanding magnetic properties, YIG is also characterized by rather strong magneto-optic coupling which enables investigation of magnons in YIG by optical methods. Faraday rotation method [81], magnetooptical Bragg diffraction method [82] and Brillouin light scattering technique [10] was successfully applied for the investigation of spin waves in YIG. Due to its high informativity, the latter has become a main experimental technique for these studies. Utilization of thin film samples allows for the investigation of long wavelength spin waves in forward scattering geometry, at which light passes through the sample.

For the current experiments monocrystalline epitaxial YIG films grown on substrates of GGG are used. The films are grown in a way, that the direction along its normal corresponds to the <111> crystallographic axis. All films have a thickness of 5.1 μm and differ in lateral dimensions. Samples are characterized by saturation magnetization $4\pi M_0$=1750 G, exchange constant $\alpha=3\times10^{-12}$ cm$^2$ and negligible pinning of spins at the surfaces (unpinned surface spins).

### 3.2 Microwave excitation and detection of magnons

For the excitation and detection of the spin waves in ferrite films thin metal conductors at the surface of the film are usually used. Normally, these are microstrip line structures with the film being placed on top of it. A conventional structure, used for the excitation of spin waves in ferrite films is shown in Fig. 7 The microwave magnetic field created by the current flowing in the antenna acts on the magnetization of the film and excites magnons. From theoretical analysis of linear spin wave excitation by a given current it follows that the amplitude of the wave with a certain $\vec{k}$ is proportional to the $k$-th space Fourier harmonic of the current [47]. This, in particular, means that the maximum value of the wave vector of the spin wave, which can be effectively excited by the antenna with the width $w$ is $k \sim \frac{\pi}{2w}$. For the typical values of $w \geq 10$ $\mu$m this gives $k \leq 10^3$ cm$^{-1}$ resulting in the natural limitation on the application of this technique by the range of dipolar spin waves only.

On the other hand, under the condition of nonlinear excitation by parametric pumping the only restriction on the wave vectors of the excited spin waves is that their sum should be equal to the wave vector of the pumping field $\vec{k}_1 + \vec{k}_2 = \vec{k}_p$,

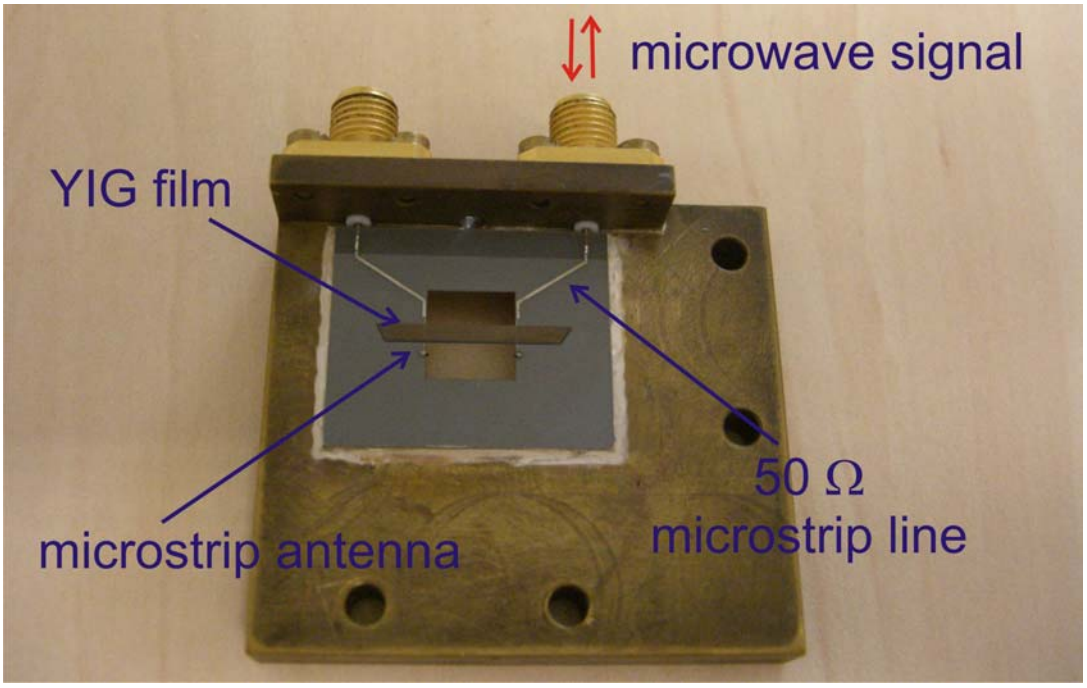


**Figure 7.** Conventional structure with a planar microstrip antenna used for the excitation and detection of spin waves in ferromagnetic films.

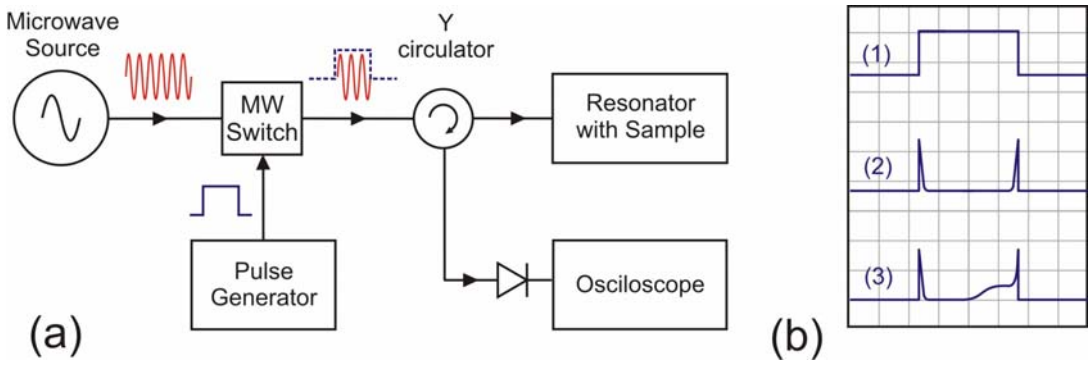


**Figure 8.** (a) Typical experimental setup for the parametric excitation of spin waves. (b) Oscillograms of microwave pulses: (1) incident pulse; (2) pulse, reflected from resonator below the threshold of parametric excitation; (3) reflected pulse, above the threshold.

allowing, therefore, excitation of exchange-dominated spin waves with large wave vectors. For practical realization of parametric excitation of spin waves microwave resonators are normally used to create the intense pumping field which is higher than the threshold of the parametric process. A sketch of the typical experimental setup for the parametric excitation of spin waves is shown in Fig. 8. The experiments are usually carried out in pulse regime (to avoid the thermal overheating of the sample). Microwave signal from the generator is modulated by the switch and applied to the resonator. The latter is matched with the transmission line, so when the frequency of the signal is equal to the resonant frequency of the resonator almost all power is absorbed by it and the reflected signal close to zero is observed on the oscilloscope (Fig. 8(b)). However, this is valid only for the low power levels up to the threshold value. When the magnetic field of the resonator inside the sample reaches the threshold, additional losses arise due to the energy transfer to the parametrically excited spin waves and the quality factor $Q$ of the system resonator/sample decreases, which, in turn, affects the coefficient of reflection from the resonator. This can be indicated by the appearance of a specific kink at the end of the reflected pulse envelope (Fig. 8(b)).

In classical pumping experiments samples are placed inside cavity resonators. This hampers investigation of the pumped magnons by other techniques. To allow application of optical techniques, open resonant systems are used. These are open dielectric resonators [83] or microstrip resonators [84]. In all cases sample is placed in an immediate proximity to the resonator, to provide the maximum of the pumping field created by the resonator inside the sample.

Above described parametric excitation is a main technique for experimental investigations of kinetic processes in magnon systems. Utilization of resonators makes it possible to create pumping fields that significantly exceed threshold values and provide excitation of high numbers of magnons. For instance, in YIG the densities of parametric magnons up to $10^{18}$-$10^{19}$ $cm^{-3}$ can be reached.

### 3.3 Brillouin light scattering spectroscopy

Brillouin light scattering (BLS) is an optical spectroscopic method for investigation of excitations in solids in the GHz frequency region. Owing to its high informativity, it has become in the last decades one of main experimental method for investigation of dynamic processes in magnetic materials [10]. The idea of the BLS experiments is rather simple: The probing laser beam is sent to the sample under consideration and the scattered light is analyzed. As it has been mentioned in the theoretical section, while propagating in magnetic material, light can be inelastically scattered by spin waves. The frequency and the wave vector of the scattered light are changed in accordance with the conservation laws:

$$\begin{aligned} \omega_S &= \omega_I \pm \omega_m \\ \vec{k}_S &= \vec{k}_I \pm \vec{k}_m \end{aligned} \qquad (57)$$

and its intensity is proportional to the density of magnons with the given $\omega_m$ and $k_m$. Hence, the scattered light contains information about the frequency, wave vector and the density of the spin wave at the same time. Besides, since the BLS spectroscopy is an optical method it provides rather high spatial resolution, which can reach down to the half of the wavelength of the probing light.

Typical frequencies of the excitations investigated by BLS spectroscopy are $10^9$-$10^{11}$ Hz, which is several orders of magnitude smaller than that of the probing light ($\omega_m/\omega_S \sim 10^{-4} \div 10^{-6}$). This means that the magnitude of the wave vector of the light $\left|\vec{k}_S\right| = \frac{\omega_S}{c}$ is actually not changed and only its direction is rotated by an angle determined by $\vec{k}_m$. This fact is often taken into account when the particular geometry of the experimental optical arrangement is chosen.

Three basic types of scattering geometries are usually described in the literature. These are: forward scattering, right-angle scattering and backscattering (see Fig. 9). The right-angle scattering appears to be the first one in historical respect and is widely used for optically transparent materials. The fact is that in scattering experiments there is always elastically scattered light (caused by the elastic scattering from imperfections of the sample). The intensity of the elastically scattered light is several

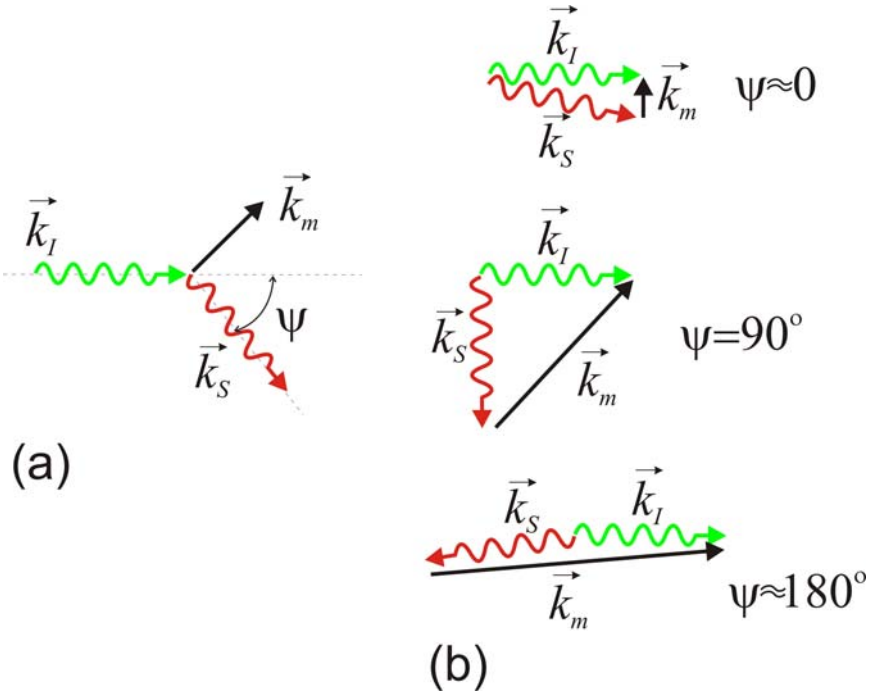


**Figure 9.** Kinematics of scattering process (a) – determination of the scattering angle; (b) types of scattering geometries

orders of the magnitude higher than that of the inelastically scattered light. This fact significantly hinders the application of BLS. For bulk transparent samples the influence of this parasitic elastic component will be minimal for the right-angle scattering geometry. For investigations of opaque samples and for studies of surface excitations the backscattering geometry is preferable. At that the surface of the sample should be optically smooth to decrease the contribution of the parasitic elastic component. The forward scattering is mostly used for the investigation of long-wavelength ($k_m << k_{I,S}$) excitations in transparent samples.

### 3.4 Fabry-Perot interferometer

In the previous section it has been shown that the smallness of the frequency of the scattering particle (magnon) with respect to that of the light results in the fact, that its wave vector can be determined from simple measurement of the scattering angle. However, due to this smallness a frequency analyzing technique with extremely high resolution is required for BLS. The device capable of providing such frequency resolution and used at present in the BLS spectroscopy is the Fabry-Perot interferometer.

A Fabry-Perot interferometer is made of two parallel flat plates separated by distance $d$ (see Fig. 10(a)). The inner surfaces of the plates are optically coated to create mirrors. It is well known, that due to the interference effects of the light beam reflected by the mirrors such system will efficiently transmit only the light, which frequency satisfy the condition

$$m\lambda_m = m\frac{c}{\nu_m} = 2nd\cos\varphi, \qquad (58)$$

where $m$=0, 1, 2… is the order of the interference, $n$ is the refractive index of the

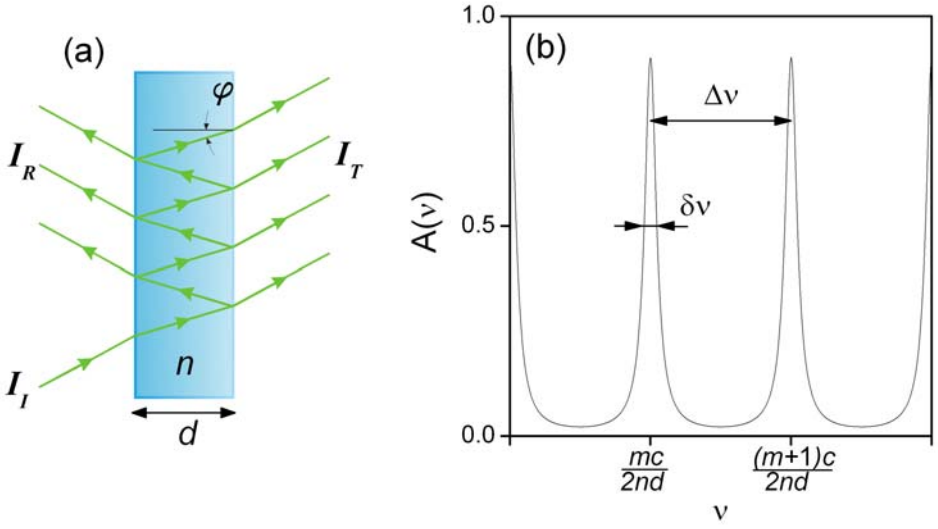


**Figure 10.** Schematics of the simplest Fabry-Perot interferometer (a) along with its transmission function (b).

medium between the mirrors (in most cases $n$=1 for air), $c$ is the speed of light and $\varphi$ is the light incidence angle (in most relevant cases $\varphi = 0$, therefore it will be omitted hereinafter), and $\nu_m$ is the linear frequency of the light corresponding to the $m$-th transmission maximum. More detailed analysis of the many-beam interference provides the transition coefficient of the Fabry-Perot interferometer

$$I_T = I_0 \left( \frac{T}{1-R} \right)^2 \frac{1}{1+\left(2F/\pi\right)\sin^2\left(\frac{2\pi n}{c}\nu d\right)} \qquad (59)$$

Corresponding dependence is plotted in Fig 10(b). Here $T$ and $R$ are transmission and reflection coefficients of the mirrors and $F$ is the finesse, which determines the width of the transmission peaks, $\delta\nu$: $F = \Delta\nu / \delta\nu$. The frequency difference between two neighboring transmission peaks

$$\Delta\nu = \frac{c}{2nd} \qquad (60)$$

is called the free spectral range (FSR).

In the ideal case the finesse is determined solely by the reflection of the mirrors $F = F_R = \pi\sqrt{R}/(1-R)$, but when another factors are taken into account (not ideal flatness across the mirrors, non-parallelism of the incident light, diffraction loses, etc.) the total finesse should be calculated as $1/F^2 = 1/F_R^2 + \sum 1/F_i^2$, where $F_i$ are the contributions of all possible imperfection factors.

From (59) it follows that changing the distance between the mirrors $d$ (sometimes $n$) one can make the condition for the maximum transition (58) to be fulfilled for different frequencies, i.e. to scan the frequency spectrum of the incident light. The width of the separate transmission peak (Fig. 10b)

$$\delta\nu = \frac{c}{2ndF} = \frac{\Delta\nu}{F} \qquad (61)$$

determines the frequency resolution, i.e. the minimal frequency difference between two lines, which can be separated by the interferometer.

Since in any BLS spectrum a strong elastic (Rayleigh) component is always present, the problem one should solve by analyzing the BLS-spectrum is not to distinguish between two close lines having similar intensities. One has to detect a weak line, corresponding to the inelastically scattered light, which has its frequency very close to a strong line caused by the elastic scattering. Therefore, another important characteristic of Fabry-Perot interferometer is the contrast. It is defined as the ratio of the maximum and minimum transition of a line and it is connected with the finesse as follows:

$$C = 1 + \frac{4F^2}{\pi^2} \qquad (62)$$

For the typical distances of $d$=3 mm and reflection coefficient of the mirrors $R$=0.95 (assuming that $F=F_R$) one gets $\Delta\nu$ =50 GHz, $\delta\nu \approx 0.8$ GHz and C≈1500. In principle, the interferometer with such a finesse and FSR is capable to resolve the frequency shifts of the Stokes and anti-Stokes components typical for magnon BLS. However, the intensity of the elastic component is usually $10^5$-$10^6$ times higher than that of the Brillouin lines, i.e. the contrast is not enough to distinguish the BLS line from the elastically scattered light, attenuated by a factor of C. This problem was solved by J.R. Sandercock [85, 86] who designed an efficient multi-pass system, in which light passes through the interferometer several times. This increases the contrast and the finesse of the system as $C_n = C_1^n$ and $F_n = F_1 \big/ \sqrt{2^{1/n} - 1}$, where $C_1$ and $F_1$ are the parameters of a one-pass interferometer. Further improvement of the system is achieved by the implementation of two interferometers in tandem, mounted to the same mechanical stage so that the spacing between their mirrors is controlled by one driver. The arrangement of the interferometers and the principle of their operation is illustrated in Fig 11. The optical axes of the interferometers FP1 and FP2 are at a small angle $\theta$ with respect to each other (see Fig. 11a), so when the mirrors are moving the spacing between them is $d_1$ and $d_2 = d_1 \cos\theta \neq d_1$ for FP1 and FP2 respectively. This results in different instrumental transmission functions of the interferometers $I_{T1}(\nu) = I_{T1}(\nu, d_1) \neq I_{T2}(\nu)$. However, for some numbers $n$ and $m$ the frequency of the $n$-th transmission maxima of FP1 can coincide with that of the $m$-th

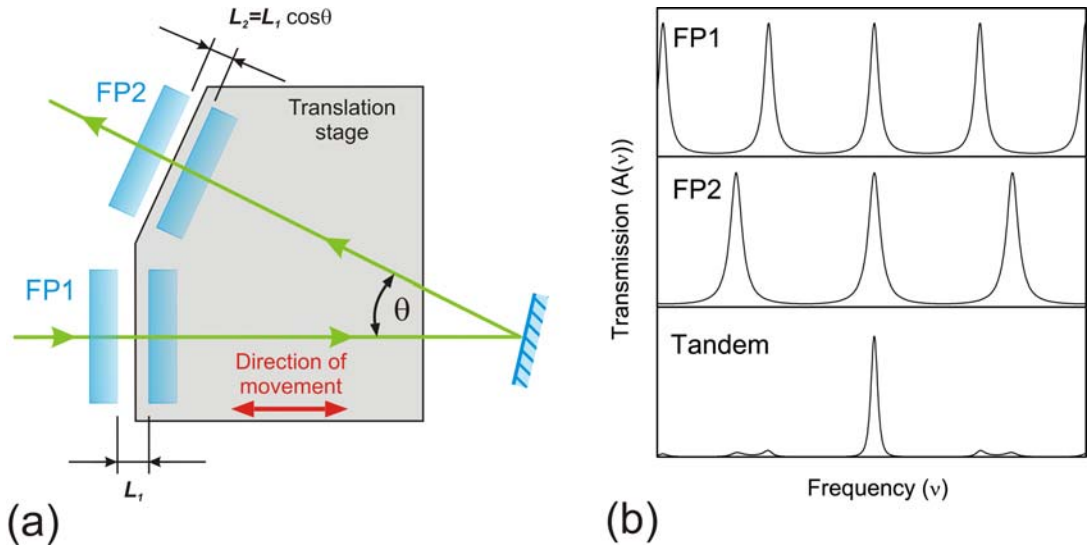


**Figure 11.** The arrangement (a) and the principle of operation (b) of tandem interferometer.

maxima of FP2 $\nu_n^{(1)} = \nu_m^{(2)}$ (see Fig 11b). At that, since for the neighboring peaks $\nu_{n\pm1}^{(1)} \neq \nu_{m\pm1}^{(2)}$ the instrumental transmission function of the tandem system, which is the simple product of those of the both interferometers, will be characterized by the essentially larger FSR.

Modern interferometers are usually realized in (3+3) arrangement (light passes three time through each of the interferometers in tandem). The motion of the mirrors (frequency scan) is realized by means of piezoelectric transducers (PZT). For the normal operation of the system, a parallelity of the mirrors of $\lambda/100$ is required. To provide such accuracy of the mirror alignment a good isolation of the interferometer from any vibration is necessary. Moreover, this parallelity should be maintained during the whole measurement (up to several hours), which requires sophisticated active stabilization procedure. The latter is realized by means of multiscan procedure: a series of quick scans of the spectrum is made, with data being accumulated by a computer. Each scan is followed by the automatic mirrors alignment procedure, for which the non-shifted elastically scattered light (or reference beam from the laser) is used (the mirrors are slightly tilted to get the maximum transmission). Frequency selected in above-mentioned way light is then detected by photomultiplier, the output of which is then accumulated for each frequency value.

### 3.5 Experimental setup

The schematic arrangement of the experimental setup for study of magnon BEC is shown in Fig. 12. It can be divided into two parts: microwave, which serves for the excitation of magnons, and optical, which provides their detection.

The sample under consideration, optically transparent YIG film on gadolinium gallium garnet (GGG) substrate, is placed between the poles of an electromagnet, used to create static magnetic field $\vec{H}_0$. The pumping magnetic field $\vec{h}_p$ with frequency $\nu_p$ for the parametric excitation of magnons is created by the resonator attached to the film surface. Half-wavelength resonators, made on the base of a microstrip line are used in the experiments, to provide an access of the probing light to the pumping region. The pumping is performed in a pulse regime, which preserves the sample from overheating by microwave. The clock pulse generator generates pulses with duration in (0.01-2) $\mu$s range and typical duty cycle value of 0.05, which are used to modulate the output of the microwave generator. Obtained microwave pulses are than amplified by amplifier and send to the resonator. The peak microwave power in the pulses is set by the attenuator. An *Y*-circulator is introduced at the input of the resonator to provide the possibility of the observation of the reflected signal and, hence, to mark the onset of the parametric instability process. The calculation of the absolute value of the pumping magnetic field $h_p$, created by the resonator inside the sample, as a function of

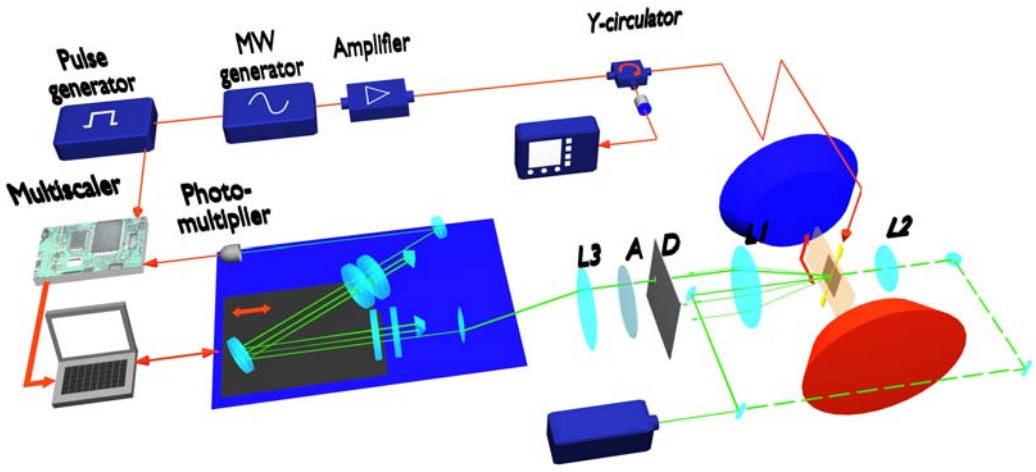


**Figure 12.** Schematic layout of experimental setup (further explanation are given in text).

the microwave power $P$ is rather complicated task, since it depends on many parameters of the setup. On the other hand, the onset of the parametric instability corresponds to $h_p(P_{thr1}) = h_{thr}$, which depends only on the properties of the sample. Thus, the power $P_{\text{thr1}}$ can be used as a reference point to compare the degree of magnon excitation in different experiments.

The optical arrangement of the experimental setup enables the investigation of magnons by means of BLS spectroscopy. The probing light from a single-frequency laser with the wavelength $\lambda_0$=532 nm and vertical polarization is focused onto the surface of the sample (YIG film). The setup can operate in backscattering and forward scattering geometry (the corresponding light paths are indicated by the solid and dashed lines). In the backscattering geometry the same lens $L_1$ is used to focus the probing beam and to collect the scattered light. For the forward scattering an additional lens $L_2$ is used for the focusing of the incident light. The aperture of the collecting lens $L_1$ determines the maximum angle of the scattered light which can be detect by the setup, i.e. the maximum value of the magnon wave vector $\vec{k}_m$. The lens used in setup has a focal distance of 55 mm and a numerical aperture of 0.42, which corresponds to the maximum angle of the scattered light with respect to the optical axis $\theta_{\text{max}}$=25º. Due to the direct correspondence between the scattering angle $\theta$ and the magnon wave vector $\vec{k}_m$ a selective detection with respect to the latter can be realized by simple introduction of the diaphragm ($D$) just after the collective lens $L_1$. The polarization analyzer $A$ is used to reduce the intensity of the elastic line at the entrance of the interferometer (as it was mentioned above the polarization of inelastically scattered light is rotated by 90º). The collected light is then focused by the lens $L_3$ onto the input pinhole of the interferometer for further frequency analysis. A 3+3 pass tandem Fabry-Perot interferometer is used to analyze the scattered light. A typical frequency resolution of the interferometer, corresponding to the optimal magnon detection regime is $\delta\nu$=250 MHz. For particular measurements it can be made as good as $\delta\nu$=50 MHz but at the expense of the sensitivity. During the scan interferometer changes the position of the transmission maximum in a given frequency range $\nu_{start} \div \nu_{stop}$. For convenience this range can be divided into $n$ frequency channels $\nu_i$ with a width of each channel $\Delta\nu = (\nu_{stop} - \nu_{start})/n$. Correspondingly, when during the scan the centre of the transition maximum is within the $i$-th frequency channel and the

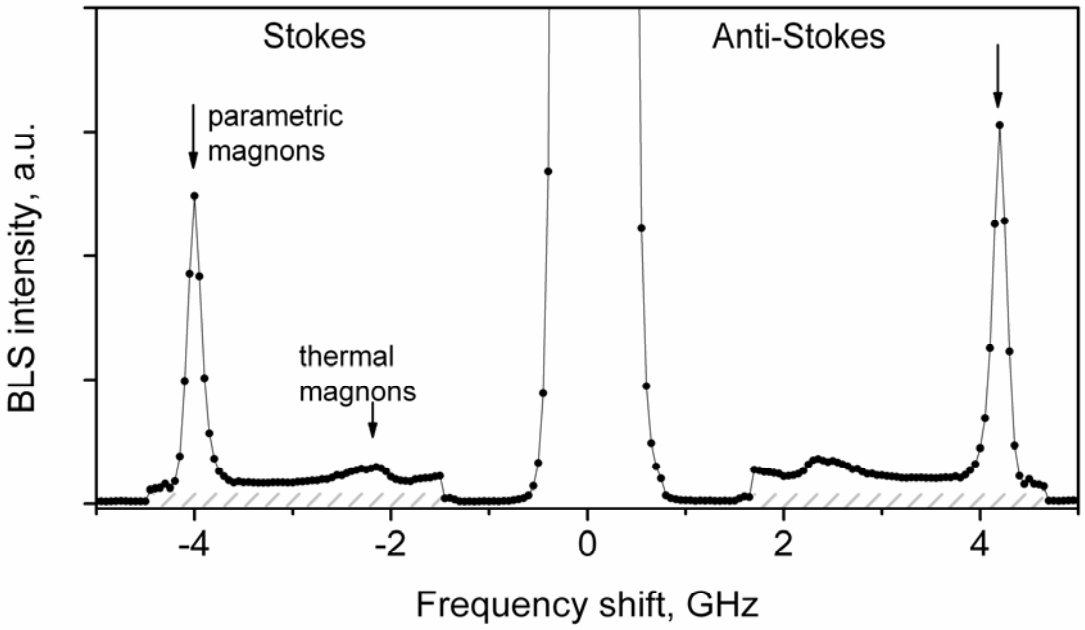


**Figure 13.** Experimental BLS spectrum obtained in back scattering on 5 μm thick tangentially magnetized YIG film under continuous excitation by parametric pumping of frequency $f_p$=8.1 GHz. Static magnetic field $H_0$=700 Oe, pumping power $P_p$=17 mW

photomultiplier detects a photon, it is regarded as to have the frequency $\nu_i = \nu_{start} + i(\nu_{stop} - \nu_{start})/n$. The number of such detected photons gives the spectral intensity of the signal. Accumulating the signal for many sweeps of the interferometer, one can obtain the BLS spectrum of the scattered light, and, as discussed above, investigate the distribution of magnons over the possible magnon states.

The example of the measured spectrum is shown in Fig 13. It represents the spectrum of the light, scattered in the in-plane magnetized YIG film, continuously excited by parametric pumping of frequency $f_0$=8.1 GHz. Along with an intense not shifted elastic line inelastic BLS components can be clearly distinguished in the spectrum. Note here, that the scanning speed of the interferometer was reduced by factor of 4 in the range of interest (1.5-4.5) GHz resulting in larger accumulation time in this region and, hence, in higher BLS intensities. The well pronounced peak near 4 GHz apparently corresponds to the parametric magnons excited in the film by the pumping and whose frequency is equal to the half of the pumping frequency (Sec. 2.5) $f_p$=$f_0$/2=4.05 GHz. Besides, a broader contribution from thermal magnons also presents in the spectrum. The observed difference in intensities of the Stokes and

anti-Stokes components is caused by the peculiarities of magneto-optical interaction [59].

Beside frequency resolution provided by the interferometer a possibility of the temporal analysis of the scattered light is crucial for the investigation of non-stationary spin wave processes. For the latter a widely used time correlated single-photon counting method [87] can be applied. The measurements are carried out by the fast time of flight multichannel scaler. A general principle of its operation is to switch through subsequent cells of high speed memory and to record events into the corresponding memory locations (time bins) as signal arrives at the stop input of the multiscaler. The latter, in turn, corresponds to the time elapsed from the triggering start event, which launches the sweep. The multiscaler, used in the setup has time resolution down to 250 ps (determined by maximal switching speed between memory cells) and maximum counting rate of 4 GHz (defined by the recording speed). As a triggering event starting the sweep of the multiplier a signal from the clock pulsed generator *P*, which modulates the microwave power and forms pumping pulses, is used. The stop input of the multiscaler, in turn, is connected with the output of the photomultiplier, so the detection of single photon by the detector is a stop event for the multiscaler. Thus, after each pumping period the fast memory of the multiscaler contains the information about the arrival time of the photons, scattered by magnons, with respect to the start of the pumping pulse. This information is then stored taking into account the current scanning position of the interferometer, which determines the frequency of the detected photons. Thus, repeating such measurements for many periods and accumulating the results one can investigate time evolution of magnon distribution.

The possibility of the measurements with spatial resolution is also provided in the setup. For this purpose the sample is mounted to the movable stage with position can be changed by electronically controlled step-motors in three spatial dimensions with respect to the optical axis of the setup. The movement along this axis is used to set the sample in the focal plane of the collecting lens. Then, moving the sample in this plane in other two dimensions with respect to the probing beam, one can measure the spatial distribution of the magnon intensity in the film. The maximal resolution is, apparently, limited by the size of the focal spot, which in turn depends on the focusing lens and the accuracy of the sample positioning. In the present setup one can achieve the resolution down to 10 $\mu$m.

# Chapter 4

# Results and discussion

## 4.1 Kinetics of magnons under parametric excitation and thermalization of magnon gas

When considering a relaxation of excitations in ferromagnets, all other (thermal) magnons, on which the scattering of the excited mode occurs, are usually regarded as a reservoir of an infinitive capacity, so that its thermodynamical characteristics (chemical potential and temperature) do not change during the relaxation process ( $\mu=\mu_0=0, T=T_0$ ). This is justified by the fact that the number of excited magnons $N$ is always much smaller than the total number of thermal magnons $N << N_T = \sum_k n_k^0$ which, in turn, are coupled to the phonon bath, so the magnetic system does not deviate from the equilibrium state. Thus, the evolution of the secondary magnons is not considered at all - after the excited magnon leaves the initial packet, it disappears in the bath. There are, however, several aspects, which can lead to another scenario of relaxation. First, the necessity of the energy and momentum conservation laws to be held allows for the participation in a relaxation of the initial wave packet only of small part of the thermal magnon reservoir $N' = \sum_{k\in K} n_k^0$ . Therefore, even at $N<<N_T$, the occupation numbers of secondary magnons in this "allowed" spectral region can differ noticeably form the equilibrium value $n_k^0$ if $N_T >> N' \sim N$. Thus, the relaxation of initially excited wave packet can result in an appearance of a non-equilibrium distribution of magnons in some spectral region away from the initially excited packet. Second, the coupling of the magnon system of the crystal to the phonon one is often week, allowing for the former to be considered as an adiabatically quasi-isolated. Thus, under intense excitation secondary magnons are accumulated in the system and, owing to their interaction with each other, magnon gas is thermalized and a quasi equilibrium distribution is settled. This quasi equilibrium state can be characterized by its own temperature $T \neq T_0$ and chemical potential $\mu \neq \mu_0 = 0$ deviating from that of the phonon system. The possibility of magnon thermalization

and creation of magnon gas with $\mu \neq 0$ is of great importance, since it opens a way to a novel type of Bose-Einstein condensation of magnons. It is worth noting that both above mentioned effects do not conclude each other, rather second of them is preceded by the first. Any strongly non-equilibrium distribution of secondary magnons, arising in some narrow spectral range due to the primary process of relaxation, then evolves into the quasi-equilibrium one.

Realization of the first scenario was observed in the experiments on so called kinetic instability [88-91]. In these studies samples of YIG (spheres [88, 89] or films [90, 91]) were exited by means of parallel parametric pumping. As a result of four-magnon relaxation of parametrically excited magnons secondary magnons are created in the spectral regions allowed by the energy and momentum conservations laws. As the intensity of parametric magnons increases, the rate of secondary magnon creation is increased as well. When latter exceeds the relaxation rate of the secondary magnons the instability arises. Since the magnons at the bottom of the spin-wave spectrum are characterized by minimal relaxation, they first become unstable. In the experiment the onset of the instability was recorded by means of observation of electro-magnetic radiation from the sample at the frequency corresponding to the bottom of magnon spectrum. It exists only in certain range of magnetic fields, in which the processes of a direct scattering of parametric magnons into the magnons at the bottom of the spectrum are allowed by the conservation laws.

The problem of accumulation of the secondary magnons was also addressed theoretically in [92-95]. In particular, a creation of quasi-equilibrium gas of magnons with $\mu \neq 0$ was considered in [93-95] in connection with possibility of Bose-Einstein condensation of magnons. However, no direct experimental verification of this prediction followed. At the same time the problem of the thermalization plays crucial role in the field of Bose-Einstein condensation of quasiparticles [70, 71], determining the possibility of the observation of this effect in particular system.

The findings, described below, represent the results of experimental investigation of the processes of redistribution of secondary magnons and thermalization of magnon gas under the parametric excitation in YIG films by means of time-resolved Brillouin light scattering technique. Contrary to the previously used microwave techniques, the Brillouin light scattering spectroscopy provides a possibility to study the distribution of magnons over their spectrum and its evolution with time directly; being, therefore, very informative for the above mentioned investigations. At the same time, YIG is

known as a material with very low magnetic losses (week magnon-phonon interaction, $\tau_{mp}$~0.5 μs) and high nonlinearity (strong magnon-magnon interaction, $\tau_{mm}$<0.1 μs) providing possibility of investigation of multiple magnon scattering processes.

A 5.1 $\mu$m thick YIG film with lateral sizes 2×2 mm$^2$ was used in the experiment. It was placed into a static magnetic field $H_0$=(600-1000) Oe parallel to its surface. Excitation of magnons in the sample was performed by means of parallel pumping instability process. For this purpose, a half-wavelength wire resonator with a diameter of 25 μm was attached to the sample. The resonator was fed by microwave pulses of 1 $\mu$s duration with the repetition period of 11 μs at the carrier frequency of $f_0$=8.04 GHz, which is the resonant frequency of the resonator. The pumping field of the resonator excited in the film primary parametric magnons with the frequency $f_p$= $f_0$/2=4.02 GHz, which then redistributed over the magnon spectrum due to magnon-magnon scattering processes. This redistribution was then studied with a temporal resolution of 10 ns using the time-resolved BLS spectroscopy in the quasi-backscattering geometry. The probing beam was focused onto the surface of the resonator so that the light from the laser passes through the film, is reflected diffusively by the resonator and passes through the film again. Although the aperture of the objective lens is capable of detection of photons with maximal value of in-plane wave vector component $k_{max}$=1×10$^5$ cm$^{-1}$, diffusive reflection of the light by the resonator allows to extend the range of wave vectors of magnons which can be detected far beyond this limit ($k'_{max} = k_{max} + k_L$, where $k_L$ is a wave vector of light).

Figure 13 illustrates the idea of the experiment. It shows the spectrum of magnons in an in-plane magnetized ferromagnetic film along with the schematics of the parametric process. The spectrum is calculated for the parameters of the YIG film (thickness $d$=5.1 μm, saturation magnetization $M_0$=1750 G and exchange constant $\alpha=q/(4\pi)$=3×10$^{-12}$ cm$^2$) and the value of static magnetic field ($H_0$=700 Oe) typical for the experiment. The lowest laying dispersion branch is shown in the figure. The solid lines represent the dispersion curves for the two limiting cases of magnons with wave vectors $\vec{k}$ oriented parallel (the so-called backward volume waves) or perpendicularly (the so-called surface waves) to the static magnetic field $\vec{H}_0$as indicated in Fig. 13. The both curves merge for $k$=0 at the frequency of the uniform ferromagnetic resonance $f_\perp$=3.67 GHz. The magnon states for intermediate angles fill

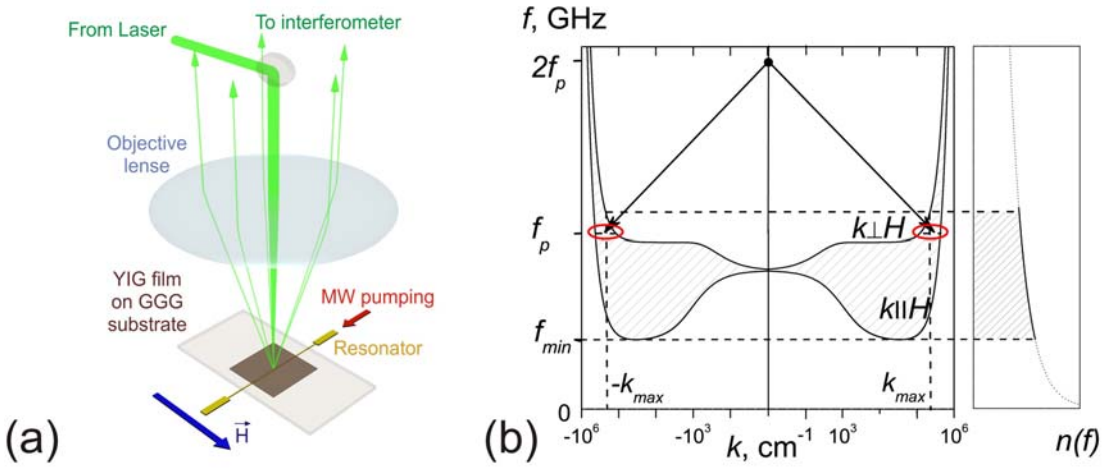


**Figure 13.** (a) The arrangement of the film, pumping resonators and the probing light, used in the experiment (b) The low-frequency part of the magnon spectrum in tangentially magnetized 5 μm thick YIG film at $H_0$=700 Oe. Arrows illustrate the pumping process. Right panel explains the limitations on the accessible frequencies range.

the manifold between these two boundaries. The minimal frequency $f_{min}$=2.1 GHz is achieved for magnons with wave vector parallel to the magnetic field at $k_{min}\approx 3.5\times 10^4$ cm$^{-1}$.

The process of the parametric pumping of the magnon gas is shown schematically by the arrows. This process can be considered as a splitting of a microwave photon of the pumping field with the frequency $f_0$ and wave vector $k_0 = \frac{2\pi f_0}{c} \approx 0$ into two magnons with frequencies $f_{p1} = f_{p2} = f_p = f_0/2$ and wave vectors $\vec{k}_{p1} = -\vec{k}_{p2} = \vec{k}_p$. When the value of the pumping field exceeds some threshold level, determined by the magnon relaxation rate, the instability arises and a rapid growth of magnon occupation numbers starts. At moderate power levels, when the threshold value is slightly exceeded, this condition is fulfilled only for one type of magnons (with certain value of $\vec{k}_p$) corresponding to the minimal threshold and only these magnons are excited (for the parallel parametric pumping process these are magnons with $\theta = \angle(\vec{k}, \vec{H}_0) = 90°$). However, the pumping powers, used in the experiments, correspond to the magnetic fields of the resonator of several orders of magnitude larger than the threshold one, allowing, therefore, for the excitation of pairs of magnons with all accessible values of $\vec{k}_p$ at $f = f_p$ (marked by red line in Fig. 13).

Moreover, at very high powers non-degenerate pumping excitation with $f_{p1} \neq f_{p2}$ (but keeping, of course $f_{p1} + f_{p2} = f_0$) becomes possible [47]. The pumping initiates a strongly non-equilibrium magnon distribution: a very high density of primary parametric magnons (up to $10^{18}$-$10^{19}$ cm$^{-3}$) is created close to the frequency $f_p$. Although the primary magnons are excited by a coherent pumping, they are not coherent to each other: two magnons are excited simultaneously, and only the sum of their phases, but not the phase of each magnon, is locked to the phase of the microwave photon.

The relaxation of the intense packet of primary parametric magnons is then studied. As it was mentioned above, the magnon system of YIG crystal is weakly coupled to the lattice, which means that the relaxation occurs mainly due to magnon-magnon processes and the energy pumped into the crystal stays within the magnon system for a certain time. Besides, the choice of the magnetic field allows to exclude unfavorable influence of three-magnon processes, namely to cancel the splitting process for primary magnons (which limits the maximal number of parametrically injected magnons at level significantly smaller then $10^{18}$-$10^{19}$ cm$^{-3}$) and to reduce to the minimum the confluence process. Thus only the two- and four-magnons scattering processes, which conserve the number of magnons, are responsible for the relaxation and an accumulation of substantial number of magnons within the magnetic system becomes possible. Although all magnons, which are injected into the system, are injected by the parametric pumping, for the sake of clarity hereinafter only primary magnons, directly excited by the pumping and having frequency $f_p$ are referred as parametric magnons. Correspondingly, all other magnons, which arise as a result of scattering of parametric magnons, are referred as secondary magnons.

It is worth noting, that the main, four-magnon, scattering process is most efficient for the exchange part of the spectrum, were the exchange interaction is dominant. For low-frequency dipole magnons, it is mainly caused by dipole-dipole interaction (as a second order of three-magnon dipole Hamiltonian) and usually is weaker. However, for film samples the conservation of only in-plane components of the magnon wave vector is obligatory, which gives an additional degree of freedom for four-magnon energy redistribution at the low dipole part of spectrum.

Fig. 14 shows the evolution of magnon distribution under the excitation by parametric pumping for the pumping power $P_p$=52 mW and magnetic field

$H_0$=700 Oe. This value of the pumping power exceeds the threshold of the parametric instability by ζ=20 dB. Figure represents the BLS spectra, accumulated for different delay times after the start of the pumping pulse. The experimentally measured BLS intensity at a given frequency *I(ω)* is proportional to the reduced frequency density of magnons

$$I(\omega) \sim \frac{dN'_{\omega}}{d\omega} = \frac{1}{d\omega} \sum_{\substack{\omega<\omega(k)<\omega+d\omega \\ k<k_{\max}}} n_k = D'(\omega)n(\omega), \qquad (63)$$

i.e. to the number of magnons with frequency laying within the interval $\omega \div \omega + d\omega$ accessible in the experiment. The latter differs from the total spectral density since the optical arrangement of the experimental setup allows for the detection of magnons only with $k<k_{\max}<<k_B$, where $k_B$ defines the Brillouin zone of the lattice. This limitation results in the fact, that reduced density of the states $D'(\omega)$ should be used when analyzing experimental BLS spectra, whereas *n(ω)* in (63) is still the Bose-Einstein occupation function $n(\omega) = [\exp(\frac{\hbar\omega - \mu}{\kappa T}) - 1]^{-1}$, depending on the thermodynamical parameters of the magnon gas.

Figure 14(a) illustrates the reference BLS spectrum of thermal magnons accumulated without pumping. These magnons are at the thermodynamical equilibrium with the phonon system of the crystal. They are excited and annihilated due to the interaction between the spin system and the lattice and their total number is defined by the temperature. Consequently, these magnons are described by the statistical Bose-Einstein occupation function with zero chemical potential $\mu$=0. As seen from the figure, the measured spectrum is bounded in frequency. The low-frequency limit apparently corresponds to the minimal magnon frequency $f_{\min}$. The presence of the upper limit is due to the lack of sensitivity of the experimental setup to the magnons with large wave vectors ($k>k_{\max}$). In this sense the spectrum of thermal magnons is also important since it contains the information about the reduced density of magnon states $D'(\omega)$ entering (63). In other words, the spectrum, showed in Fig. 14(a) depicts the Bose-Einstein occupation function $n(\omega) = [\exp\left(\frac{\hbar\omega}{\kappa T}\right) - 1]^{-1}$ in representation of the experimental setup.

As the pumping is switched on primary magnons are excited, which is clearly seen in Fig. 14(b) by the appearance of the sharp peak in magnon spectrum at the frequency $f_p$. The intensity of the peak grows with time as pumping injects more and

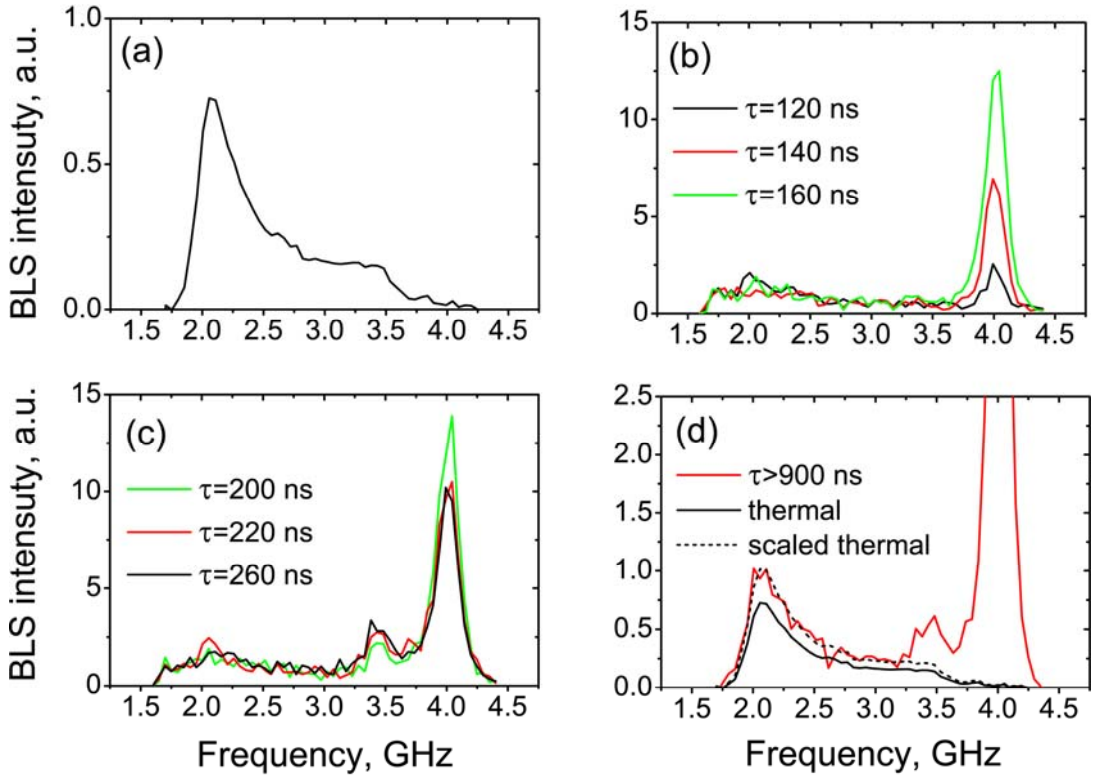


**Figure 14.** Evolution of the magnon frequency distribution for pumping power $P_p$=52 mW. (a) the BLS spectrum of thermal magnons, measured without pumping; (b), (c) magnon spectra recorded at different delays after the start of the pumping; (d) steady state distribution of magnons which is settled in the system.

more magnons into the system. At the same time a process of redistribution of the injected magnons over the magnon spectrum takes place due to the above-mentioned four-magnon scattering processes.

First of all, injected parametric magnons interact with each other. Corresponding interaction Hamiltonian term can be written as $T_{12,34}c_{p_1}c_{p_2}c^+_{p_3}c^+_{p_4}$, with $p$ denoting the parametric magnons (i.e. $f_1 \approx f_2 \approx f_3 \approx f_4 \approx f_p$). The processes of this type are described in details in Chapter 6 in [46]. Corresponding theory of interaction of parametric magnons with each other is called $S$, $T^2$-theory. In particular, these processes lead to a slight spreading of the distribution of parametric magnons around the resonance surface $f(k) = f_p$ in phase space.

Second, since the distribution of magnons with the sharp intense peak of parametric magnons at $f_p$ is highly non-equilibrium, system tends to redistribute them over the whole spectral range by means of four-magnon scattering processes of parametric

magnons with the magnons from other parts of the spectrum. In general case these processes are presented by Hamiltonian $T_{p1,23}c_p c_{k_1} c_{k_2}^{+} c_{k_3}^{+}$ which describes a scattering of parametric magnon by a thermal magnon $\overrightarrow{k_1}$ with further creation of magnons $\overrightarrow{k_2}$ and $\overrightarrow{k_3}$. It allows for participation of thermal magnons practically from the whole spectrum, providing therefore efficient redistribution of parametric magnons over the wide spectral range.

Besides, when dealing with the relaxation of intense packet of magnons one often considers separately the process of a type $T_{p_1p_2,23}c_{p_1}c_{p_2}c_{k_2}^{+}c_{k_3}^{+}$ which is a special case of general four magnon scattering processes. In this particular process two parametric magnons are annihilated and two magnons in other spectral regions are created. A rate of this process is very high since it is proportional to the second order of the population of parametric magnons $n_p = n(f_p)$, which significantly exceeds thermal equilibrium value $n_p^0$. At the same time it is allowed only for very narrow spectral region for which $\overrightarrow{k_1} + \overrightarrow{k_2} = \overrightarrow{k_{p_1}} + \overrightarrow{k_{p_2}}$ and $f_1 + f_2 = 2f_p$. The small additional peak in magnons population at FMR frequency $f_\perp$=3.67 GHz that appears in experimental spectrum at delays $\tau$>200 ns (Fig. 14(c)) is evidently the result of such processes: two parametric magnons with frequencies $f_p$=4.05 GHz are annihilated and two magnons with frequencies $f_1 = f_\perp = 3.67$ GHz and $f_2 = 2f_p - f_\perp = 4.43$GHz correspondingly are created. The emergence of the peak at $f_\perp$ means that the rate of magnons creation due to annihilation of the parametric magnons exceeds the relaxation rates in this spectral region, i.e. the situation in some sense can be treated as the kinetic instability mentioned at the beginning of this section. Apparently the radiation of electromagnetic waves by exactly these magnons was detected in [90] in the range of magnetic fields, where classical kinetic instability has not been observed.

Fig. 14(d) shows quasi-stationary distribution of magnons which is settled in the system after $\tau$=900 ns. This distribution corresponds to the flow equilibrium between the pumping, which injects magnons into the film, and the spin-lattice relaxation processes, which are responsible for the energy transfer into the lattice. Noteworthy is the fact, that beside highly non-equilibrium distribution of magnons near the pumping frequency $f_p$, caused by the continuous injection of the parametric magnons the occupation numbers of magnons at other frequencies exceed those of the thermal as well (for the sake of comparison the spectrum of thermal magnon is also shown in Fig

14(d) by solid black line). This is, apparently, the result of redistribution of the injected magnons over the entire spectrum, which reflects the inherent tendency of the system to the thermodynamically equilibrium state (maximum of the entropy). However, the observed settled distribution, obviously, do not corresponds to a quasi-equilibrium thermodynamic state, since it is characterized by the relatively higher occupations near the upper frequency limit (above-mentioned peak at $f_{\perp}$) then those at the bottom in compare with the reference thermal spectrum. This can be seen from the comparison of the stationary settled distribution with the thermal one, scaled in a way to match the occupation numbers at the bottom frequency $f_{\min}$ (dashed line in Fig. 14(d)).

The peculiarities of the kinetics of injected magnons can be revealed from figure 15, where the time evolution of magnon spectrum under the excitation by more intense pumping ($P_p$=171 mW, $\zeta$=25 dB) is illustrated. Similar to the previous case, an appearance and a growth of the peak of primary magnons is observed at the initial stage just after the pumping is switched on (Fig. 15(a)). At the same time the processes responsible for the redistribution of the parametric magnons over the other parts of the spectrum start to act. Analysis of the experimentally obtained spectra at delays $\tau$>100 ns, illustrated in Fig. 15(a), shows that the redistribution of the injected magnons happens in a gradual wave-like manner starting from the frequencies close to the frequency of parametric magnons $f_p$ toward the bottom of the spectrum. Such behavior of magnons can be explained by the properties of the four-particle scattering processes considered above, which are responsible for the energy redistribution within the gas of magnons. Consider first small delays, when only parametric magnons are excited, and their occupation numbers significantly exceed equilibrium values (

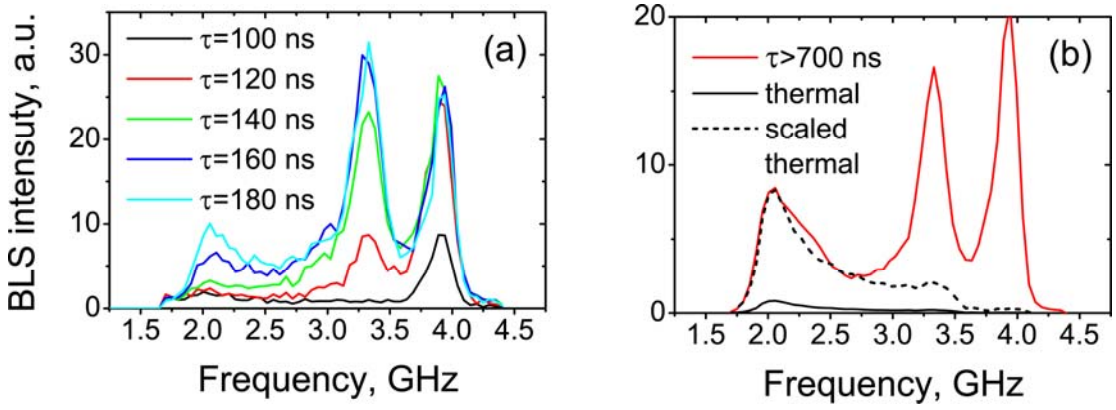


**Figure 15.** Time evolution of magnon distribution for pumping power $P_p$=171 mW

$n_p >> n_p^0$) and are continuously sustained by the pumping. As mentioned above, in this case the processes of the type $T_{12,34} c_{p1} c_{p2} c_{k_3}^+ c_{k_4}^+$ became also important. The frequencies and the wave vectors of magnons created as a result of this process are determined by the energy and momentum conservation laws. However, a remarkable property of the four particle scattering processes of 2→2 type is that they are allowed by all dispersion laws when the values of the wave vectors and the frequencies of the particles involved are close to each other. Process of this type is well known in physics; in particular, it is responsible for the effect of modulation instability during a propagation of an intense wave in a medium [7]. Thus, not depending on the value of external magnetic field, a process of scattering of parametric magnons with further creation of magnons at frequencies $f_p \pm \Delta f$ will occur at high pumping powers. For convenience, such process can be called four-magnon decay process in contrast to general process of scattering of highly excited magnons by thermal ones. Denoting magnons occupation numbers at frequencies $f_p \pm \Delta f$ as $n_\pm$ correspondingly, one can write down the matrix element of such process:

$$\left\langle n_p - 1, n_p - 1, n_+ + 1, n_- + 1 \left| H^{(4)} \right| n_p, n_p, n_+, n_- \right\rangle = \\ = T_{pp,12} \sqrt{n_p^2 (n_+ + 1)(n_- + 1)} \delta(k_p + k_p - k_+ - k_-) \quad (64)$$

and kinetic equation, giving the rate of decrease of number of parametric magnons due to this process

$$\frac{dn_p}{dt} \sim \left| T_{pp,34} \right|^2 [-n_p^2 (n_+ + n_- + 1) + (2n_p + 1) n_+ n_-], \quad (65)$$

where the second term stands for the reverse process. From (65) it follows that under $n_p >> n_\pm$ the rate of the parametric magnon flow-out will be proportional to $n_p^2$. At the same time the occupation numbers $n_\pm$ will grow as well until they start to exceed noticeably thermal level and the four-magnon decay process comes into play. In this way, above mentioned process allows avoiding a presence of sharp, strongly non-equilibrium peaks in magnon spectrum. At the same time it cannot be responsible for

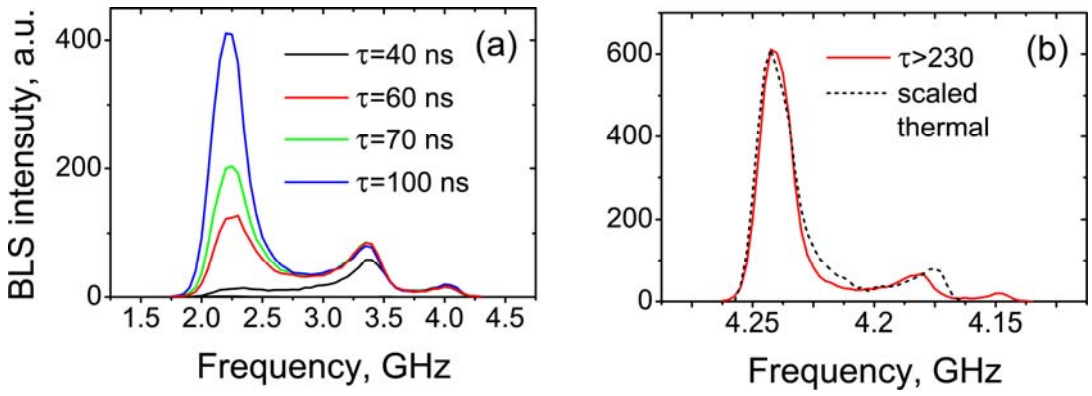


**Figure 16.** Time evolution of magnon distribution for pumping power $P_p$=0.7 W.

the settlement of thermodynamically equilibrium state on large frequency scales, since it is sensitive only to high gradients of magnon population. Apparently, this is achieved by processes of scattering on thermal magnons.

Figure 15(b) illustrates the steady-state distribution of magnons, which is settled in the system after $\tau$=700 ns. The time, necessary for the stationary state to be reached is now smaller than that in the previous measurements with the lower pumping power, which can be explained by increased role of decay processes which provide fast pre-redistribution of strongly excited magnon states. Again, a comparison of the relative occupation numbers at different frequencies for the settled distribution and that of the thermal magnons indicates a non-thermalized character of the magnon spectrum, namely overpopulation of the high-frequency states with respect to the bottom of the spectrum is observed. Decisive for this point is, apparently, the relation between the time, necessary for the stationary state to be settled and the average life time of magnons (with respect to the spin-lattice relaxation). In fact, as follows from the Figure 15, the steady state sets in when the magnon occupation at minimum frequency $n(f_{\min})$ saturates. At the same time, the magnons at the bottom of the spectrum appears as a result of multiple scattering processes and, hence, need some time to arrive at $f_{\min}$. If then this time is larger the life time they disappear before reaching the minimum frequency, resulting in relative under-population of the lowest part of the spectrum.

It is obvious, that the efficiency of magnon-magnon interaction, which determined the characteristic time of their redistribution over the spectrum, can be decreased by increase in pumping power. This is further illustrated by Figure 16, which shows magnon distributions measured at the pumping power level $P_p$=0.7 W ($\zeta$=31 dB). Indeed, as seen from the figure, the processes of magnon redistribution now occur at shorter time scales. More interesting, however, is the fact, that the distribution, which

is settled in the system at $\tau$=230 ns, now fully corresponds with the spectrum of thermal magnons (Fig. 16(b)), which means that it can be described by an equilibrium statistical population function with chemical potential $\mu$=0 and turn out to be thermodynamically quasi-equilibrium. Accordingly, the time of 230 ns can be considered as the thermalization time at a given pumping power $P_p$=0.7 W. It is worth to note, that further slight change of magnons distribution is observed after the magnon gas is thermalized (for $\tau$>230 ns), which is characterized by slow quasi-adiabatic increase of magnons population at low frequency. It will be shown in the next section that such distribution is also thermodynamically quasi-equilibrium but characterized by non-zero chemical potential.

Due to nonlinearity of the four-magnon scattering the thermalization should occur at smaller delays as pumping power is further increased above its values of 0.7 W. This is corroborated by measurements at higher pumping levels. The results of these measurements are summarized in Fig. 17, where the characteristic time, corresponding to either steady distribution appearance (for low powers) or thermalization of magnon gas (high powers), is plotted as a function of pumping power. A crossover between these two regimes happens around the threshold value of

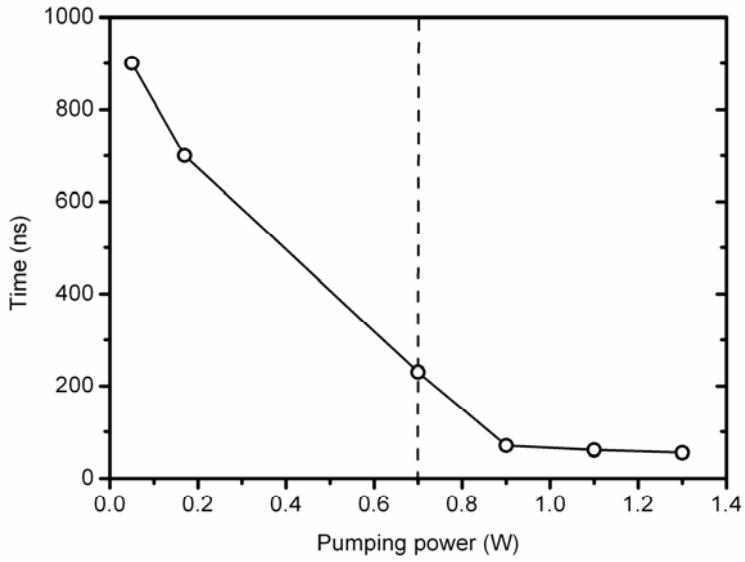


**Figure 17.** Time, corresponding to the appearance of a characteristic state of the magnon spectrum, as a function of pumping power. For low powers, corresponding to the left half of the graph characteristic state is described by the flow equilibrium between the pumping and the spin-lattice relaxation processes, whereas for the right one, characteristic time is the thermalization time.

0.7 W. As seen from the Figure, the thermalization time approaches a value of about 50 ns at the pumping power of 1.3 W, which is significantly smaller than the lifetime of magnons in YIG films due to the spin-lattice interaction.

Thus, concluding this section it can be pointed out that the obtained results on the kinetics of magnon gas under the parametric excitation clearly show that a redistribution of parametrically injected magnons occurs in a series of multiple scattering events. Due to nonlinear character of the four magnon interaction, responsible for the magnon scattering, the rate of the energy redistribution within the system of magnons depends on the pumping power, increasing with the latter. At high enough power levels, the characteristic time of magnon thermalization becomes smaller than their lifetime and quasi-equilibrium state with thermalized magnon gas can be achieved, which, in turn, opens a way for the observation of Bose-Einstein condensation of magnons.

### 4.2 Bose-Einstein condensation of magnons

The concept of Bose-Einstein condensation (BEC) [64] was introduced by Einstein in 1925 after he applied statistical approach developed by Bose for photons [96] for a gas of non-interacting atoms. It followed from his consideration that in a gas of bosonic particles solely due to the quantum statistical properties of the latter, without any interaction between them, a formation of collective quantum state, comprising macroscopic number of bosons, should occur when the concentration of particles $n$ exceeds critical value

$$n > n_c(T) = N_c(T)/V = 0.165\left(m\kappa T/\hbar^2\right)^{3/2}, \qquad (66)$$

where $m$ is the mass of the particles and $T$ the temperature of the gas. Followed shortly after the Einstein's work discovery of superfluidity in fluid $^4$He (see e.g. [97, 98]) had indirectly confirmed his prediction. Although this system noticeably differs from that, considered by Einstein, BEC is proven to underlie the effect of superfluidity in $^4$He [99, 100]. Recent experimental observation of BEC in dilute atomic gases [12-14] has unambiguously proved Einstein's prediction and has renewed interest to this effect. The 70-year delay between theoretical prediction and experimental realization is explained by extremely low temperatures required for

condensation condition (66) to be fulfilled for atomic gases. The fact is, that the concentration of atoms $n$ is limited since at high $n$ they form molecules or vapor starts to condensate in real space. Therefore, one needs to reduce $T$ and hence $n_c$ and make it smaller than $n$. This results in transition temperatures as small as $T\sim(10^{-7}\text{-}10^{-6})$ K, which requires sophisticated cooling techniques.

Beside atomic gases systems of bosonic quasiparticles in solids were also proposed as candidates for BEC. First theoretical works, addressing possibility of condensation in the system of longitudinal electric modes [101] and excitons [102, 103] date back to 60-ies years of the last century. The main advantage of quasiparticle in compare with atoms is that the condition of condensation (66) for them appears to be easier to fulfill. First of all, there is no such strict limitation on their concentration and the latter can be easily increased by external pumping. Second, their effective mass is much smaller than that of atoms resulting in possibility of achieving required values of critical densities $n_c$ at higher temperatures. However, as mentioned above, the lifetime of quasiparticles is finite (since they cannot be isolated from the phonon system of the solid), and to observe BEC one should provide conditions for condensation transition to occur faster than this time, which appears to be not always possible. Of course, in this case one can speak only about quasi-equilibrium condensation, which, however, does not cancel the effect, and merely brings it to another time scale. Strictly speaking, BEC is always quasi-equilibrium. Even for atomic gases the state with Bose-Einstein condensate is never a true equilibrium state: being left on his own gas will always, sooner or later, evolve into liquid or solid state, or gaseous one without condensate [104]. To date BEC has been reported to be experimentally observed in systems of excitons [22, 23], polaritons [24], and magnons in superfluid $^3$He [69] and YIG [25].

The possibility of BEC of magnons in ferromagnetic dielectrics was addressed theoretically by different authors [93-95, 105]. BEC of magnons was also proposed as one of possible explanations of effects of microwave radiation from the bottom of spin wave spectrum in YIG samples [91]. However, there were no sufficient experimental data to prove this suggestion in early experiments. Nevertheless, none fundamental constraints, which could prevent from observation of BEC of magnons, were suggested in all works.

In fact, it appears that magnons in YIG are very attractive candidates for BEC observation. They have all advantages of quasiparticles, namely the mass of magnons

in YIG is $m_{eff} = \hbar\left(\frac{\partial^2\omega}{\partial k^2}\right)^{-1} \sim \hbar(\gamma q M_0)^{-1} \approx 12.6 m_e$ ($m_e$ is a mass of an electron) is much smaller than the mass of any atoms, and they can be easily excited in considerably large amount by means of parametric pumping. At the same time, as it was shown in the previous section, the main quasiparticle's problem of finite lifetime appears to be solvable for magnons in YIG: under certain conditions magnons can interact fast enough for quasi-equilibrium state to be settled during their lifetime.

Another advantage of magnons in YIG as a system for BEC experiments is the fact, that being in equilibrium state at room temperature unlike atomic gases magnon gas is degenerate Bose gas with occupation numbers $n_k$>>1, i.e. is close to the Bose-Einstein transition. Indeed, in thermodynamically equilibrium state chemical potential $\mu$ of magnon gas is equal to zero. At the same time, condensation condition (66) is fulfilled at $\mu = \varepsilon_{\min} = \hbar\omega_{\min}$. For magnetic field values $H_0$~1 kOe one obtains $\frac{\hbar\omega_{\min}}{\kappa T} \approx \frac{\hbar\gamma H_0}{\kappa T} \approx 4.5\times10^{-4}$, which means that only slight increase in magnons concentration is required to achieve Bose Einstein condensation. Simple estimation can be made in a way, similar to how the concentration of thermal magnons was equated for calculation of magnetization of ferromagnet in the theoretical section. Within this approach equations (41) and (58) can be rewritten as

$$
\begin{aligned}
n(\mu=0) &= \frac{1}{\sqrt{2}}\left(\frac{\kappa T}{2\pi\hbar\gamma q M_0}\right)^{3/2} \mathrm{Li}_{3/2}\left(e^{-\frac{\hbar\omega_{\min}}{\kappa T}}\right) \\
n_{cr} = n(\mu=\hbar\omega_{\min}) &= \frac{1}{\sqrt{2}}\left(\frac{\kappa T}{2\pi\hbar\gamma q M_0}\right)^{3/2} \varsigma\left(\frac{3}{2}\right) \qquad (67) \\
\frac{\Delta n}{n} &= \frac{\varsigma\left(\frac{3}{2}\right) - \mathrm{Li}_{3/2}\left(e^{-\frac{\hbar\omega_{\min}}{\kappa T}}\right)}{\mathrm{Li}_{3/2}\left(e^{-\frac{\hbar\omega_{\min}}{\kappa T}}\right)} \approx \frac{\varsigma\left(\frac{3}{2}\right) - \mathrm{Li}_{3/2}\left(1-\frac{\hbar\omega_{\min}}{\kappa T}\right)}{\mathrm{Li}_{3/2}(1)} \approx \frac{2\sqrt{\pi}}{\varsigma(3/2)}\sqrt{\frac{\hbar\omega_{\min}}{\kappa T}} = 0.028
\end{aligned}
$$

i.e. approximately 3% increase in magnons concentration should be enough for condensation.

For films this value should be even smaller, since continuous $k$-space of a bulk splits into a set of discrete planes perpendicular to $\vec{k}_\perp$. However, complex nontrivial

dispersion relation of magnons in films do not allows obtaining of a simple analytical expression for $n_{cr}$. To calculate the critical concentrations for magnons in a film sample one should perform a direct summation over the cites of reciprocal lattice

$$n(\mu,T)=\frac{N}{V}=\frac{1}{L_xL_yL_z}\sum_{k_xk_yk_z}\frac{1}{\exp(\frac{\hbar\omega(k_x,k_y,k_z)-\mu}{\kappa T})-1},$$
$$k_x=\frac{\pi j_x}{L_x},\ j_x=0,1,...\frac{L_x}{a}, \qquad (68)$$
$$k_{y,z}=\frac{2\pi j_{y,z}}{L_{y,z}},\ j_{y,z}=-\frac{L_{y,z}}{2a},-\frac{L_{y,z}}{2a}+1,...,\frac{L_{y,z}}{2a},$$

where $L_\alpha$ are the dimensions of the sample (axis *0x* is normal to the film surface), and *a* is the lattice constant. Frequency $\omega(k_x,k_y,k_z)$ can be calculated using dispersion relation (20). Performing calculations for the values of parameters corresponding to the experimental situation (5.1 μm thick YIG film, magnetic field $H_0$=700 Oe, room temperature $T$=300 K) one obtains for the concentration of thermal magnons $n(\mu=0)=4.11\times10^{20}$ cm$^{-3}$. For calculation of critical concentration $n_{cr}$ the lateral dimensions are important, since they determine the separation between neighboring quantum states $\Delta\varepsilon_i=\varepsilon_{i+1}-\varepsilon_i$ in magnon spectrum. The lower is the value of this separation for the states just above the lowest energy state $\varepsilon_{\min}$ the higher is the population of this states at $\mu\to\varepsilon_{\min}$ ($n(\varepsilon_{\min}+\Delta\varepsilon,\mu=\varepsilon_{\min})=[\exp(\frac{\Delta\varepsilon}{\kappa T})-1]^{-1}\approx\frac{\kappa T}{\Delta\varepsilon}$) and, consequently, the higher densities are required to achieve BEC. The lateral sizes of the sample used in the experiment are 2×2 mm$^2$. Substituting this values into (68) with $\mu=\varepsilon_{\min}$ and excluding bottom states $(\pm\vec{k}_{\min},\omega_{\min})$, for which $n_k(\mu\to\varepsilon_{min})\to\infty$, one obtains for the maximal concentration of magnons which can be accommodated by thermal states $n_{cr}=n(\mu=\varepsilon_{\min})=4.16\times10^{20}$ cm$^{-3}$ and $\Delta n=5.5\times10^{18}$ cm$^{-3}$. Such densities of magnons can well be achieved under the excitation of magnons by intense parametric pumping.

It is worth to note, that not only the chemical potential of the magnon gas is changed when additional pumping magnons are added. The temperature of the gas should change as well. However, until the number of magnons injected is small this change should also be negligible. The value of this change can be estimated from

simultaneous account of energy and magnons number balance condition in the pumping experiment.

$$\begin{aligned} n(\mu = 0, T_0) + n_p &= n(\mu = \hbar\omega_{\min}, T_0 + dT) \\ E(\mu = 0, T_0) + \hbar\omega_p n_p &= E(\mu = \hbar\omega_{\min}, T_0 + dT) \end{aligned}, \quad (69)$$

where $E(\mu, T) = \sum_{k_x k_y k_z} \frac{\hbar\omega(k_x, k_y, k_z)}{\exp(\frac{\hbar\omega(k_x, k_y, k_z) - \mu}{\kappa T}) - 1}$, $n_p$ and $\omega_p$ is the number and the frequency of magnons created by the pumping. Apparently, the sign of the change of the temperature will depend on whether the pumped magnons are "hotter" or "colder" than the initial magnon gas, i.e. whether their energy $\varepsilon_p = \hbar\omega_p$ bigger or smaller then $\langle\varepsilon\rangle \sim \kappa T_0$. For example, for the pumping frequency used in the previous experiments ($f_p=\omega_p/2\pi$=4.02 GHz) solution of (69) yields $dT$=-200 mK. The main conclusion is, however, that $dT<<T_0$. Thus, the results of the calculations cited above shows the principal possibility of BEC of magnons in YIG films at room temperature.

In the previous section it was shown that parametric magnons excited in the film by parametric pumping can be distributed over the whole spectrum fast enough to provide thermalization of magnon gas. Thus, injecting sufficient number of parametric magnons one can expect to observe a formation of a quasi-equilibrium state corresponding to the gas with increased concentration, i.e. with non-zero chemical potential $\mu>0$. This was verified in a series of experiments similar to those described in the previous section. The idea of the experiment remains the same: electromagnetic pumping pulse of 1 μs duration with carrying frequency $f_0$=8.04 GHz following in a sequence with the repetition period of 11 μs is applied to the 5 μm thick tangentially magnetized YIG film and excites magnons in it. Excited magnons then redistribute over the spectrum and settled distribution is measured by means of BLS spectroscopy. However, the power of the pumping is increased in compare with the previous experiments to provide an excitation of considerable number of magnons.

Fig 18(a) illustrates the spectrum of thermal magnons in the film at magnetic filed $H_0$=700 Oe existing without pumping. As it was already mentioned, this spectrum contains important information about reduced density of states $D'(\omega)$. In general

case, spectral density, i.e. number of magnons within frequency interval $\omega \div \omega + d\omega$ is given by $dN_\omega = D(\omega)n(\omega)d\omega$, where $n(\omega) = [\exp(\frac{\hbar\omega - \mu}{\kappa T}) - 1]^{-1}$ number of magnons in quantum state with frequency $\omega$ and $D(\omega)$ is a number of quantum states $(k_x, k_y, k_z)$ with frequency $\omega(k_x, k_y, k_z)$ lying within interval $\omega \div \omega + d\omega$. In the experiments, however, only magnons in quantum states with such values of wave vector $k = (k_x, k_y, k_z)$ which can be detected by optical arrangement of the setup should be taken into account (these are magnons with in-plane wave vectors $k_\parallel = (k_y, k_z) < k_{max}$). Therefore, spectral density of magnons accessible in the experiment is $dN_\omega^{exp} = D'(\omega)n(\omega)d\omega$. Correspondingly, the BLS intensity obtained at the output of the interferometer and plotted in graph 18(a) is

$$I(\omega) = \int A(\omega - \omega')D'(\omega')n(\omega')d\omega', \qquad (70)$$

where $A(\omega)$ is the instrumental function (or amplitude frequency characteristic) of the interferometer (see (59)). Direct calculation of its shape using (59) require exact value of finesse, which depend on many factors, however the instrumental function is directly defined by the shape of elastic line. Indeed, since elastically scattered light

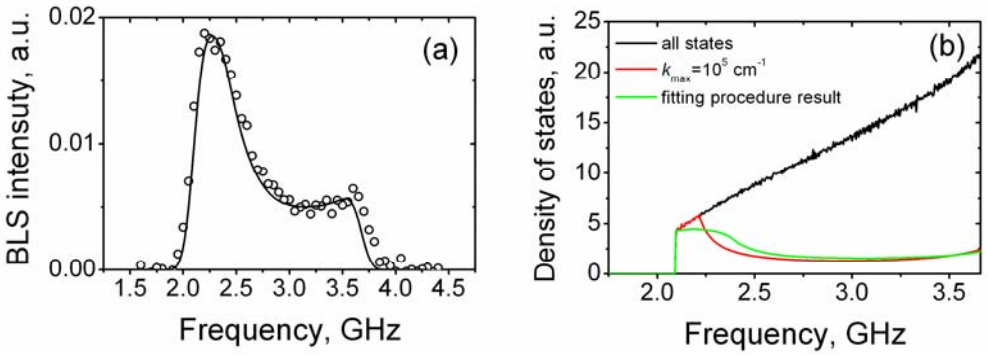


**Figure 18.** (a) Spectrum of thermal magnons at $H_0$=700 Oe: circles – experiment, solid line –fit, using Eq. (70). (b) Magnons density of states in the frequency range ($f_{min}$, $f_\perp$): black line – calculation using dispersion relation (20) with accounting for all states; red line – density of states with $k<10^5$ cm$^{-1}$; green line - result of best fit optimization procedure.

contains only one frequency component $\omega=\omega_L$ its BLS spectrum is $I(\omega)=\int A(\omega-\omega')\delta(\omega'-\omega_L)d\omega'=A(\omega-\omega_L)$. Thus, knowing $A(\omega)$ and taking into account that for thermal magnons $n(\omega)=n(\omega,\mu=0)$ one can use (70) for determining reduced density of states $D'(\omega)$ from experimentally measured BLS spectrum of thermal magnons. For this, $D'(\omega)$ is first calculated theoretically for a given maximum in-plane wave vector of magnons $k_{\max}$ and then obtained density of state function is slightly varied to achieve the best coincidence with the experimental spectrum. Figure 18(b) represents the results of calculation of density of magnons states in the frequency range $(f_{\min}, f_{\perp})$ by means of direct counting over the sites of reciprocal unit, using dispersion relation (20). Black line in the graph shows the density of all states in the given frequency region. Red line represents calculated density of states function $D'(\omega)$ where only magnons with wave vectors $k<k_{\max}=10^5$ cm$^{-1}$ are taken into account. This function was then substituted in Eq. 70 and was slightly varied to obtain the best fit of experimentally measured thermal spectrum. Green line shows the density of the states function $D'(\omega)$ obtained as a result of such procedure, i.e. the BLS intensity spectrum $I(\omega)$ calculated with this function appears to give the best fit of experimental results. The difference between the green and the red lines is easy to understand: the sensitivity of the setup does not go to zero stepwise; it rather fast decreases as soon as $k>k_{\max}$. Corresponding calculated BLS intensity is shown in Fig. 18(a) by solid line. Obtained in such manner value of $D'(\omega)$ is then used for the analysis of the experimental spectra parametrically driven thermalized magnon gas.

Figure 19 shows the results of measurements of evolution of magnons distribution under the excitation by parametric pumping of power $P_p$=4.0 W ($\zeta$=38 dB). Magnons spectra in different panels correspond to different time delays after the start of pumping pulse. A growth of number of magnons with time can be clearly seen from the figure. In particular, noticeable increase in magnons population at low frequencies is observed. According to previous results magnon gas at such pumping powers quickly thermalizes (with thermalization time $\tau_{\text{therm}}\leq$50 ns) and for all delays $\tau>\tau_{\text{therm}}$ it can be regarded as being in a thermodynamically quasi-equilibrium state. Therefore, it should be possible to describe the observed changes of magnon distribution by Bose-Einstein statistic with increasing chemical potential as

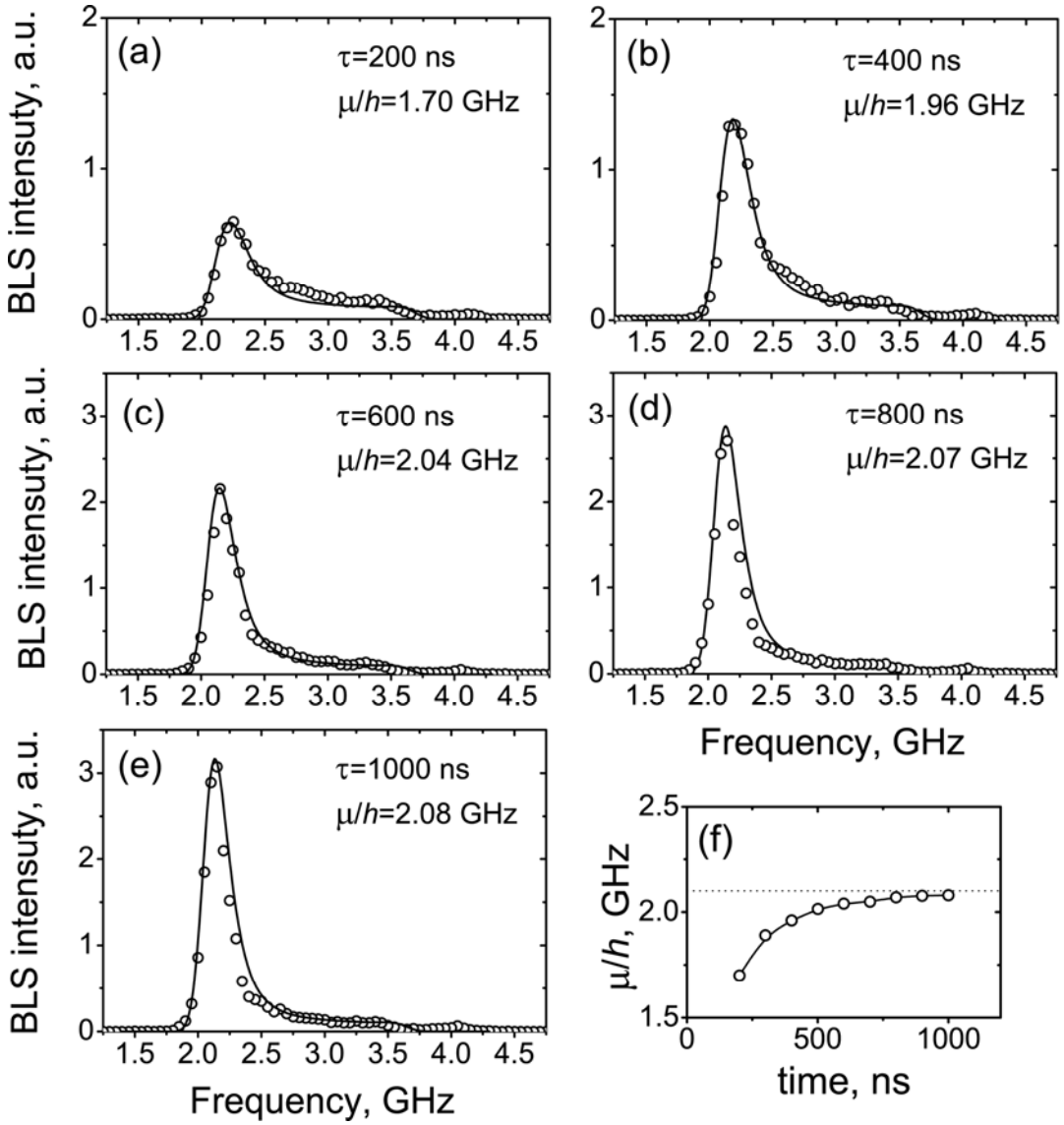


**Figure 19.** (a)-(e) BLS spectra of pumped magnons recorded for different delay times after the start of the pumping pulse ($P_p$=4 W, $H_0$=700 Oe): circles – experiment, solid lines – result of the fit based on Eq. (70); (f) dependence of the chemical potential of magnon gas on time.

pumping inject more magnons into the system. The results of the fit of the experimental spectra by Bose-Einstein distribution function

$n(\omega,\mu)=[\exp(\frac{\hbar\omega-\mu}{\kappa T})-1]^{-1}$ with $\mu$ being fitting parameter using (70) and $D'(\omega)$ extracted from thermal spectrum are shown by solid lines. The corresponding values of chemical potential are also indicated in the graphs. For the sake of better comparability it is presented in frequency units (GHz). The information about the chemical potential is summarized in Fig. 19(f). It is seen, that chemical potential grows with time and saturates at the end of the pumping pulse reaching at $\tau$=1000 ns

the value $\mu/h$=2.08 GHz. This value of the chemical potential is very close to the maximal possible value $\mu_{max}/h = f_{min}$ =2.1 GHz, which, in turn, means, that magnon gas is close to Bose-Einstein condensation.

Figure 20 illustrates magnons spectra measured at a higher pumping power $P_p$=5.9 W ($\zeta$=40 dB). For this pumping power the measured magnon spectrum at $\tau$=300 ns corresponds to the Bose-Einstein distribution function with the value of $\mu/h = f_{min}$ =2.1 GHz (Fig. 20(b)), which means that a critical density of magnons is reached at this delay ($n(\omega,\tau$=300 ns)= $n(\omega,\mu=\hbar\omega_{min})=n_{cr}(\omega)$). Nevertheless, as follows from Figs. 20(c), (d) number of magnons grows further with time. Comparison of the experimental spectra for $\tau$=400 ns and $\tau$=500 ns with the critical distribution $I(n_{cr}(\omega))$ shows, that this growth of total number of magnons affects only the states with frequencies close to the bottom of the spectrum, whereas the population of magnons at higher frequencies remains constant (for the sake of better comparison high frequency tails of magnons distributions are shown on an increased scale). This is further visualized in Fig. 20(e), where the difference $\Delta I(\omega)=I(\omega,\tau>300$ ns)-$I(n_{cr}(\omega))$ is plotted for $\tau$=400 ns and $\tau$=500 ns. As seen from the graph, this difference has a shape of a peak with the width $\Delta\omega=2\pi\Delta f=2\pi\cdot$250 MHz which is equal to the frequency resolution of the interferometer. This allows to conclude that the observed difference in experimental spectra $\Delta I(\omega)$ is caused by very narrow magnons population peak $\Delta n(\omega)$. In fact, it appears that that $\Delta I(\omega)$ is nicely fitted by instrumental function $\Delta I(\omega) = \int A(\omega-\omega')D'(\omega')\Delta n(\omega')d\omega' = \alpha A(\omega-\omega_{min})$ (corresponding fits are shown by solid lines) which directly implies $\Delta n(\omega) = n_0\delta(\omega-\omega_{min})$. Thus, a fully correspondence between the observed situation and BEC transition scenario can be pointed out: after the concentration achieves some critical value all newly introduced particles are accumulated at the lowest energy state.

To prove further the conclusion that the finite width of the observed peak at minimal frequency is caused solely by the limited frequency resolution of the spectrometer additional measurements with better resolution were carried out. In all cases the width of the peak correlated with the value of the spectral resolution of the interferometer. Minimal width, obtained with the best achieved resolution value is 50 MHz (see inset in Fig. 20(e)).

It is worth noting, that based on the estimation, made in the beginning of this section temperature of magnon gas was regarded as to be constant in all fitting procedures.

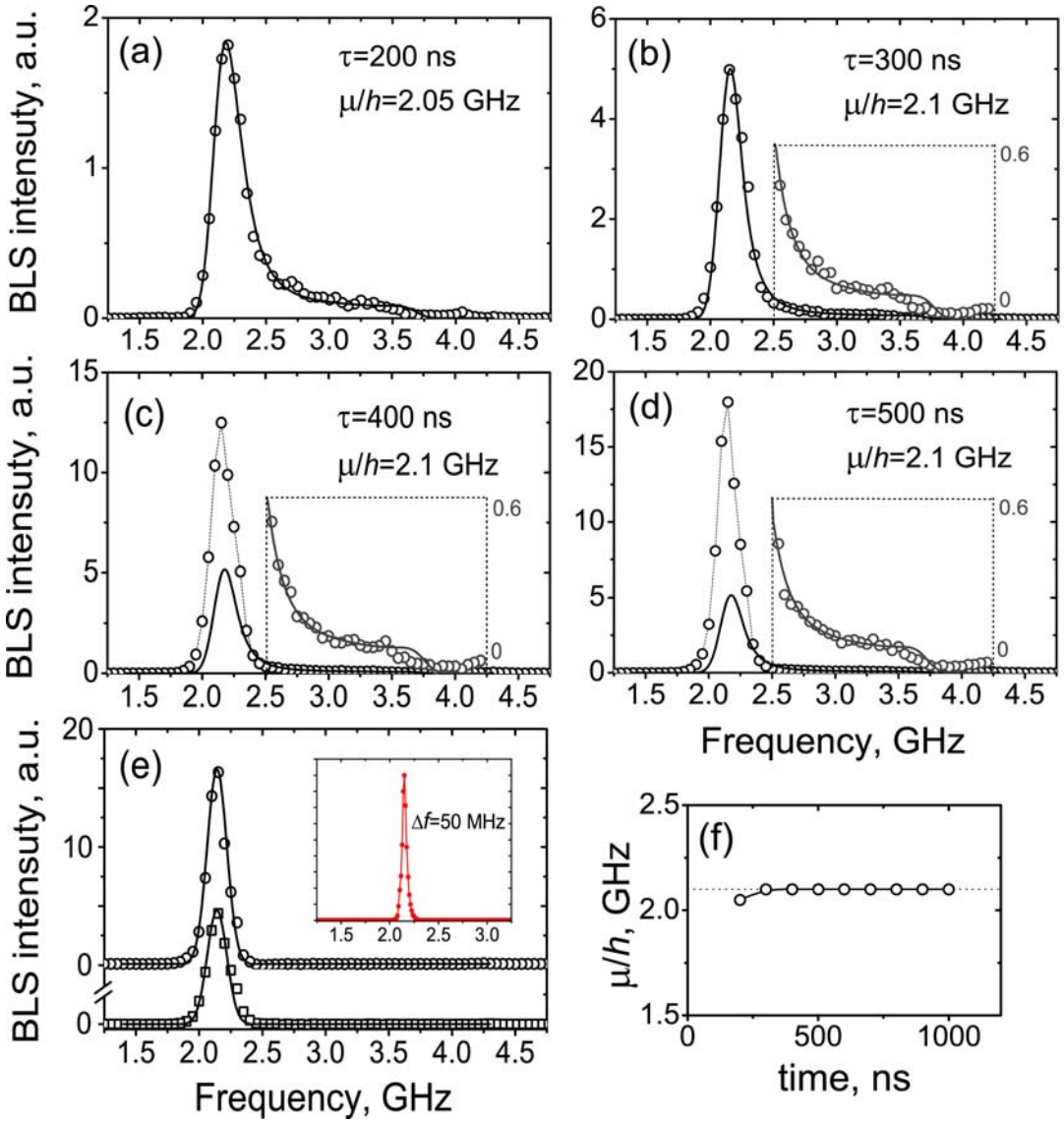


**Figure 20.** (a)-(d) Time evolution of magnons BLS spectrum for pumping power $P_p$=5.9 W: circles – experiment, solid lines in (a), (b) best fit using Eq. (20), lines in (c), (d) –calculated critical magnon distribution with $\mu=hf_{\min}$. (e) Differences between spectra measured at $\tau$=400 ns and $\tau$=500 ns (squares and circles) and critical magnon distribution; lines – results of fit with the instrumental function of the interferometer; inset – magnon distribution measured with the ultimate resolution of the interferometer. (f) Dependence of the chemical potential of magnon gas on time.

This approach, being fairly reasonable, however is not the only reason for temperature can be omitted in the current consideration. In fact, since the energies of magnons $\hbar\omega$ are much smaller than the mean thermal energy of the gas $\kappa T$ the shape of the magnons distribution $n(\omega)=\left[\exp\left(\frac{\hbar\omega-\mu}{\kappa T}\right)-1\right]^{-1}\approx\frac{\kappa T}{\hbar\omega-\mu}$ appears not to depend on

the temperature, since $\kappa T$ serves just as a multiplication factor. Thus, the value of the chemical potential, obtained by the fitting procedure and the assignment of the critical distribution ($n_{cr}(\omega)$) to the certain experimental conditions, described above, is insensitive with respect to changes of $T$ (until $\hbar\omega << \kappa T$).

Thus, experimental results cited here provide a direct evidence of quasi-equilibrium Bose-Einstein condensation in pumped magnon gas at room temperature. Pumped magnons, initially observed to be distributed over the whole accessible frequency range at some critical pumping power form extremely narrow ($\Delta f \leq 50$ MHz) peak at the minimal frequency of magnons spectra. Besides being observed at room temperature the effect of magnon BEC has another intrinsic feature, which distinct it from all other known BEC transitions: the minimum energy is doubly degenerated, namely two points in $k$-space correspond to minimal frequency of magnons ($\pm k_{min}$, $\omega_{min}$). That means that magnon condensate is composed of two sorts of magnons with opposite directed wave vectors. This fact demonstrates universal nature of BEC and makes further investigation of magnon condensation attractive from the general point of view.

### 4.3 Spatiotemporal dynamics of magnon Bose-Einstein condensate

Being itself one of the most fascinating phenomena BEC opens way for further investigation, implying the condensation being is not only the ultimate goal to be reached but rather assuming experiments with the condensates as macroscopic quantum objects and the interaction of two or more of them. In fact, since the all particles in the condensate behave as a single wave (described by the wave function of the lowest energy state) one can expect to observe coherent wave-like effects involving macroscopic number of particles. Moreover, the presence of interaction between single particles allow for nonlinear dynamics. In particular, formation of solitons [106, 107] and collapse [108] in atomic Bose-Einstein condensate was experimentally observed. Besides experiments on single condensate dynamics, interference [109] and linear Josephson oscillations [110] along with effect of nonlinear self trapping [111] in the system of two interacting condensate were reported. The fact that the experiments are mainly carried out with atomic condensates is explained by their relatively long lifetimes allowing for them, once being prepared,

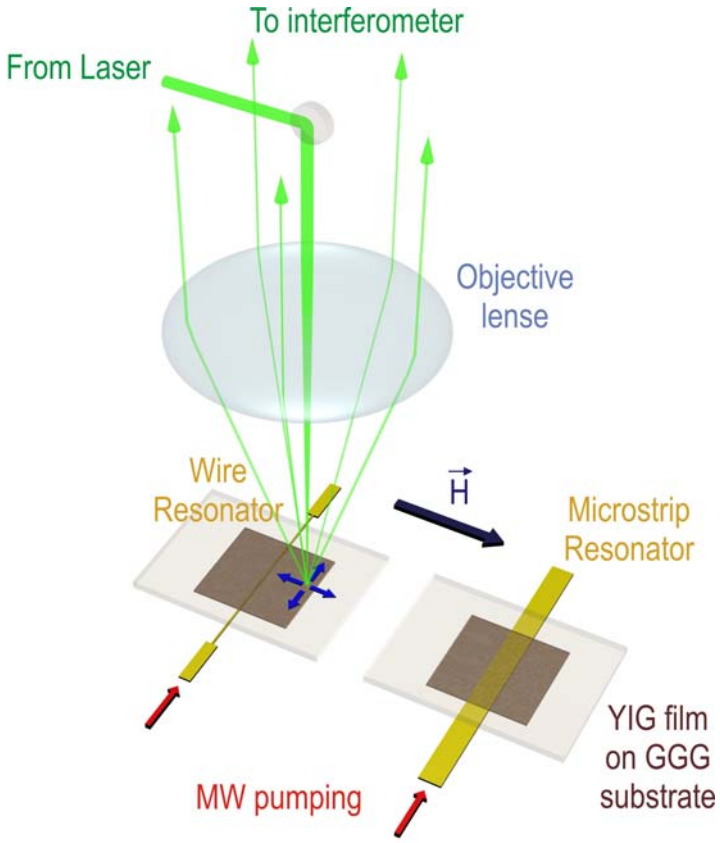


**Figure 21.** Arrangement of the film, pumping resonators and the probing light, used in the experiment

to be manipulated by means of applying of energy potentials with different spatial configuration.

The disadvantage of magnons BEC caused by the fact that it can be observed only under the action of external pumping can, however, play positive role. In fact, instead of manipulations with prepared condensate one can, apparently, make use of correlation between the spatial configuration of the pumping and the condensate, excited by it.

This section represents results of investigation of spatial characteristics of magnon condensate and its temporal evolution by means of space and time resolved BLS spectroscopy. In particular, the problem of control over the spatial characteristics of magnon condensate through the configuration of pumping field is addressed.

The experiments were performed on 5.1 μm thick YIG film in quasi-backscattering geometry. The measurement procedure similar to that, described in the previous sections, was applied for these studies at different positions of the focal laser spot over the film surface. The only difference was that additional small space gap was introduced between the film and the resonator and the probing light was now reflected from YIG-air interface. This provided constant reflectivity for all points on film surface, allowing to avoid problems with different reflection condition for region

directly above the resonator, which might cause uncontrolled fluctuations of the BLS-intensity (see Fig. 21).

In order to examine possible influence of the shape of the pumping resonator on the spatial distribution of the condensate two sets of measurements with two resonators were performed. Along with the 25 μm diameter wire resonator used in the previous experiments, rather wide microstrip resonator with the width of 500 μm was also employed (Fig. 21). Both resonators were tuned to have the same resonant frequency $f_0 \approx 8.1$ GHz.

All measurements of spatial distribution of the condensate were preceded by the preliminary measurements in phase space. The distribution of magnons over the entire range of the frequencies was examined in order to determine the minimum frequency of the magnon spectrum i.e. the frequency of the condensed magnons $f_{min}$. After that, the pass band of the interferometer was constricted to $f=f_{min}\pm150$ MHz. That ensured that the detected signal corresponded to the condensate and was free from the contribution from the other magnons. As one would expect from the symmetry reasons, the measured spatial distributions of magnons were found to be uniform along the length of the resonators. Therefore, one can restrict himself to the analysis of one-dimensional distributions of the condensate density over the spatial coordinate $z$ perpendicular to the axis of the resonator and their temporal dependences.

Figure 22 represents typical results of the spatio-temporal measurements for the case of the wire resonator obtained at $H_0=1000$ Oe and $P_p=4$ W. The dependence of the condensate density on the spatial coordinate $z$ is shown for different time delays $t$ with respect to the onset of the pumping pulse (Fig. 22(a)). The graph shows a certain time delay in appearance of the condensate with respect to the start of the pumping. As described above, this delay is due to magnon thermalization, which is necessary for formation of the condensate. As soon as the thermalization process is over, magnon condensate arises. The figure reveals some initial spatial expansion of the condensate, but after the certain time its width is decreased and a steady state with a constant spatial distribution is formed. As it is seen from the figure, the condensate cloud is concentrated over the resonator, and has a maximum density at its center. This result is in a good agreement with the conception of BEC of magnons developed in previous sections. Since the condensation arises as a consequence of the injection of magnons due to the parallel pumping instability process, its spatial characteristics should map the properties of the pumping. This fact is further illustrated in Fig. 22(b),

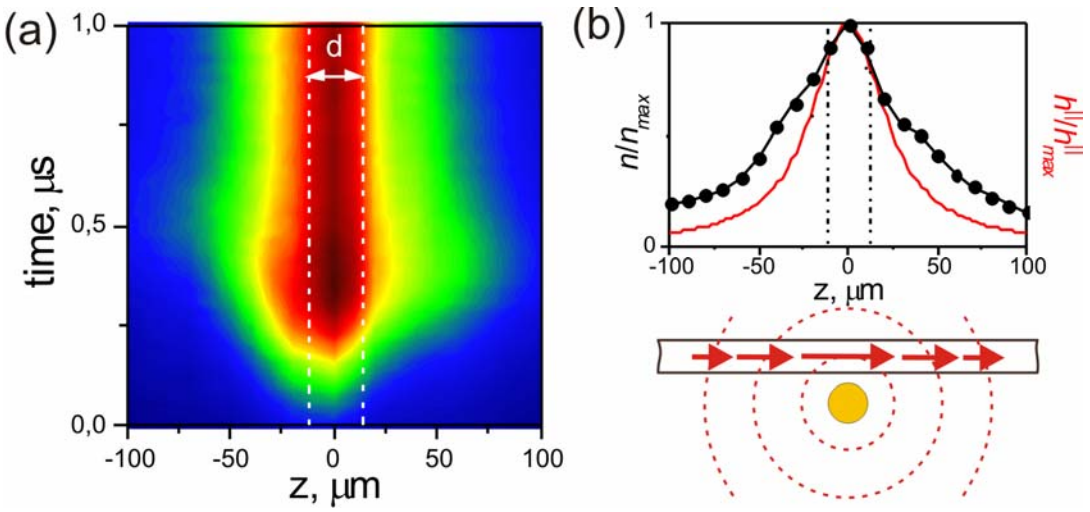


**Figure 22.** (a) Experimentally measured distribution of the condensate density as a function of time and distance from the centre of wire resonator in colour-coded representation; static magnetic field $H_0$=1000 Oe, pumping power $P_P$=4 W. (b) Top: settled distribution of the spatial density of the condensate measured at the time delay $\tau$=1 μs and the calculated dependence of the parallel component of the pumping field $h_{||}(z)$; bottom: schematic layout of the cross-section of the experimental structure.

where the settled distribution of the condensate along with the dependence of the parallel component of microwave field $h_{||}$ over the coordinate $z$ in the plane of the film is plotted. For the calculation of the latter a well known expression for the magnetic field of a straight current-carrying wire $(\vec{h}(r) = \frac{2}{c}\frac{\vec{I}\times\vec{r}}{r^2})$ was used: $h_{||}(z) = h_0 \frac{1}{1+z^2/\Delta^2}$, where Δ - is a distance from the center of the wire resonator to the plane of the film. Direct correspondence between the pumping field profile and the distribution of magnons in condensate can be nicely observed. Slightly larger spatial size of the condensate cloud should be addressed to the spreading of the initially exited magnons during the thermalization.

To further investigate the influence of the configuration of pumping field on the distribution of magnons in condensate measurements with the wide ($w$=500 μm) microstrip resonator were carried. Typical picture of the spatial-temporal dynamics of the magnon condensate, excited by the microstrip resonator, is shown in Fig. 23(a). Observed distribution drastically differs from that, presented in Fig. 22(a) - instead of one condensate cloud, concentrated over the resonator, two separate condensates are

formed. By mapping the position of the microstrip onto the observed distribution (dashed line) one concludes that the condensates arise at the edges of the resonator, so that the spatial separation between them is equal to the width of the microstrip $w$. Despite completely different spatial distributions of the condensate density, the time evolution of each separate condensate is similar to that, observed for wire resonator: after some initial expansion, a slight decrease of the width of the condensate cloud followed by stabilization is seen.

The shape of the observed distribution is, apparently, connected with the properties of the pumping process. An explanation can be found if one recalls that there are two different types of parametric instability in ferromagnets: parallel pumping, caused by the dynamic magnetic field $\vec{h}$ parallel to the static magnetization $\vec{M}_0$, and perpendicular pumping, which arises when $\vec{h} \perp \vec{M}_0$ (see section 2.5). Since the pumping field, created by the resonators in our experiments has components both parallel and perpendicular to the static field, both kinds of instability are potentially possible. The case of oblique pumping, when both components of the pumping fields are present was addressed in details in [112, 113]. The main conclusion of these

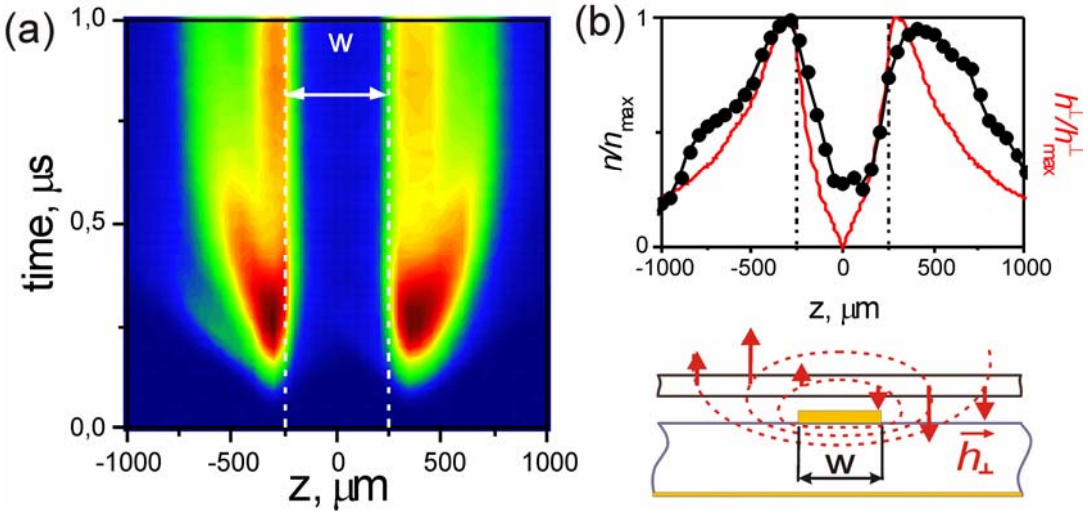


**Figure 23.** (a) Experimentally measured distribution of the spatial density of the condensate as a function of time in colour-coded representation for the case of microstrip resonator; static magnetic field $H_0$=1000 Oe, pumping power $P_P$=4 W. (b) Top: settled distribution of the spatial density of the condensate measured at the time delay $\tau$=1 μs and the calculated dependence of the parallel component of the pumping field $h_{||}(z)$; bottom: schematic layout of the cross-section of the experimental structure.

works is that under given experimental conditions the instability characterized by a smaller power threshold dominates over the other. In general case the threshold of the parallel pumping is lower for the low fields (when frequency of pumped magnons corresponds to the exchange part of the spectrum) while the perpendicular pumping dominates at high fields (when dipole magnons are pumped). Using the theory developed in [48] one can calculate the thresholds values of the dynamic magnetic field for the parallel and the perpendicular instability for given experimental conditions (YIG film, $H_0$=1000 Oe). They were found to be $h_{thr}^{\parallel} \approx 0.99$ Oe and $h_{thr}^{\perp} \approx 0.75$ Oe, i.e. they are rather close to each other. At the same time calculation of field configuration for wire resonator gives for the maximal values of the components $h_{\max}^{\parallel} = 2h_{\max}^{\perp}$ ($\vec{h}(r) = \frac{2}{c}\frac{\vec{I} \times \vec{r}}{r^2}$), whereas for microstrip resonator, using approach developed in [114], one obtains $h_{\max}^{\parallel} \approx h_{\max}^{\perp}$. Thus, for given experimental conditions, parallel pumping dominates for a wire resonator whereas regime of perpendicular pumping is realized for a microstrip. As a further proof of this fact, a good correspondence between the condensate density distribution and the profile of perpendicular component of dynamic field of the microstrip resonator plotted in Fig. 23(b) can be pointed out.

As a next step the spatial width of the single condensate cloud in the two-condensate regime was investigated. Figure 24(a) represents the time evolution of the full width at a half maximum (FWHM) value of the observed condensate distribution for different pumping powers. The initial growth of the width can be referred to the flow of the magnons from the pumping to the condensate. Since the condensation is a threshold process and the flow of magnons from the pumping to the condensate is provided by the four-magnon scattering, which depends on magnon density, condensate first arises at the point corresponding to the maximum of the pumping field. Then it spreads as the critical density is reached locally for the other spatial points. This continues until the energy flow from the pumping is balanced by the decay of the condensate. The further decrease of the width observed for high powers can be caused by the spatial dynamic of already formed condensate. This compression of condensate cloud fully corresponds with the fact that the interaction between magnons in current experimental configuration is attractive [115]. Thus it is not

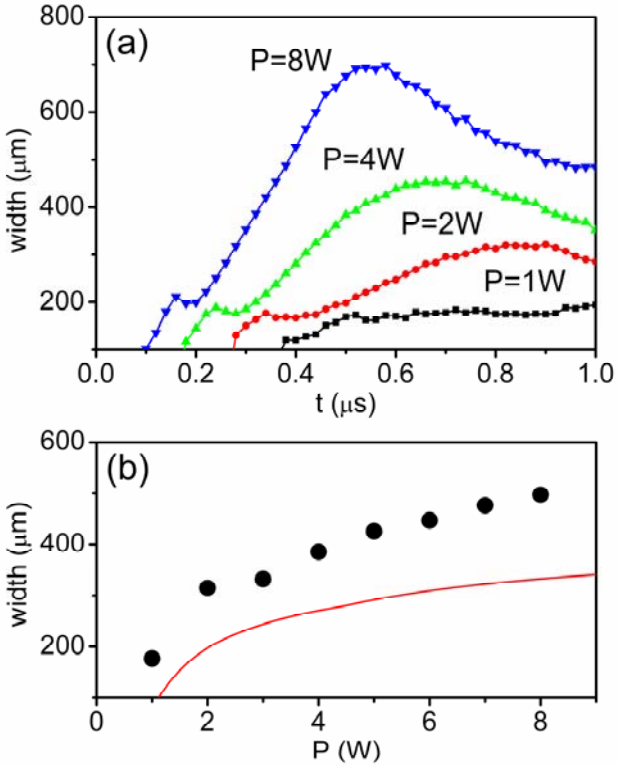


**Figure 24.** (a) Temporal dependences of the spatial width of the condensate clouds for the case of the two-condensate regime for different pumping powers $P$, as indicated. (b) Width of the condensate clouds corresponding to the end of the pumping pulse as a function of the pumping power. Points – experiment, line – theory.

surprising, that the compression becomes more pronounced with increase in pumping power.

In spite of the presence of some spatial dynamics an important conclusion about common increase of the width of the condensate cloud with the pumping power $P_p$ can be made. This is also a consequence of the threshold character of the condensation process, which demands the density of magnons to be larger than some critical value $n > n_{cr}$. It is obvious, that with the increase in the pumping power the size of the spatial region were the threshold of the condensation is reached increases as well. This width can be estimated based on the distribution of the pumping field, shown in Fig. 23(b), and the fact, that the number of magnons excited by pumping is $n \sim \sqrt{h^2 - h_{thr}^2} > n_{cr}$, where $h$ - is the microwave pumping field applied to the sample and $h_{thr}$ is its threshold of parametric pumping process. Taking into account that $h_{thr} << h$ one obtains following condition for the condensation region $h(z) > h_{cr} \sim \sqrt{n_{cr}}$, where $h_{cr}$ is the field corresponding to the onset of the BEC. The results of these calculations are shown in Fig. 24(b) by the line. Comparing the

experimental and the theoretical data one can see their good qualitative agreement. Note that the experimentally determined width of the condensate appears to be slightly larger than the theoretical one. This result is expected, since the additional spreading of the condensate cloud due to the non-zero velocities of the magnons, existing at the intermediate stage between the pumping and the condensate is not taken into account in the estimation cited above. The same effect leads to the absence of an abrupt decrease of the condensate intensity at the spatial point, where the pumping field becomes smaller than the threshold field on the observed experimental distributions (Figs. 22(a), 23(a)).

Concluding this section one can point out that obtained results on spatiotemporal dynamics of magnon condensate demonstrate a possibility of control over the spatial distribution of magnons through the geometry of pumping resonator. In particular, two separated condensates can be excited with controllable separation and spatial width, which creates a perfect base for further study of interaction of magnon Bose-Einstein condensates.

### 4.4 Radiation of magnon Bose-Einstein condensate

In the previous sections it was shown that magnons in YIG being pumped by parametric pumping can undergo BEC transition when power of the pumping exceeds some critical value. As a result of such transition an essential part of magnons is accumulated in the lowest energy state and forms Bose-Einstein condensate – a macroscopic quantum state of coherent magnons. In classical interpretation formation of magnon condensate means appearance of intense dynamical component of magnetization over a macroscopic area of the sample, which should radiate electromagnetic waves. Experimental observation of such radiation would be a clear proof of the coherent nature of the condensate. This section represents the result of experimental investigation of microwave radiation generated by Bose-Einstein condensate of magnons in YIG films. The properties of the radiation are examined in details with respect to the properties of the pumping signal, to prove the possibility of above discussed energy conversion.

The layout of the experimental setup is shown in the Fig. 25(a). The standard arrangement of the microwave part (see Fig. 12) was slightly changed, due to the necessity of microwave detection of the radiation of the condensate. The pumping

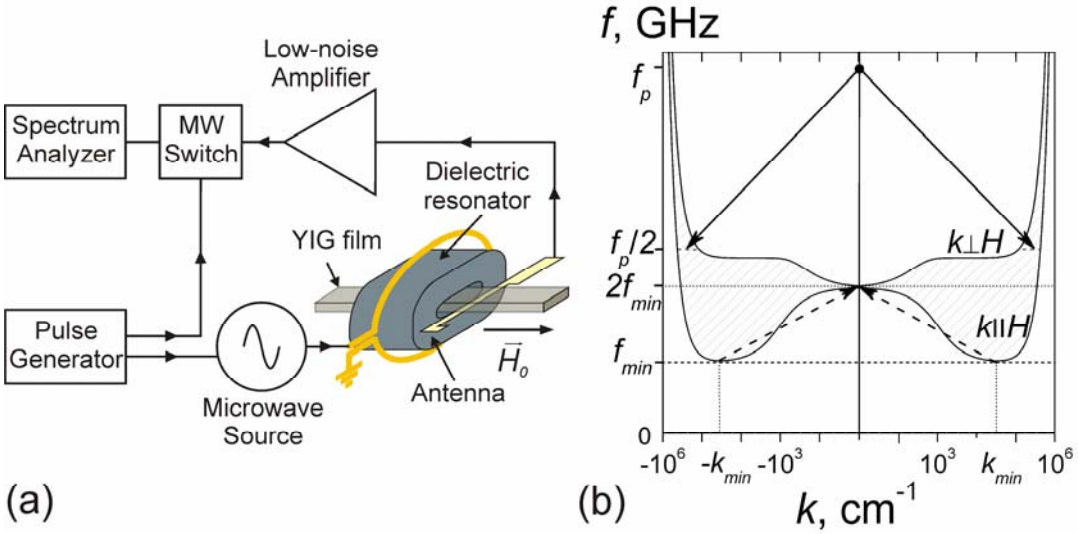


**Figure 25.** (a) Schematic layout of the experimental setup. (b) Spectrum of magnons for 5 μm thick YIG film at $H_0$=520 Oe. Solid lines illustrate parametric pumping process, dashed lines – confluence process of two magnons from the bottom of the spectrum.

field is now created by open dielectric resonator which is driven by means of conducting-wire loop serving as a coupling element between the resonator and the microwave transmission line. The system is fed with microwave pumping pulses with a duration of 5 μs and a repetition period of 5 ms. The pumping frequency of about $f_p$=8.21 GHz, corresponds to the $TM_{110}$ oscillation mode of the resonator. The utilization of open dielectric resonator allows to minimize the mutual coupling between the pumping channel and the part of the experimental setup, serving for detection and analysis of the electromagnetic radiation arising in the system. The detection of the radiation is performed by means of 40 μm wide microstrip pickup antenna attached to the surface of the film close to the edge of the resonator. The microwave signal induced in the antenna is amplified by a low-noise microwave amplifier and then is sent to a spectrum analyzer. A microwave switch is introduced between the antenna and the spectrum analyzer in order to have a possibility to analyze the received signal after the pumping pulse, which excludes any influence of the pumping on the observed spectra.

The spectrum of magnons along with the schematic representation of main processes occurring in the system during the experiment is shown in Fig. 25(b). As in previous experiments, pumping injects substantial number of magnons into the film, which then quickly redistribute over the spectrum (thermalize) and a quasi-equilibrium state is settled. For high pumping powers most of the pumped magnons

are accumulated in the states with the minimal frequency $f_{min}$, (the overpopulation of this state reaches several orders of magnitude) and form a condensate. As discussed above, for magnons in tangentially magnetized films there are two states with minimal frequency ($\pm k_{min}$, $\omega_{min}$) corresponding to two oppositely-directed wave vectors. The value of the minimal frequency depends on the magnetic field $H_0$ ($\omega_{min} = 2\pi f_{min} \sim \gamma H_0$) whereas the value of the wave vector is mainly determined by the thickness of the film. For 5 μm thick YIG film and $H_0$~0.5 kOe one obtains for the magnons at the bottom of the spectrum $f_{min}$~1.5 GHz and $k_{min}$~$3.5\times10^4$ cm$^{-1}$ which is significantly larger than the wave vector of electromagnetic waves of the same frequency $k_{em}=2\pi f_{min}/c\approx0.3$ cm$^{-1}$. This means that although the transverse dynamic magnetization, corresponding to these magnons, is huge, there is almost none direct electromagnetic radiation at frequency $f_{min}$ due to the significant mismatch in their wave vectors (i.e., direct radiation of photons by condensed magnons is forbidden by the momentum conservation law).

However, using the process of confluence of magnons from different minima (see dashed arrows in Fig. 25(b)), one can reduce the wave vector of the magnetization oscillations corresponding to magnons at the lowest states. In fact, since the both minima in magnon spectrum ($\pm k_{min}$, $\omega_{min}$) are symmetric with respect to each other, the resulting magnon, created by confluence of two magnons from different minima will have frequency $f=2f_{min}$ and almost zero wave vector $k\approx0$. Such magnons can easily radiate photons, the latter being detected by the pickup antenna.

Fig. 26(a) represents the results of measurements of the power of the electromagnetic signal at frequency $2f_{min}$ detected by the pickup antenna as a function of pumping power. A radiation of the condensate is undoubtedly observed, confirming the coherent nature of the created condensate. From figure it also follows that there is a certain threshold in pumping power ($P_{th}\approx4.5$ W), above which a radiation is observed. For pumping powers just below this value the power of the radiation lays below the noise level $P^{(rad)}(P_p< P_{th})\leq0.05$ μW. This is, apparently, caused by the threshold character of both BEC and the process of confluence of magnons from bottom states ($\pm k_{min}$, $\omega_{min}$).

Fig. 26(b) shows the spectra of the signal discussed above recorded for pumping powers corresponding to different parts of the dependence illustrated in Fig. 26(a): just above the threshold value, for intermediate powers and in the saturation region. All spectra were measured during 1 μs time window starting 100 ns after the end of

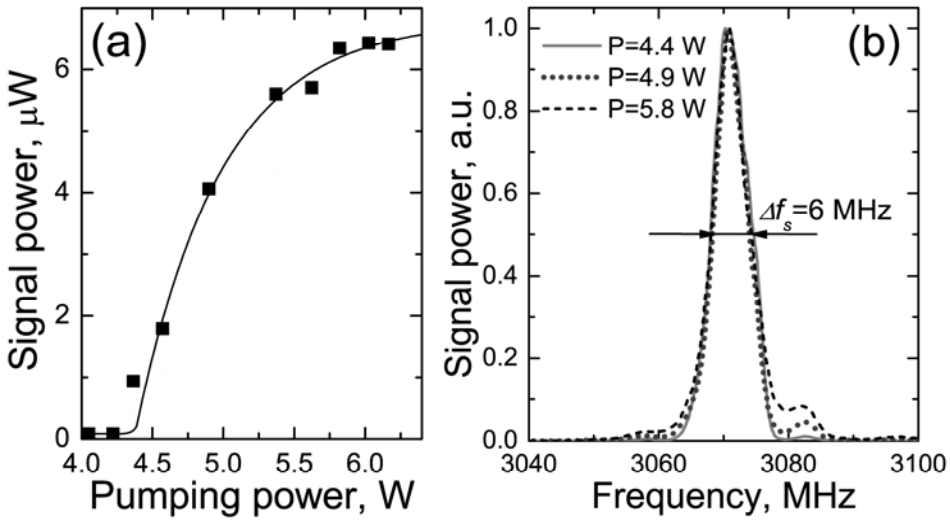


**Figure 26.** (a) Dependence of the power of microwave radiation vs pumping power. (b) Normalized spectra of the radiation for different pumping powers. $H_0$=520 Oe.

the pumping pulse. The chosen delay guaranties that the measured spectra are free from direct influence of the pumping and represent properties of the thermalized magnon gas. On the other hand, the chosen width of the window exceeds the magnon lifetime excluding, therefore, any effects of additional spectrum broadening due to the finite measurement time. The spectra are normalized at their maxima for convenience of the comparison. As follows from the graph, the width of the spectra of the radiated signal practically does not change with the pumping power being equal $\Delta f_S$=6 MHz in the whole observable range.

The constant value of the linewidth for different pumping power indicates that the observed spectra at $2f_{min}$ is a result of confluence of magnons from single states rather than from states in some frequency band near $f_{min}$. The fact is that according to previous observations the distribution of magnons near the bottom of the spectrum converges with increase in pumping power, whereas none narrowing is observed for spectrum of radiation at double frequency. However, although being rather small, the obtained value of the linewidth is still larger than the value one would expect to obtain for radiation caused by the confluence of magnons from single quantum states. In fact, the intrinsic linewidth of the single mode, corresponding to certain magnon, is determined by its lifetime $\Delta f = (2\pi\tau_0)^{-1}$. For typical values of spin-lattice relaxation times of $\tau_0$~0.25 μs one obtains $\Delta f$≈0.6 MHz. A possible explanation of this

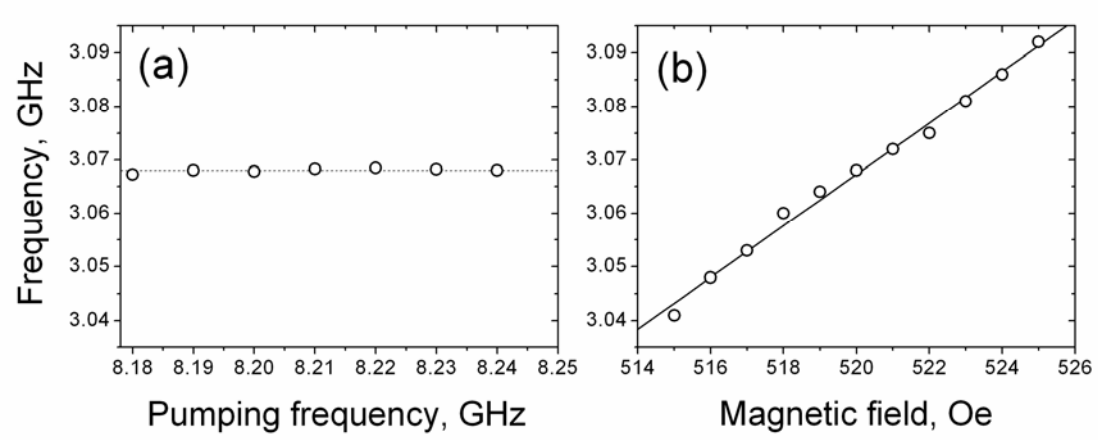


**Figure 27.** Dependence of the frequency of the radiation vs pumping frequency (solid squares) and magnetic field (open circles); solid line is the best linear fit of the field dependence.

discrepancy can lie in the fact that the confluence process itself, as a process which leads to an annihilation of magnons at the lowest energy state, can be treated as an additional relaxation channel, increasing, therefore, the linewidth of the emitted microwave signal.

Figure 27 summarizes the results of the measurements of the frequency of the radiated signal as a function of the pumping frequency $f_0$ (Fig. 27(a)) and static magnetic field $H_0$ (Fig. 27(b)). Obtained results fully correspond to the ideas discussed at the beginning of this section. As seen from the figure, the frequency of the emitted radiation does not depend on the frequency of the pumping. During the measurements the latter was varied in the range allowed by the width of the resonant line of the pumping resonator ($\Delta f_0$=60 MHz). At the same time the frequency of the microwave signal remained constant with the accuracy within the experimental error ($\delta f$<3 MHz). This results directly indicates on the possibility of the system to convert any frequency into the monochromatic radiation with $f$=2$f_{min}$. Thus, it can be successfully used for the purposes of spectral compression of the energy of broadband incoherent radiation, provided the latter is powerful enough to ensure magnon thermalization and condensation. The required density of energy of incoherent radiation can be provided by its focusing on the sample or, in some cases, conventional coherent pumping can be used as seeding. As also follows from the figure, the frequency of the resulting radiation can be controlled by tuning the static magnetic field. In accordance with the fact that the observed microwave signal is a

result of confluence of two magnons with $\omega_{min}=2\pi f_{min}=\gamma H_0$ obtained dependence of its frequency on the magnetic field is linear and characterized by the slope equal to $2\gamma$.

Thus, obtained results demonstrate an ability of the system of pumped magnons for conversion of arbitrary frequency pumping into a signal with constant microwave frequency controlled by the applied magnetic field. The conversion is based on the effect of BEC of pumped magnons. The linewidth of the emitted radiation is relatively small and appears to be independent on the external characteristics (magnetic field, frequency and the power of the pumping) being, therefore, determined by the properties of the processes inside the magnon system.

One can, apparently, make use of the observed radiation for purposes of generation of coherent microwaves in a way similar to applications of uniform precession mode in YIG oscillators [47]. An efficiency of a BEC-based device appears to be doubtful at the first glance, since to obtain a microwave signal from condensate one needs first to apply parametric pumping (a microwave signal of different frequency). However, intrinsic properties of BEC can result in certain advantages, making reasonable the utilization of such conversion. In fact, since BEC occurs as a result of multi-step thermalization process of pumped magnons with their further accumulation in the lowest energy state, whose frequency is determined solely by the applied magnetic field there is, obviously, no principal constrains on the frequency of the pumping field. Moreover, spectrally wide pumping signal containing different frequencies appears to be even more preferable for condensation, since it favors faster thermalization of pumped magnons [116]. Thus, under condition of BEC a conversion of the energy of broadband electromagnetic radiation into a monochromatic signal generated by the condensate becomes possible. This effect might be very attractive if used in far-infrared frequency region, since radiation of these frequencies dominates in the room-temperature environment and can easily be focused on such a converter.

# Chapter 5

# Summary and outlook

The presented thesis addresses experimental study of kinetic processes in parametrically driven magnon gas in YIG films. Besides providing novel experimental data on magnetic relaxation processes, the main motivation for the current investigation was a possibility of experimental observation of Bose-Einstein condensation in quasi-equilibrium magnon gas. Successfully achieved in experiments BEC of magnons was then further investigated, addressing, mainly, properties of the magnon condensate. In particular, its spatiotemporal dynamics and properties of microwave radiation, generated by the condensate, were studied. Space- and time-resolved Brillouin light scattering technique in combination with standard microwave technique for excitation and detection of magnons were used for the current investigations.

At the first step a detailed investigation of thermalization of parametric magnons was carried out. Taking advantage of high temporal resolution of BLS technique it was possible to observe directly all stages of the thermalization process: excitation of primary magnons by the parametric pumping, their interaction with thermal magnons and creation of secondary magnons with subsequent redistribution of the latter over the magnon spectrum. This redistribution was found to happen as a result of multiple magnon-magnon scattering events. The main mechanism for this scattering, four-magnon interaction, depends on the concentrations of magnons involved. Thus, increasing the pumping power and, consequently, the number of injected magnons it was possible to observe an increase in efficiency of magnons redistribution over the spectrum. Moreover, at some critical power, the efficiency of the redistribution process was high enough to provide total thermalization of injected magnons with the entire magnon gas. As a result, a quasi-equilibrium state of pumped magnon gas described by Bose-Einstein statistics was observed to be settled in the system within the lifetime of magnons. For pumping powers higher then this critical value, thermalization time was found to decrease quickly and to reach the value of 50 ns, which is about order of magnitude smaller than magnon lifetime. Observed quick thermalization of magnons straightforwardly opens a way to the experimental investigation of Bose-Einstein condensation, since it shows a possibility of creation of quasi-equilibrium pumped gas with increased number of magnons.

The experiments on thermalization of magnon gas were then directly followed by measurements at higher pumping powers. Experimentally measured distributions of

magnons were used to determine a chemical potential $\mu$ of the quasi-equilibrium pumped magnon gas, created in these experiments. The chemical potential $\mu$ characterizes a quantum degeneracy of magnon gas. It was found to increase with the pumping, reflecting the growth of the total concentration of magnons due to their parametric excitation. At high enough pumping power the value of the chemical potential $\mu$ reached its maximum value $\mu = \hbar\omega_{min}$, which indicated the onset of Bose-Einstein condensation. At the same time an appearance of an intense narrow peak of magnon population at the lowest magnon frequency was observed in experimentally measured spectra. The conclusion about Bose-Einstein condensation was also supported by the analysis of the experimentally measured distributions for higher densities of magnons. It appeared that the injection of additional magnons above the critical value changes the distribution of magnons only close to the minimal frequency (within the limits of the peak at the bottom), whereas the population of magnons at all other frequencies remains constant. The above mentioned behavior allowed to associate the observed peak with the Bose-Einstein condensate of magnons.

To verify the assumption about the BEC of magnons, further measurements of the spectral width of the peak at the bottom were carried out. Its observable width was found to be determined solely by the frequency resolution of the setup, which means that the intrinsic width of the peak is much smaller than this value. BLS measurements with the ultimate resolution have shown that it is less than 50 MHz.

As a next step in investigation of magnon Bose-Einstein condensation the spatial properties and the dynamics of the condensate were studied experimentally. In accordance with the fact that the condensate arises as a result of action of parametric pumping a direct correspondence between the spatial profile of the condensate cloud and the configuration of the pumping field was observed. In particular, using a specific character of dynamic fields produced by a pumping resonator, simultaneous excitation of two spatially separated condensate clouds was realized. Moreover, it follows from the measurements that the separation between the condensates excited in this experiment, as well as their spatial width, can be varied in a controllable way.

Finally, a radiation of microwave signal by the condensate was observed in a series of experiments with microwave detection of magnons. An existence of such radiation is a clear evidence of the coherent nature of magnon condensate. The frequency of the radiation, as well as its linewidth, was found not to depend on the frequency and the

power of the parametric pumping (as long as its value is above the threshold of condensation). At the same time, the frequency of the radiation can be controlled by the applied static magnetic field.

## References


1. F. Bloch, *Zur Theorie des Ferromagnetismus*, Z. Phys. **61**, 206 (1930).

2. J. H. E. Griffiths, *Anomalous High-Frequency Resistance of Ferromagnetic Metals*, Nature **158** 670 (1946).

3. N. Bloembergen and R. W. Damon, *Relaxation Effects in Ferromagnetic Resonance*, Phys. Rev. **85**, 699 (1952).

4. N. Bloembergen and S. Wang, *Relaxation Effects in Para- and Feromagnetic Resonance*, Phys. Rev. **93**, 72 (1954).

5. H. Suhl, *The Theory of Ferromagnetic Resonance at High Signal Powers*, J. Phys. Chem. Solids **1**, 209 (1957).

6. M. G. Cottam, *Linear and Nonlinear Spin Waves in Magnetic Films and Superlattices*, World Scientific Publishing, Singapore (1994).

7. P. E. Wiegen, *Nonlinear Phenomena and Chaos in Magnetic Materials*, World Scientific Publishing, Singapore (1994).

8. M. Sparks, *Ferromagnetic Relaxation Theory*, McGraw-Hill, New York (1964).

9. A. S. Borovik-Romanov and N. M. Kreines, *Brillouin-Mandelstam Scattering from Thermal and Excited Magnons*, Phys. Rep. **81**, 351 (1982).

10. S. O. Demokritov, B. Hillebrands and A. N. Slavin, *Brilluoin Light Scattering Studies of Confined Spin Waves: Linear and Nonlinear Confinement*, Phys. Rep. **348**, 441 (2001).

11. P. Kabos, G. Wiese, and C. E. Patton, *Measurement of Spin Wave Instability Magnon Distributions for Subsidiary Absorption in Yttrium Iron Garnet Films by Brillouin Light Scattering*, Phys. Rev. Lett. **72**, 2093 (1994).

12. M. H. Anderson, J. R. Ensher, M. R. Matthews, C. E. Wieman, and E. A. Cornell, *Observation of Bose-Einstein Condensation in a Dilute Atomic Vapor*, Science **269**, 198 (1995).

13. C. C. Bradley, C. A. Sackett, J. J. Tollett, and R. G. Hulet, *Evidence of Bose-Einstein Condensation in an Atomic Gas with Attractive Interactions*, Phys. Rev. Lett. **75**, 1687 (1995).

14. K. B. Davis, M.-O. Mewes, M. R. Andrews, N. J. van Druten, D. S. Durfee, D. M. Kurn, and W. Ketterle, *Bose-Einstein Condensation in a Gas of Sodium Atoms*, Phys. Rev. Lett. **75**, 3969 (1995).

15. A. Griesmaier, J. Werner, S. Hensler, J. Stuhler and T. Pfau, *Bose-Einstein Condensation of Chromium*, Phys. Rev. Lett. **94**, 160401 (2005).

16. G. Modugno, G. Ferrari, G. Roati, R. J. Brecha, A. Simoni, and M. Inguscio, *Bose-Einstein Condensation of Potassium Atoms by Sympathetic Cooling*, Science **294**, 1320 (2001).

17. A. Robert, O. Sirjean, A. Browaeys, J. Poupard, S. Nowak, D. Boiron, C. I. Westbrook, and A. Aspect, *A Bose-Einstein Condensate of Metastable Atoms*, Science **292**, 461 (2001).

18. F. Pereira Dos Santos, J. Léonard, Junmin Wang, C. J. Barrelet, F. Perales, E. Rasel, C. S. Unnikrishnan, M. Leduc and C. Cohen-Tannoudji, *Bose-Einstein Condensation of Metastable Helium*, Phys. Rev. Lett. **86**, 3459 (2001).

19. D. G. Fried, T. C. Killian, L. Willmann, D. Landhuis, S. C. Moss, D. Kleppner and T. J. Greytak, *Bose-Einstein Condensation of Atomic Hydrogen*, Phys. Rev. Lett. **81**, 3811 (1998).

20. T. Weber, J. Herbig, M. Mark, H.- C. Nägerl and R. Grimm, *Bose-Einstein Condensation of Cesium*, Science. **299**, 232 (1998).

21. Y. Takasu, K. Maki, K. Komori, T. Takano, K. Honda, M. Kumakura, T. Yabuzaki and Y. Takahashi, *Spin-Singlet Bose-Einstein Condensation of Two-Electron Atoms*, Phys. Rev. Lett. **91**, 040404 (2003).

22. S. A. Moskalenko and D. W. Snoke, *Bose Einstein Condensation of Excitons and Biexcitons*, Cambridge University Press, Cambridge (2000).

23. L. V. Butov, A. L. Ivanov, A. Imamoglu, P. B. Littlewood, A. A. Shashkin, V. T. Dolgopolov, K. L. Campman, and A. C. Gossard, *Stimulated Scattering of Indirect Excitons in Coupled Quantum Wells: Signature of a Degenerate Bose-Gas of Excitons*, Phys. Rev. Lett. **86**, 5608 (2001).

24. J. Kasprzak, M. Richard, S. Kundermann, A. Baas, P. Jeambrun, J. M. J. Keeling, F. M. Marchetti, M. H. Szymaska, R. André, J. L. Staehli, V. Savona, P. B. Littlewood, B. Deveaud, and L. S. Dang, *Bose-Einstein Condensation of Exciton Polaritons*, Nature **443**, 409 (2006).

25. S. O. Demokritov, V. E. Demidov, O. Dzyapko, G. A. Melkov, A. A. Serga, B. Hillebrands, and A. N. Slavin, *Bose-Einstein Condensation of Quasi-Equilibrium Magnons at Room Temperature under Pumping*, Nature **443**, 430 (2006).

26. J. D. Jackson, *Classical Electrodynamics*, John Wiley and Sons, New York, 3rd Edition (1998).

27. P. A. M. Dirac, *Quantum Mechanics of Many-Electron Systems*, Proc. R. Soc. London, **A123**, 714 (1929).

28. L. D. Landau and E. M. Lifshitz, *Theory of the Dispersion of Magnetic Permeability in Ferromagnetic Bodies*. Phys. Z. Sowietunion **8**, 153 (1935).

29. A. I. Akhiezer, V. G. Bar'yakhtar, and S. V. Peletminskii, *Spin Waves*, North-Holland, Amsterdam (1968).

30. C. Herring and C. Kittel, *On the Theory of Spin Waves in ferromagnetic Media*, Phys. Rev. **81** 869 (1951).

31. C. Kittel, On the Theory of Ferromagnetic Resonance Absorption, Phys. Rev. **73**, 155 (1948).

32. T. L. Gilbert, *A Phenomenological Theory of Damping in Ferromagnetic Materials*, IEEE T. Magn. **40**, 3443 (2004).

33. N. Bloembergen, E. M. Purcell, and R. V. Pound, *Relaxation Effects in Nuclear Magnetic Resonance Absorption*, Phys. Rev. **73**, 679 (1948).

34. R. W. Damon and J. R. Eshbach, *Magnetostatic Modes of a Ferromagnetic Slab*, J. Phys. Chem. Solids **19**, 308 (1961).

35. D. D. Stancil, *Theory of Magnetostatic Waves*, Springer Verlag, New York (1993).

36. P. Kabos and V. S. Stalmachov, *Magnetostatic Waves and Their Applications*, Chapman and Hall, London (1994)

37. M. J. Hurben and C. E. Patton, *Theory of Magnetostatic Waves for In-Plane Magnetized Isotropic Films*, J. Magn. Magn. Mater. **139**, 263 (1995).

38. M. Sparks, *Ferromagnetic Resonance in Thin Films*, Phys. Rev. B **1**, 3831 (1970).

39. B. A. Kalinikos, *Excitation of Propagating Spin Waves in Ferromagnetic Films*, IEE Proc. **127**, (H1), 4 (1980).

40. B. A. Kalinikos and A. N. Slavin, *Theory of Dipole-Exchange Spin Wave Spectrumfor Ferromagnetic Films with Mixed Exchange Boundary Conditions*, J. Phys. C **19**, 7013 (1986).

41. C. Kittel, *Excitation of Spin Waves in a Ferromagnet by a Uniform RF Field*, Phys. Rev. **110**, 1295 (1958).

42. G. T. Rado and J. R. Weertman, *Spin-Wave Resonance in a Ferromagnetic Metal*, J. Phys. Chem. Solids **11**, 315 (1959).

43. M. I. Kaganov, *Excitation of Standing Spin Waves in a Film*, Sov. Phys. JETP **12**, 114 (1961).

44. E. Schlöman, J. J. Green, U. Milano, *Recent Developments in Ferromagnetic Resonance at High Power Levels*, J. Appl. Phys. **31**, 386S (1960).

45. W. H. Louisell, *Coupled Modes and Parametric Electronics*, Wiley, New York (1960).

46. V. S. L'vov, *Wave Turbulence under Parametric Excitation*, Springer Verlag, Berlin (1994).

47. G. Gurevich, G. A. Melkov, *Magnetization Oscillations and Waves*, CRC Press, New York (1996).

48. O. G. Vendik, B. A. Kalinikos, and D. N. Chartorizhskii, *Instability of Spin Waves in Tangentially Magnetized Ferromagnetic Films*, Fiz. Tverd. Tela (Leningrad) **19**, 387 (1977); Sov. Phys. Solid State **8**, 222 (1977).

49. G. Wiese, *Theory for the First-Order Spin-Wave Instability Threshold in Ferromagnetic Insulating Thin Films*, Z. Phys. B **91**, 57 (1993).

50. G. Wiese, L. Buxman, P. Kabos and C. E. Patton, *Parallel Pumping Fine Structure at 9.4 GHz for In-Plane Magnetized Yttrium Iron Garnet Thin Films*, J. Appl. Phys. **75**, 1041 (1994).

51. G. Wiese, P. Kabos and C. E. Patton, *Subsidiary-Absorption Spin-Wave Instability Process in Yttrium Iron Garnet Thin Films: Coupled Lateral Standing Modes, Critical Modes, and the Kink Effect*, Phys. Rev. B **51**, 15085 (1995).

52. T. Holstein and H. Primakoff, *Field Dependence of the Intrinsic Domain Magnetization of a Ferromagnet*, Phys. Rev. **58**, 1098 (1940).

53. L. D. Landau and E. M. Lifshitz, *Course of Theoretical Physics*, Vol. 3, *Quantum Mechanics: Non-relativistic Theory*, Pergamon Press, Oxford, 3rd Edition (1977).

54. W. Nolting, *Grundkurs Theoretische Physik 5/2*, *Quantenmechanik-Methoden und Anwendungen*, Vieweg, Braunschweig (1997).

55. Y. R. Chen and N. Bloembergen, *Interaction between Light Waves and Spin Waves*, Phys. Rev. **143**, 372 (1966).

56. P. A. Fleury and R. London, *Scattering of Light by One- and Two-Magnon Excitations*, Phys. Rev. **166**, 514 (1968).

57. A. K. Zvezdin and V. A. Kotov, *Modern Magnetooptics and Magnetooptical Materials*, Taylor & Francis Group, New York (1997).

58. L. D. Landau and E. M. Lifshitz, *Course of Theoretical Physics*, Vol. 8, *Electrodynamics of Continuous Media*, Pergamon Press, Oxford, 3rd Edition (1984).

59. W. Wettling, M. G. Cottam and J. R. Sandercock, *The relation between one-magnon light scattering and the complex magneto-optic effects in YIG*, J. Phys. C **8**, 211 (1975).

60. M. G. Cottam, *Magnetistatic Theory of the Response Functions for a Finite-Thickness Ferromagnetic Slab and the Application to Brillouin-Scattering*, J. Phys. C: Solid State Phys. **12**, 1709 (1979).

61. R. E. Camley, T. S. Rahman and D. L. Mills, *Theory of Light Scattering by the Spin-Wave Excitations of Thin Ferromagnetic Films*, Phys. Rev. B **23**, 1226 (1981).

62. J. F. Cochran and J. R. Dutcher, *Calculation of the Intensity of Light Scattered from Magnons in Thin Films*, J. Magn. Magn. Mater. **73**, 299 (1988).

63. S. Demokritov and E. Tsymbal, *Light Scattering from Spin Waves in Thin Films and Layered Systems*, J. Phys. : Condens. Matter **6**, 7145 (1994).

64. A. Einstein, *Quantentheorie des Einatomigen Idealen Gases*, Part I, Sber. Preuss. Akad. Wiss. **22**, 261 (1924); *Quantentheorie des Einatomigen Idealen Gases*, Part II, Sber. Preuss. Akad. Wiss. **1**, 3 (1925).

65. J. F. Annett, *Superconductivity, Superfluids, and Condensates*, Oxford University Press, New York (2004).

66. B. Pethick and H. Smith, *Bose-Einstein Condensation in Dilute Gases*, Cambridge University Press, Cambridge (2002).

67. R. Balili, V. Hartwell, D. Snoke, L. Pfeiffer, and K. West, *Bose-Einstein Condensation of Microcavity Polaritons in a Trap*, Science **316**, 1007 (2007).

68. T. Giamarchi, C. Rüegg, and O. Tchernyshyov, *Bose–Einstein Condensation in Magnetic Insulators*, Nat. Phys. **4**, 198 (2008).

69. Yu. M. Bunkov and G. E. Volovik, *Bose-Einstein Condensation of Magnons in Superfluid $^3$He,* J. Low Temp. Phys. **150**, 135 (2008).

70. D. W. Snoke and J. P. Wolfe, *Population Dynamics of Bose Gas near Saturation*, Phys. Rev. B **39**, 4030 (1989).

71. H. T. C. Stoof, *Nucleation of Bose-Einstein Condensation*, Phys. Rev. A **45**, 8398 (1992).

72. G. Winkler, *Magnetic Garnets*, Vieweg, Braunschweig (1981).

73. V. Cherepanov, I. Kolokolov and V. L'vov, *Saga of YIG: Spectra, Thermodynamics, Interaction and Relaxation of Magnons in a Complex Magnet*, Phys. Rep. **229**, 81 (1993).

74. R. A. Laudise, *The Growth of Single Crystals*, Prentice-Hall, New York (1970), ch. 7.

75. D. Elwell and H. J. Sheel, *Crystal Growth from High-Temperature Solutions*, Academic Press, New York (1975), ch. 10.

76. H. J. Levinstein, S. Licht, R. W. Landorf, and S. L. Blank, *Growth of High-Quality Garnet Thin Films from Supercooled Melts*," Appl. Phys. Lett. **19**, 486 (1971).

77. E. A. Giess, J. D. Kuptsis, and E. A. D. White, *Liquid Phase Epitaxial Growth of Magnetic Garnet Films by Isothermal Dipping in a Horizontal Plane with Axial Rotation*, J. Cryst. Growth **16**, 36 (1972).

78. S. L. Blank and J. W. Nielsen, Thegrowth of magneticgarnets by liquid phase epitaxy, J. Cryst. Growth **17**, 302 (1972).

79. H. L. Glass, *Ferrite Films for Microwave and Millimeter-Wave Devices*, IEEE Proc. **76**, 151 (1988).

80. R. Krishnan, H. Le Gall and Tran Khan Vien, *Optical and Magnetooptical properties of Epitaxial YIG Films*, Phys. Status Solidi (a) **17**, K65 (1973).

81. A. A. Solomko, Y. A. Gaidai, and O. V. Kolokoltsev, Abstracts of ICM-94, p. 368 Warsaw, Poland (1994).

82. B. S. Tsai, D. Young and S. A. Nikitov, *Microwave and Magnetooptic Measurements of Nonlinear Dispersive Magnetostatic Waves in a Yttrium-Iron-Garnet-Gadolinium-Gallium-Garnet Waveguide*, J. Appl. Phys. **84**, 1670 (1998).

83. S. J. Fiedziuszko, *Microwave dielectric resonators*, Microwave Journal **29**, 189 (1986).

84. T. Koryu Ishii, *Handbook of Microwave Technology* Vol. 1 *Components and Devices*, Academic Press, London (1995).

85. J. R. Sandercock, *Some Recent Development in Brillouin Scattering*, RCA Rev. **36**, 89 (1975).

86. J. R. Sandercock, *Light Scattering in Solids* III, ed. M. Cardona and G. Güntherodt, Springer Verlag, Heidelberg (1982).

87. W. Becker, *Advanced Time-Correlated Single Photon Counting Technique*, Springer Verlag, Berlin Heidelberg (2005).

88. A. V. Lavrinenko, V. S. L'vov, G. A. Melkov and V. B. Cherepanov. *Kinetic Instability of a Strongly Nonequilibrium System of Spin Waves and Tunable Radiation of a Ferrite*, Zh. Eksp. Teor. Fiz. **81**, 1022 (1981); Sov. Phys. JETP **54**, 542 (1981).

89. V. S. Lutovinov, G. A. Melkov, A. Yu. Taranenko and V. B. Cherepanov, *Kinetic Instability of 1$^{st}$ Order Spin Waves in Ferrite*, Zh. Eksp. Teor. Fiz. **95**, 760 (1989); Sov. Phys. JETP **68** 432 (1989).

90. G. A. Melkov and S. V. Sholom, *Kinetic Instability of Spin Waves in Thin Ferrite Films*, Zh. Eksp. Teor. Fiz. **99**, 610 (1991); Sov. Phys. JETP **72**, 341 (1991).

91. G. A. Melkov, V .L. Safonov, A. Yu. Taranenko and S. V. Sholom, *Kinetic Instability and Bose Condensation of Nonequilibrium Magnons*, J. Magn. Magn. Mater. **132**, 180 (1994).

92. V. B. Cherepanov, *Accumulation of the Relaxation Products of a Stationary Magnon Packet*, Zh. Eksp. Fiz. **91**, 235 (1986); Sov. Phys. JETP **64**, 136 (1986).

93. Yu.D. Kalafati and V.L. Safonov, *Possibility of Bose Condensation of Magnos Excited by Incoherent Pump*, Pis'ma Zh. Eksp. Fiz. **50**, 135 (1989); JETP Lett. **50**, 149 (1989).

94. Yu.D. Kalafati and V.L. Safonov, *The Theory of Quasi Equilibrium Effects in a Magnon System Excited with Incoherent Pumping*, Zh. Eksp. Teor. Fiz. **100**, 1511 (1991); Sov. Phys. JETP **73**, 836 (1991).

95. Yu.D. Kalafati and V.L. Safonov, *Theory of Bose Condensation of Magnons Excited by Noise*, J. Magn. Magn. Mater. **123**, 184 (1993).

96. S.N. Bose, *Planks Gesetz und Lichtquantenhypotese*, Z. Phys. **26**, 178 (1924).

97. P. Kapitza, *Viscosity of Liquid Helium below the λ-point*, Nature **141**, 74 (1938).

98. J.F. Allen and A.D. Misener, *Flow of Liquid Helium II*, Nature, **141**, 75 (1938)**.**

99. F. London, *On the Bose-Einstein Condensation*, Phys. Rev. **54**, 947 (1938).

100. N. N. Bogoliubov, *On the Theory of Superfluidity*, Izvestia Academii Nauk USSR **11** 77 (1947); J. Phys. USSR **11**, 23 (1947).

101. H. Fröhlich, *Bose Condensation of Strongly Excited Longitudinal Electric Modes*, Phys. Lett. A **26**, 402 (1968).

102. S. A. Moskalenko, *Reversible Optico-Hydrodynamic Phenomena in a Nonideal Exciton Gas*, Sov. Phys. Solid State **4**, 199 (1962).

103. J. M. Blatt, K. W. Böer and W. Brandt, *Bose-Einstein Condensation of Excitons*, Phys. Rev. **126**, 1691 (1962).

104. E. A. Cornell, C. A. Wieman, *Nobel Lecture: Bose-Einstein Condensation in a Dilute Gas, the First 70 Years and Some Recent Experiments*, Rev. Mod. Phys. **74**, 875 (2002).

105. M. I. Kaganov, N. Pustylnik and T. I. Shalaeva, *Magnons, Magnetic Polaritons and Magnetostatic Waves*, Uspekhi Fiz. Nauk **167**, 191 (1997); Sov. Phys. Usp. **40**, 181 (1997).

106. K. E. Strecker, G. B. Partridge, A. G. Truscott and R. G. Hulet, *Formation and Propagation of Matter-Wave Solitone Trains*, Nature **417**, 150 (2002).

107. L. Khaylovich, F. Schreck, G. Ferrari, T. Bourdel, J. Cubizolles, L. D. Carr and Y. Castin, *Formation of a Matter-Wave Bright Soliton*, Science **296,** 1290 (2002).

108. E. A. Donley, N. R. Claussen, S. L. Cornish, J. L. Robert, E. A. Cornell and C. E. Wieman, *Dynamics of collapsing and exploding Bose-Einstein condensates,* Nature **412**, 295 (2001).

109. M. R. Andrews, C. G. Townsend, H.-J. Miesner, D. S. Durfee, D. M. Kurn, and W. Ketterle, *Observation of Interference between Two Bose Condensates*, Science **275**, 637 (1997).

110. F. S. Cataliotti, S. Burger, C. Fort, P. Maddaloni, F. Minardi, A. Trombettoni, A. Smerzi, and M. Inguscio, *Josephson Junctions Array with Bose-Einstein Condensates*, Science **293**, 843 (2001).

111. M. Albiez, R. Gati, J. Fölling, S. Hunsmann, M. Cristiani, and M. K. Oberthaler, *Direct Observation of Tunneling and Nonlinear Self-Trapping in a Single Bosonic Josephson Junction*, Phys. Rev. Lett. **95**, 010402 (2005).

112. Y. H. Liu and C. E. Patton, *Spin-Wave Instability Threshold in Single-Crystal Yttrium Iron Garnet for Oblique Pumping*, J. Appl. Phys. **53**, 5116 (1982).

113. T. Neumann, A. A. Serga, V. I. Vasyuchka, and B. Hillebrands, *Field-Induced Transition from Parallel to Perpendicular Parametric Pumping for a Microstrip Transducer*, Appl. Phys. Lett. **94**, 192502 (2009).

114. A. Krawczyk and S. Wiak, *Electromagnetic Fields in Electrical Engineering* IOS Press, Amsterdam (2002).

115. I. S. Tupitsyn, P. C. E. Stamp, and A. L. Burin, *Stability of Bose-Einstein Condensates of Hot Magnons in Yttrium Iron Garnet Films*, Phys. Rev. Lett. **100**, 257202 (2008).

116. A. V. Chumak, G. A. Melkov, V. E. Demidov, O. Dzyapko, V. L. Safonov, and S. O. Demokritov, *Bose-Einstein Condensation of Magnons under Incoherent Pumping*, Phys. Rev. Lett. **102**, 187205 (2009).